• Institute of Fundamental Technological Research
• Polish Academy of Sciences
• Warsaw • Poland

LECTURE NOTES 10

Andrei Constantinescu
Ky Dang Van

# A Global Computational Approach in Engineering Problems

## Identification and Fatigue

Centre of Excellence for
Advanced Materials and Structures

WARSAW 2004

# AMAS LECTURE NOTES



*Production of this volume has been partially supported by the European Commission*

*Published and distributed by*
Institute of Fundamental Technological Research
Świętokrzyska 21, 00-049 Warszawa, Poland

ISSN 1642-0578

Papier offset. kl. III, 70 g, B1
Ark. wyd.: 12,1; ark. druk.: 10,25
Skład w systemie LaTeX: T.G. Zieliński
Oddano do druku i druk ukończono: III 2004
Druk i oprawa: Drukarnia Braci Grodzickich, Piaseczno, ul. Geodetów 47a

# Contents

PART I

# Identification and Inverse Problems in Solid Mechanics

ANDREI CONSTANTINESCU

# Preface

This work is a fruit of the lectures given at the Institute of Fundamental Technological Research of the Polish Academy of Sciences (IFTR PAS) in November 2001. Its purpose is to present an introduction to inverse and identification problems in solid mechanics which are ones of the fast growing areas in this engineering field with applications in both other sciences and in industry. It presents a short overview of the field and methods, without pretending to cover the field. The contents is based on classical and recent results from the literature and some results of the author and of his coworker.

A certain number of aspects are discussed here:

- reciprocity gap,
- gradient computations: direct differentiation and the adjoint state method,
- crack identification,
- identification of material parameters,
- errors functionals: least squares, error on the constitutive law, etc.

Aspects like ill-posedness and regularization, minimization algorithms, numerical implementation details, etc., have been left aside. I hope that indicating some references for further reading will help the reader and will prove enough precise for an introduction to this subject.

This work is first of all, an expression of my gratitude to HUY DOUNG BUI who was my PhD adviser. He patiently guided my steps through this field and who continuously shared his enthusiasm for these topics. I would also like to especially thank MARC BONNET, HUBERT MAIGRE, NICOLAS TARDIEU, ERIC CHARKALUK, LAETITIA VERGER and BRICE LECAMPION with whom I closely worked during the last years on different topics which are partially present in the book and who influenced my understanding of the field and underlying applications. A last thought goes to my colleagues

and friends at the Laboratoire de Mécanique des Solides and elsewhere who always encouraged me during the work of the last years.

This work would have not been possible without the kind invitation of Prof. ZENON MRÓZ to lecture in Warsaw or without the patience and kindness of the colleagues and students at the IFTR who assisted at the lectures and made my stay so enjoyable.

A special acknowledgment comes for the kind encouragements of Prof. J. JOACHIM TELEGA to bring this manuscript to its final form and to TOMASZ G. ZIELIŃSKI who helped with the LaTeX editing.

# Chapter 1

# A historical introduction

## 1.1. What are inverse problems?

One of the major difficulties in discussing inverse problems is that there is no their precise definition. As Charles W. Groetsch has very nicely expressed it [1], they are defined by "community standards". That means actually that people have for a long time accepted a familiar formulation for the problem, which they call the direct problem. Every less familiar variant is an inverse problem. The familiarity itself is determined, for example, by the facility of solving the problem, historical priority, uniqueness properties of the solution, etc.

On of the first arithmetical task children learn in school is the multiplication: given two numbers one has to compute their product:

$$(a, b) \longrightarrow a \times b = c.$$

This is the direct problem. The associated inverse problem is the factorization: given a number, find all pairs such that their product is the initial number:

$$c \longrightarrow (a, b), \quad \text{such that} \quad c = a \times b.$$

With this simple example we can already remark some characteristics to be retrieved in most direct and inverse problems. The direct problem has a unique solution, whereas the inverse problem might have a whole set of solutions.

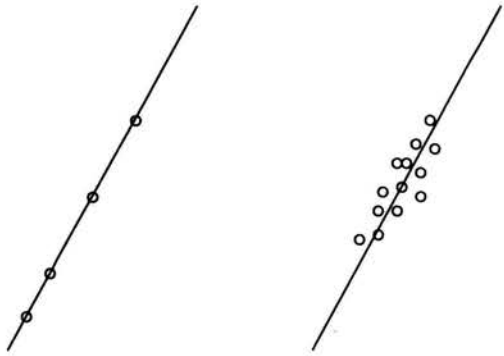

FIGURE 1.1. Extracting points from a given line (left) and finding a line passing through a set of points (right).

Another elementary pair of direct and inverse problems is that of extracting points of a line and respectively that of linear interpolation, where a line has to be drawn through a set of points (see Fig. 1.1). The direct problem is then expressed as:

$$\begin{gathered} (\boldsymbol{a}, b) \quad \longrightarrow \quad \boldsymbol{x} \\ \text{Find} \quad \boldsymbol{x} \quad \text{such that} \quad \boldsymbol{a} \cdot \boldsymbol{x} = b, \end{gathered} \tag{1.1}$$

and the inverse problem becomes:

$$\begin{gathered} \{\boldsymbol{x}_1, \ldots, \boldsymbol{x}_n\} \quad \longrightarrow \quad (\boldsymbol{a}, b) \\ \text{Find} \quad (\boldsymbol{a}, b) \quad \text{such that} \quad \boldsymbol{a} \cdot \boldsymbol{x}_i = b \quad \forall i = 1, \ldots, n. \end{gathered} \tag{1.2}$$

In this case we remark that the inverse problem does *not* possess a solution. As such, one will define a quasi-solution or a solution in the least square sense:

$$\text{Find} \quad (\boldsymbol{a}, b) \quad \text{minimum of} \quad \sum_i (\boldsymbol{a} \cdot \boldsymbol{x}_i - b)^2. \tag{1.3}$$

This quasi-solution gives at least an approximate answer, in the sense of the least squares norm, of the inverse problem.

If the direct problem is thought in terms of a model or a process with an input and and output (see Fig. 1.2), then one could imagine two corresponding inverse problems (see Fig. 1.3) as the identification of the input or as the identification of the model, generally understood as the identification of some characteristics or parameters of the model such that the generated output corresponds to the given input. In terms of classical problems of continuum mechanics the direct problem could be formulated as follows:

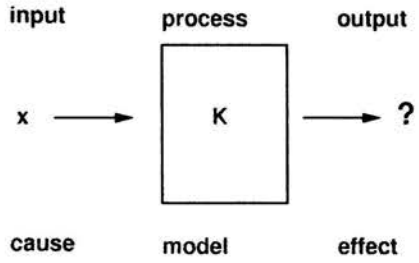


FIGURE 1.2. A scheme of generic direct problem.

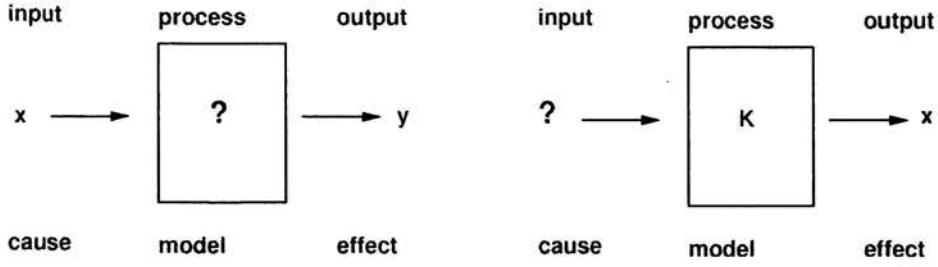


FIGURE 1.3. Two schemes of generic inverse problems: identification of input (right) and model identification (left).

- Compute the *displacements* of a *structure* provided that a system of *forces* is given.

Some corresponding inverse problems are:

- Determine the constitutive law of the structure provided that the *displacements* and the system of *forces* are given.
- Determine the initial (undeformed geometry) from the *displacements* and *forces*.
- Determine an unknown boundary condition.

Some of these problems will be discussed in the next Chapter.

Before proceeding to these topics let us recall briefly in a historical order some well-known problems, which can be considered as inverse problems.

## 1.2. Shadows from the antiquity

**Plato's allegory of the cave.** One of the most famous allegories of antiquity is Plato's allegory of the cave. It is the account of a group of pris-

oners living in an underground den. The prisoners are chained around their necks and legs, so they are unable to move and they can only see what is in front of them. Behind them there is a fire and they see their own shadows and the shadows of the other prisoners that the fire reflects onto the wall. As such the only perception of the world the prisoners have comes through the projection by the light of the fire. Obliviously, they will have a very hard task to imagine the world from this very limited information.

Now, the *direct* problem consists in the determination of shadow of an object from its outer shape and is straightforward. The associated *inverse* problem is to determine the shape of an object given its shadow and is a practically impossible task to perform since the solution is not unique (see for instance Fig. 1.4). For example, if the shadow is a circle it can be the shadow of a sphere, an ellipsoid, or of a cylinder. However, if one begins to know all shadows, coming from all directions, we can have a precise answer.

As we shall see these features are to be found in other inverse problems as well.

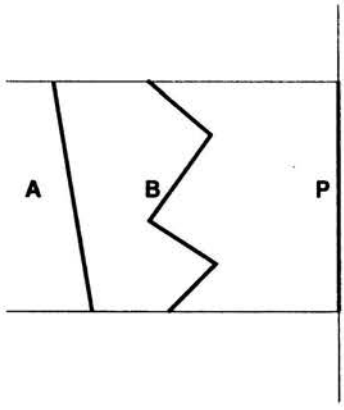


FIGURE 1.4. Two different set $A$ and $B$ having the same orthogonal projection $P$ on a given line.

**Sphericity of the earth.** The sphericity of the earth has already been accepted since ancient times. It is interesting to know that one of Aristotle's (384 BC – 322 BC) arguments for the sphericity of the earth was the shape of the shadow projected by the earth on the moon during the eclipses. The argument is therefore the result of an indirect observation and we could assert that it is the "solution" of an inverse problem.

An even finer reasoning for the solution of this inverse problem was provided by Eratosthenes of Cyrene (276 BC – 194 BC) who proposed to estimate the radius of the earth by measuring the midday shadow in Alexandria and Syene.

Eratosthenes knew that the length of an arc on a circle is directly proportional to the angle it subtends and to the radius of the circle. He also knew that the length of the way from Alexandria to Syene was about 850 km. In order to estimate the radius of the earth he had then only to estimate the angle between the two locations (see Fig. 1.5).

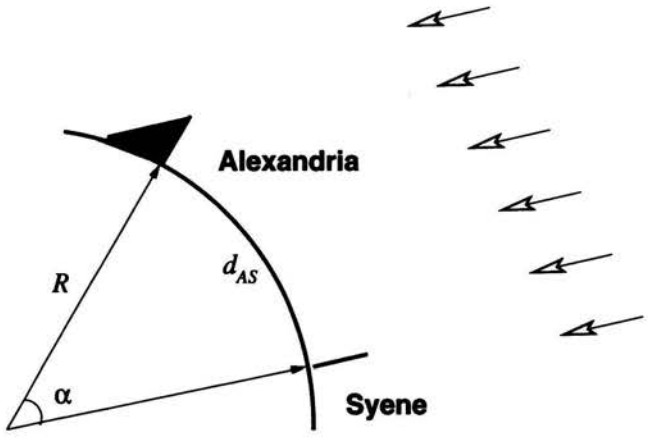


FIGURE 1.5. Scheme for Eratosthenes computation of the radius of the earth.

In order to solve the last problem he noted that in the sun Syene is directly overhead at midday on the summer solstice, this comes from the fact that Syene lies practically on the Tropic of the Cancer. He could then measure at the same moment the angle of the midday shadow in Alexandria as $\alpha \approx 12°$, which was equal to the angle between the two locations. His estimation conducts therefore to an earth radius of:

$$R = \frac{360° \cdot d_{AS}}{\alpha} = \frac{360° \cdot 850\,\text{km}}{12°} = 42500\,\text{km}, \tag{1.4}$$

which is an excellent estimation, when one takes into account the measurement techniques of that period.

**Archimedes.** Another now classical reasoning to estimate an inaccessible quantity is the famous story of Archimedes bath. King Herons (287 BC – 212 BC) suspected that the goldsmith of his new crown had cheated him

by changing partly the gold of the crown for another less noble material. As less noble materials were generally lighter that gold, the straightforward method was to melt down the crown and compare its volume to an equal volume of pure gold, however this would imply the destruction of the crown, which was to be avoided. Therefore the king asked Archimedes invent a "non-destructive" technique to tackle this question. It is told the idea came to Archimedes one day when he was taking a bath and the water was flooding out of the tube. It meant to measure the volume of the crown and of an equal weight of lump material.

## 1.3. Trajectory problems: guns and stars

Beginning with the medieval age a series of problems related to the computation of trajectories of moving bodies gained the interest of scientists. Some had direct application in the art of gunnery and provided as such funding from princes of that time.

Before to the works of Galileo Galilee (1564–1642) the scientific description was practically flawed. However, the main direct and inverse problems where already announced.

The brescian mathematician Nicolo Tartaglia, his real name was Nicolo Fontano (1500?–1557), known for his results in solving the quadratic equation along Girolamo Cardano, also claimed to be the inventor of the gunners square, a simple device to measure the shooting angle (see Fig. 1.6), also denoted as the elevation. The direct problem is the result of a test shot, giving the shooting range for a given elevation. The interesting problem is the inverse one, which consists in finding the elevation which provides a given shooting

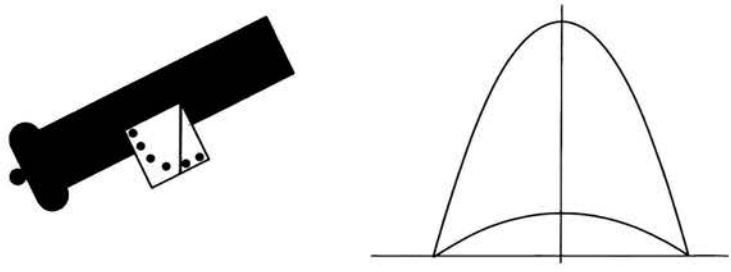

FIGURE 1.6. The gunners square (left) and two trajectories with different initial shooting angle providing the same shooting range (right).

range. This problem was solved by the gunners of that time by trial and error method: correcting at each step the elevation through a dichotomy algorithm. It is interesting to point out that the gunners had already discovered that this problem does not have a unique solution.

**Exercise:** *Solve the gunners inverse problem, i.e. find the shot angle $\theta$ (modern equivalent of the medieval punti), such that the shot attains a range $R$ in the absence of drag and assuming that the initial velocity is independent of $\theta$. Remark that the solution is not unique (see Fig. 1.6).*

The basis of elementary ballistics gained a sound basis only with the work of Galileo Galilee. He proposed the key notions of trajectory computations by transferring the problem in vacuum, thus eliminating the effect of drag. With the evolution of the mathematical and physical foundations of this domain, problems pertaining gunnery have also been evolving and are at all time more or less present in the technical community.

As impressive modern applications of the inverse gunners problem, we might cite the finding of the launch sites of the V1 bombs at Peenemuende by the Royal Air Force and the investigations of airplanes crashes from the distribution of debris.

Another application of inverse trajectory problems is the simultaneous discovery of Uranus by Urbain Le Verrier 1811–1877 and John Couch Adams 1819–1842. After the impressive work done by Newton in defining the laws of motion and the developments in calculus which followed it was a "simple" matter of direct computation to determine the path of a planet given the masses and positions of the other planets influencing its motion. The inverse problem solved by Le Verrier and Adams consisted in determining an unknown planet from the perturbation of the paths of known planets. The perturbations should be understood as a difference between astronomical measurements and the predicted path obtained by computations from the positions of the known planets. In modern times similar path problems are solved for the flight control of artificial satellites.

## 1.4. Gravity measurements

It is well known that the gravitational attraction between points is directly related to their respective masses and inverse proportional to the square of their distance. In each position we can add up the earthly attrac-

tion and express it as the local gravitational acceleration in function of the distribution of mass density. Mathematically this is written in the following integral equation [2]:

$$g_3(\boldsymbol{x}) = \mathcal{G}\frac{\partial}{\partial x_3}\int_{\Omega}\frac{1}{\boldsymbol{x}-\boldsymbol{y}}\rho(\boldsymbol{y})\,dv(\boldsymbol{y}), \tag{1.5}$$

where $\mathcal{G}$ is Newton's universal gravitational constant, $\Omega$ represents the earth and $\rho(\boldsymbol{y})$ is the mass density at the point $\boldsymbol{y}$.

The gravitational acceleration $g_3(\boldsymbol{x})$ can *directly* be measured for example from the frequency of a pendulum. Therefore one can imagine that from a precise measurement of the acceleration at the surface one could reconstruct the underground distribution of density indicating the existence of oil trap [3] or the even the position of the pharaohs chamber in a pyramid. For this type of application a good introduction is to be found in [2] (see Fig. 1.7).

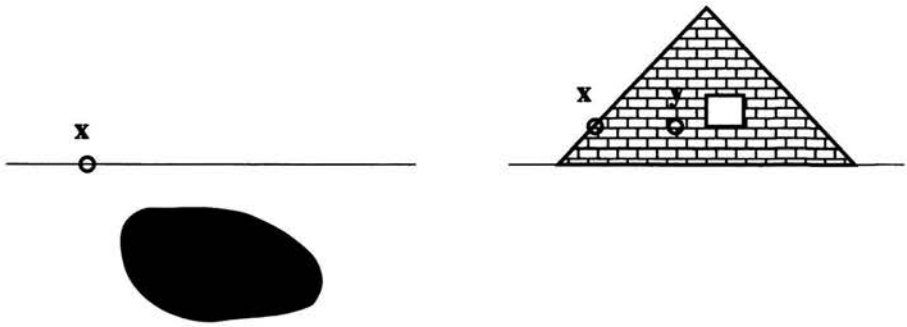


FIGURE 1.7. Configuration for the inverse gravity problem in the case of underground reservoir (left) and the pharaohs chamber (right).

This inverse gravity problem can be formalized as:

$$\text{Determine} \quad \rho(\boldsymbol{y}) \quad \text{from} \quad g_3(\boldsymbol{x}).$$

From mathematical point of view Eq. (1.5) is a Fredholm equation of the first kind. This type of equations is generally difficult to solve as they possess generally a very weak continuity of the solution with respect to the input data and are therefore numerically unstable [4].

In the special case of gravimetry one can show that the solution is not unique, as shown in the next exercise. In such a case one will add some *a priori* information has to be added, i.e. additional information known in

advance, in order to solve the problem. For example, in the determining the location of the mortuary chamber of the pyramid one can suppose that the mass density is vanishing in the chamber and is a given constant outside.

**Exercise:** *Prove the non uniqueness of the solution of this problem by taking $\psi$ a function defined on $\partial\Omega$ such that:*

$$\psi = 0 \quad \textit{and} \quad \partial_{\boldsymbol{n}}\psi = 0.$$

*Hint:*

$$\triangle \frac{1}{\boldsymbol{x} - \boldsymbol{y}} = 0;$$

*apply the Stokes theorem*

$$\int_{\Omega} (f \triangle g - g \triangle f)\, dv = \int_{\partial\Omega} (f \partial_{\boldsymbol{n}} g - g \partial_{\boldsymbol{n}} f).$$

## 1.5. X–Ray Tomography

The discovery by Wilhelm Roentgen (1845–1923) of the X-ray technique was a great achievement for the evolution of medicine in the beginning of the twentieth century as it was a first step into *non-invasive* diagnosis. His technique consisted in exposing the body to a beam of X-rays and recording the image of the rays after they passed through the body on photographic film. The record represents a shadow of passed tissues. The intensity of the image is inversely proportional to the attenuation coefficient, the capacity of each tissue to absorb X-rays. The image is therefore a sum of the tissues passed. The main main drawback of the method is that projections of different organs are overlapped on the final picture. This will always be the case independently of the projection direction of X-rays.

In the same period, in 1917, an Austrian mathematician Johann Radon (1887–1956) solved a mathematical inverse problem. The problem of Radon was to reconstruct a real valued function defined on a plane from its line integrals computed on all lines of the plane.

Half a century later, in 1955, Allan Cormack, a young lecturer at the Groote Schuur Hospital in Capetown (South Africa) succeded to solve the X-ray "overlapping" difficulty. Jointly with G.N. Hounsfiel, in 1979, he was awarded the Nobel Prize in medicine.

Allan Cormack tried to prepare isodose charts for radiotherapy, i.e. he prepared the X-ray exposure of patients such that different parts would get an equal amount of X-rays. The initial assumption was that the body was homogeneous. Then he improved the technique using an inhomogeneous body. He also understood that the spatial distribution of the attenuation coefficient could be reconstructed from external X-ray images. From a mathematical point of view, this is actually the Radon problem (for more technicalities see [2]).

Let us denote by $\mu(\boldsymbol{x})$ the attenuation coefficient in the current point $\boldsymbol{x}$. Then the intensity of the image at the point of position $\rho$ of the screen for an X-ray taken in the direction $\theta$ will be directly dependent of:

$$a(\theta,\rho) = \int\limits_{\text{line}(\theta,\rho)} \mu(\boldsymbol{x})\, dv = \int\limits_{R^2} \mu(x_1,x_2)\delta(x_1\cos\theta + x_2\sin\theta - \rho)\, dx_1 dx_2, \quad (1.6)$$

i.e., the sum of the attenuation coefficient over the line$(\theta,\rho)$ (see Fig. 1.8).

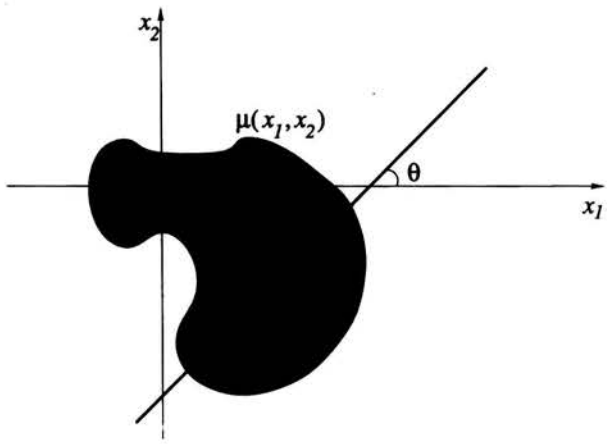


FIGURE 1.8. A scheme of generic direct problem.

The corresponding *inverse* problem is now formulated as:

$$\textit{Determine}\ \ \mu(\boldsymbol{x})\ \ \textit{from}\ \ a(\theta,\rho)\ \ \forall\theta\ \forall\rho.$$

The solution proposed by Radon was to take first the partial *Fourier*

transforms with respect to the variable $\rho$ in order to obtain:

$$\mathcal{F}_\rho[a(\theta,\rho)] = \int_{-\infty}^{\infty} a(\theta,\rho)e^{-i\rho k_\rho}\,d\rho$$
$$= \int_{-\infty}^{\infty}\int_{R^2} \mu(x_1,x_2)\delta(x_1\cos\theta + x_2\sin\theta - \rho)e^{-i\rho k_\rho}\,dx_1dx_2\,d\rho. \quad (1.7)$$

Second, denoting: $k_1 = k_\rho \sin\theta$ and $k_2 = k_\rho\cos\theta$ one can take partial Fourier transforms with respect to $k_1$ and $k_2$ to obtain the final solution in the form:

$$\mu(x_1,x_2) = \mathcal{F}_{k_1}^{-1}\mathcal{F}_{k_2}^{-1}\mathcal{F}_\rho[a(\theta,\rho)]. \quad (1.8)$$

This rough version of a solution presents actually the main idea; however, from the numerical point of view a series of additional works have been done in order to obtain the actual resolutions of X-ray tomographies.

From the physical point of view other complementary techniques, such as MRI (Magnetic Resonance Imaging) were proposed in the last decades. In spite of different physical phenomena, one will observe similar mathematical settings for these techniques. Let us simply resume that the MRI measurements are based on two steps: in the first step protons, acting like infinitesimal magnets, are oriented and set into rotation by a microwave pulse. In the second step the current induced by the moving magnetic field is recorded. A series of recordings is then obtained for different orientations and the inverse problem consists in the determination of the spatial density of protons.

## 1.6. Notes

**Further reading.** For further reading regarding different inverse problems we recommend two books:

- *Inverse Problem in the Mechanics of Materials* by H.D. Bui [2]. The book provides a fast overview of problems and equations involving inverse problems in solid mechanics. The applications discussed range from fracture mechanics and identification of cracks to vibrations and acoustic waves, demography and seismic demography, microgravity, residual stresses, etc. Each chapter has a comprehensive bibliography on various related topics.

- *Inverse Problems* by C.W. Groetsch gives a charming introduction to a series of inverse problems. It is written at an undergraduate mathematics level and presents a series of exercises and worked out examples in Matlab.

Other more technical introductions at a graduate level can be found in the DEA lectures notes of M. Bonnet [5] and S. Andrieux [6].

## 1.7. References

1. C.W. GROETSCH, *Inverse Problems*, The Mathematical Society of America, 1999.
2. H.D. BUI, *Introduction aux Problèmes Inverses en Mécanique des Matériaux*, Eyrolles, Paris / CRC Roca Baton, 1993.
3. G.E. BACKUS and F. GILBERT, Numerical applications of a formalism of geophysical inverse problems, *Geophysical J.Roy.Astr.Soc*, 13:247, 1967.
4. G.M. WING, *Primer on Integral Equations of the First Kind*, SIAM, 1991.
5. M. BONNET, *Problèmes Inverses*, DEA: Dynamique des Structures et Couplages, Ecole Polytechnique, 2001.
6. S. ANDRIEUX, *Problèmes Inverses*, DEA: Techniques Avancées de Calcul des Structures, Ecole Polytechnique, 2001.

# Chapter 2

# Applications of Betti reciprocity

## 2.1. The Betti reciprocity principle

Michael Faraday (1791–1867), one the most famous physicists of the 19th century, in 1834 designed a simple experiment with important consequences for the later theory of elasticity and electricity.

Let us consider an elastic rod. We shall impose vertical forces in two different points $P$, $Q$, and denote the pair as $\boldsymbol{f} = (f_P, f_Q)$. The measurement of the normal displacements at the same points is given by the pair: $\boldsymbol{u} = (u_P, u_Q)$. In a real experiment one can now remark [1] that for two distinct

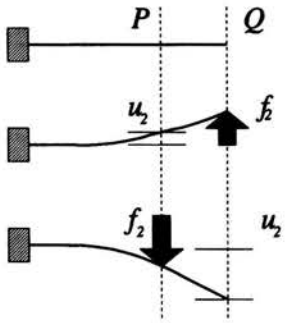


FIGURE 2.1. The Faraday experiment for what was later called the Betti reciprocity principle.

[1] A simple verification as a table top experiment can be done using a saw blade and a simple weight for the force.

experiments in which we denoted displacements and forces by $(\boldsymbol{u}_1, \boldsymbol{f}_1)$ and respectively $(\boldsymbol{u}_2, \boldsymbol{f}_2)$, that the crossed mechanical work of the displacements and forces is always equal, i.e.:

$$\boldsymbol{f}_2^{\mathrm{T}} \cdot \boldsymbol{u}_1 = \boldsymbol{f}_1^{\mathrm{T}} \cdot \boldsymbol{u}_2. \tag{2.1}$$

This relation is called the *Betti reciprocity principle* to honour Enrico Betti (1823–1892) who studied this property in the case of continuous elastic systems. Such an experiment where $\boldsymbol{f}^1 = (f_P, 0)$, $\boldsymbol{f}^2 = (0, f_Q)$ is depicted in Fig. 2.1.

As the rod has been supposed to be linear elastic therefore it is represented by a linear operator $\boldsymbol{A}$, defined by:

$$\boldsymbol{A} = \begin{bmatrix} A_{PP} & A_{PQ} \\ A_{QP} & A_{QQ} \end{bmatrix}. \tag{2.2}$$

The balance of forces and the equivalent principal of virtual work on the system is then simply written as:

$$\boldsymbol{A} \cdot \boldsymbol{u} = \boldsymbol{f} \quad \text{or} \quad \boldsymbol{v}^{\mathrm{T}} \boldsymbol{A} \cdot \boldsymbol{u} = \boldsymbol{v}^{\mathrm{T}} \cdot \boldsymbol{f} \quad \forall \boldsymbol{v}. \tag{2.3}$$

A straightforward algebraic computation (left as an exercise to the reader), shows that Eq. (2.1) is equivalent to the symmetry of $\boldsymbol{A}$, i.e. $\boldsymbol{A} = \boldsymbol{A}^{\mathrm{T}}$. This statement is of crucial importance as it also ensures the existence of a potential energy for the system:

$$W = \frac{1}{2} \boldsymbol{u}^{\mathrm{T}} \cdot \boldsymbol{A} \cdot \boldsymbol{u}. \tag{2.4}$$

Suppose now that the system has a "defect" which has to be identified, i.e. consider $\boldsymbol{A} + \delta \boldsymbol{A}$ and suppose $\boldsymbol{A}$ known and $\delta \boldsymbol{A}$ unknown.

Let us now consider one experiment, in which we measure the data $(\boldsymbol{u}_1, \boldsymbol{f}_1)$ on the system $\boldsymbol{A} + \delta \boldsymbol{A}$ and a second ficticious experiment $(\boldsymbol{u}_2^*, \boldsymbol{f}_2^*)$. We then have the following relations for the real experiment:

$$(\boldsymbol{A} + \delta \boldsymbol{A}) \cdot \boldsymbol{u}_1 = \boldsymbol{f}_1, \qquad \boldsymbol{v}^{\mathrm{T}} \cdot (\boldsymbol{A} + \delta \boldsymbol{A}) \cdot \boldsymbol{u}_1 = \boldsymbol{v}^{\mathrm{T}} \cdot \boldsymbol{f}_1 \quad \forall \boldsymbol{v} \tag{2.5}$$

and

$$\boldsymbol{A} \cdot \boldsymbol{u}_2^* = \boldsymbol{f}_2^*, \qquad \boldsymbol{v}^{\mathrm{T}} \cdot \boldsymbol{A} \cdot \boldsymbol{u}_2^* = \boldsymbol{v}^{\mathrm{T}} \cdot \boldsymbol{f}_2^* \quad \forall \boldsymbol{v} \tag{2.6}$$

for the ficticious experiment.

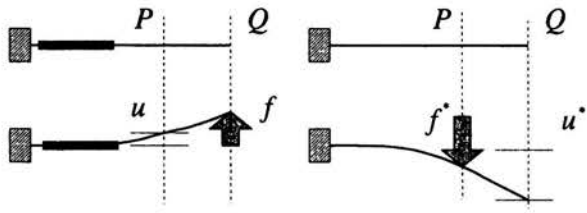


FIGURE 2.2. The real and virtual Betti reciprocity experiment for a rod.

It is obvious that the *reciprocity principle* is generally not respected for these two experiments:

$$\boldsymbol{u}_1^{\mathrm{T}} \cdot \boldsymbol{f}_2^* \neq \boldsymbol{u}_2^{*\mathrm{T}} \cdot \boldsymbol{f}_1. \tag{2.7}$$

However, we remark by a simple algebraic computation that the gap to fulfill the reciprocity principle (2.1), denoted as the *Reciprocity Gap*, is directly related to defect:

$$\mathcal{RB} = \boldsymbol{u}_1^{\mathrm{T}} \cdot \boldsymbol{f}_2^* - \boldsymbol{u}_2^{*T} \cdot \boldsymbol{f}_1 = \boldsymbol{u}_2^{*T} \cdot (\delta \boldsymbol{A}) \cdot \boldsymbol{u}_1. \tag{2.8}$$

The identification technique proposed in the sequel is based on the idea that for a given experiment, one can choose the solution of the ficticious experiments in such a way as to give an insight into $\delta \boldsymbol{A}$.

**Exercise:** *Compute the volume change of a linear elastic isotropic body due to the following load:*

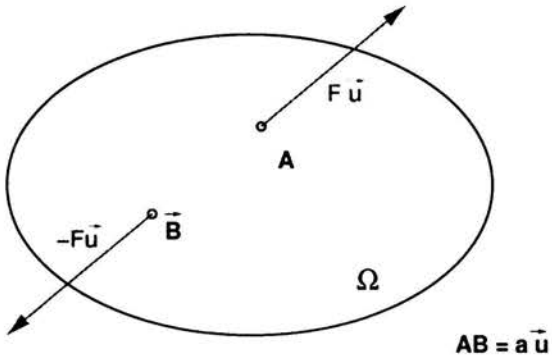


*Hint: Use as a second state the body subject to the strain:* $\boldsymbol{\varepsilon} = \frac{k}{3}\boldsymbol{I}$.

**Remark: The Betti reciprocity principle for a continuous system.** For the similar experiment performed on an elastic body occupying

the domain $\Omega$, one would classicaly write:

$$\int_{\partial\Omega} \boldsymbol{u}_1 \cdot \boldsymbol{t}_2 \, ds + \int_{\Omega} \boldsymbol{u}_1 \cdot \boldsymbol{f}_2 \, ds = \int_{\partial\Omega} \boldsymbol{u}_2 \cdot \boldsymbol{t}_1 \, ds + \int_{\Omega} \boldsymbol{u}_2 \cdot \boldsymbol{f}_1 \, ds, \tag{2.9}$$

where $\boldsymbol{u}_i, \boldsymbol{f}_i, \boldsymbol{t}_i$ $(i = 1, 2)$ are the vector fields of displacements, body forces and surface tractions respectively. We can remark that the left and the right hand side of the preceding equation are equal to:

$$\int_{\Omega} \nabla \boldsymbol{u}_1 : \boldsymbol{C} : \nabla \boldsymbol{u}_2 \, dv = \int_{\Omega} \nabla \boldsymbol{u}_2 : \boldsymbol{C} : \nabla \boldsymbol{u}_1 \, dv, \tag{2.10}$$

and the equality is equivalent to the symmetry property of the elastic tensor $\boldsymbol{C}$ $(C_{ijkl} = C_{klij},\ i, j, k, l = 1, 3)$ which also ensures the existence of the energy potential for the system.

## 2.2. Identification of cracks

In this section we shall present a series of recent mathematical results in which planar cracks are identified using the idea of the reciprocity gap introduced in the preceding section. The main difficulty is linked with the "choice" of appropriate ficticious experiment.

### 2.2.1. Elliptic equation

In this section, we shall consider a scalar potential solution of an elliptic equation. From a practical point of view this will model the electric or thermal stationary conduction problem and some practical applications are to be found in these fields.

Let us consider a body occupying the domain $\Omega \subset \mathbb{R}^3$, with boundary $\partial\Omega$ and containing a planar crack $\Gamma$ (see Fig. 2.3).

The system is repesented by an elliptic equation expressing stationary heat or electric conduction. The balance equation is written as:

$$\mathcal{A}(u) = 0, \qquad \operatorname{div}(k \operatorname{grad} u) = 0, \tag{2.11}$$

where $u$ represents the temperature distribution or the field of electric potential, $k$ denotes here the heat or the electric conduction coefficient which

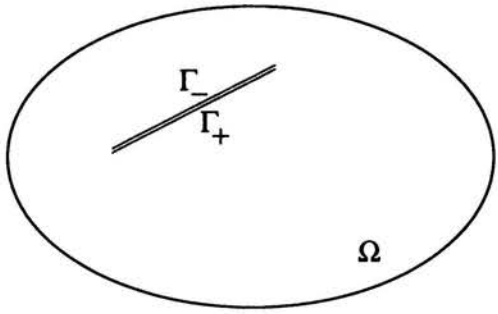


FIGURE 2.3. The body containing a planar crack.

is supposed to be known. The crack $\Gamma = \Gamma_+ \bigcup \Gamma_-$ is defined as a flux free surface:

$$k\partial_{\boldsymbol{n}} u = 0, \qquad \boldsymbol{x} \in \Gamma_+ \bigcup \Gamma_- \tag{2.12}$$

We assume that both the potential and the flux $(\xi, \varphi)$ are measured on the external boundary $\partial\Omega$ which implies the following boundary conditions:

$$u = \xi, \qquad k\partial_{\boldsymbol{n}} u = \varphi. \tag{2.13}$$

In the *direct problem* $\mathcal{P}$ one wants to determine the spatial distribution of the potential $u$ knowing the exact position of $\Gamma$ and one of the two boundary conditions (2.13).

The *inverse problem* $\mathcal{P}^{-1}$ is defined as:

> *Identify the geometry of* $\Gamma$ *from the over-specified boundary measurements* $(\xi, \varphi)$.

We are talking about over-specified boundary measurements, as in a well posed problem is sufficient to give only one of the potential or the flux on the boundary.

The solution presented here was initially proposed in a pioneering paper by Andrieux and Benabda [1]. They defined the reciprocity gap corresponding to this problem as in the previous section and proposed a series of *virtual* test fields in order to identify the crack provided its domain $\Gamma$ lies completely in a plane.

**The Betti Reciprocity Gap $\mathcal{RB}$.** The multiplication of (2.11) by a smooth field $w$ defined over $\Omega$, followed by an integration over $\Omega$ and series

of integration by parts leads to:

$$\int_{\Gamma} \left( [\![\partial_n u]\!] w - [\![u]\!] \partial_n w \right) ds$$

$$= - \int_{\Omega \setminus G} u \big( \operatorname{div} k \operatorname{grad} w \big) \, d\boldsymbol{x} + \int_{\partial\Omega} \left( w \, \partial_n u - u \, \partial_n w \right) ds. \quad (2.14)$$

We choose $w$ to be a smooth solution of the equation:

$$\mathcal{A}^*(u) = - \operatorname{div}(k \operatorname{grad} w) = 0 \quad (2.15)$$

in the domain $\Omega$ without the crack and call such a solution an *adjoint field* and the corresponding equation the *adjoint equation*. If $w$ is an adjoint field, Eq. (2.14) becomes an integral equation relating fields defined on the exterior boundary $\partial\Omega$ and on the crack $\Gamma$. We define the *reciprocity gap* $\mathcal{RB}$, as:

$$\mathcal{RB}(w; \xi, \varphi) = \int_{\partial\Omega} \left( \xi \partial_n w - w\varphi \right) ds, \quad (2.16)$$

which is also equal to:

$$\mathcal{RB}(w; \xi, \varphi) = \int_{\Gamma} \left( [\![\partial_n u]\!] w - [\![u]\!] \partial_n w \right) ds. \quad (2.17)$$

From the point of view of the inverse problem we can remark that the reciprocity gap, depends only on measurable quantities $(\xi, \varphi)$ and on an arbitrary adjoint field $w$.

**Identification of the planar crack.** In order to identify the crack, we suppose that its position and shape is completely revealed by the jump of the potential over the crack $[\![u]\!]$. This is a restrictive definition as not all potentials are discontinuous over the crack, and as such does not preserve the geometry completely. However, we accept this definition and suppose that we dispose of an experiment giving a potential with a non zero jump.

The crack is supposed to be planar, i.e. completely included in a plane and as such it will be identified in three distinct steps using for each one a special adjoint function:

- *Orientation of the plane*
  Let us define the following family of adjoint functions, parametrized by $\boldsymbol{p} \in \mathbb{R}^3$:

$$w_{\boldsymbol{p}}(\boldsymbol{x}) = \boldsymbol{p} \cdot \boldsymbol{x} + c, \qquad \nabla w_{\boldsymbol{p}} = \boldsymbol{p}.$$

A simple computations shows that the normal to the plane of the crack is given by:

$$\boldsymbol{n} = \frac{\mathcal{RB}(w_{\boldsymbol{e}_i}; \varphi, \psi)}{k \int_\Gamma [\![u]\!]\, ds}\, \boldsymbol{e}_i,$$

where $\boldsymbol{e}_i$ are the vector of the basis. The condition: $\|\boldsymbol{n}\| = 1$ gives the the relation:

$$\int_\Gamma [\![u]\!]\, ds = \frac{1}{k}\Big(\sum_{i=1}^{3} \mathcal{RB}(w_{\boldsymbol{e}_i}; \varphi, \psi)^2\Big)^{\frac{1}{2}},$$

which completes the proof.

- *Position of the plane*
  The next family is defined by:

$$w = 3(\boldsymbol{n} \cdot \boldsymbol{x})^2 - (\boldsymbol{x} \cdot \boldsymbol{x}).$$

  Similar computations provide:

$$\boldsymbol{n} \cdot \boldsymbol{x} = \frac{\mathcal{RB}(w; \varphi, \psi)}{4k \int_\Gamma [\![u]\!]\, ds}\, \boldsymbol{e}_i.$$

- *Extension of the crack in the plane*
  Consider a transformed coordinate system such that the plane of the crack is now defined by $x_3 = 0$.
  By $(\omega_i)_{i\in\mathbb{N}}$, we denote the solutions of the following eigenvalue problem:

$$-\triangle \omega_i(x_1, x_2) = \lambda_i \omega_i(x_1, x_2), \quad i \in \mathbb{N},$$

  and recall that the eigenfunctions of such a problem form a complete basis in $L^2(\mathbb{R}^2)$.
  If the third family of adjoint functions $\{w_i\}_{i\in\mathbb{N}}$ is defined by

$$w_i(x_1, x_2, x_3) = \omega_i(x_1, x_2) \frac{\mathrm{sh}(\sqrt{\lambda_i} x_3)}{\lambda_i},$$

  then

$$\partial_n w_i(x_1, x_2, 0) = \omega_i(x_1, x_2).$$

  The reciprocity relation for this family of adjoint functions becomes:

$$\int_\Gamma [\![u]\!]\, \partial_n w_i\, ds = \int_\Gamma [\![u]\!]\, \omega_i(x_1, x_2)\, dx_1 dx_2 = \mathcal{RB}(w_i; \varphi, \psi).$$

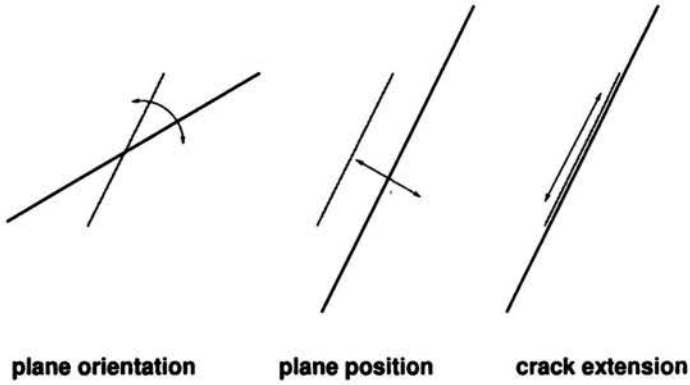


FIGURE 2.4. The identification of the three characteristics of the crack.

Consequently, the coefficients of $[\![u]\!]$ in the basis $L^2$ given by$(\omega_i)_{i\in\mathbb{N}}$ are known. We conclude that $[\![u]\!]$ is completely known and its support revealed by the crack opening the exact shape of the crack:

$$\text{supp}[\![u]\!] = \Gamma.$$

**Exercise:** *Check the preceding equations!*

A series of enhancements of these results have recently been proven: some numerical results [2], extension to elastostatics [3], uniqueness and stability results [4].

### 2.2.2. Hyperbolic equation: acoustic case

In this section we will show how the Betti reciprocity gap can be defined in the case of an acoustic equation, i.e. which is a hyperbolic equation with scalar potential, and used to identify a crack in a similar way as has been shown in the last section. In a similar way we will define as before three families of adjoint solutions which will permit us to define the complete geometry of a planar crack by identifying the orientation of the plane of the crack, its position and finally its complete extension. These results were obtained by Bui et al. [5].

Let us consider a body occupying the domain $\Omega \subset \mathbb{R}^3$, with the boundary $\partial\Omega$ and containing a planar crack $\Gamma$ (see Fig. 2.3).

The system is repesented by a *hyperbolic equation* expressing scalar wave propagation. The balance equation is written as:

$$\mathcal{A}(u) = \partial_t \partial_t u - \Delta u = 0, \tag{2.18}$$

where $u$ is the scalar field of the acoustic pressure. The crack $\Gamma = \Gamma_+ \bigcup \Gamma_-$ is defined as before as a flux free surface:

$$k \partial_{\boldsymbol{n}} u = 0. \tag{2.19}$$

The initial conditions are specified by

$$u(\boldsymbol{x}, t \leq 0) = 0, \quad \partial_t u(\boldsymbol{x}, t \leq 0) = 0, \quad \forall \boldsymbol{x} \in \Omega. \tag{2.20}$$

We assume, as before, that both the history of the potential and of the flux, $(\xi, \varphi)$ are measured on the external boundary $\partial\Omega$ in the time interval $[0, T]$, which implies the following boundary conditions:

$$u = \xi, \quad k \partial_{\boldsymbol{n}} u = \varphi. \tag{2.21}$$

The *inverse problem* $\mathcal{P}^{-1}$ can be defined as:

> *Identify the geometry of* $\Gamma$ *from the histories of boundary measurements* $(\xi, \varphi)$.

**The Betti reciprocity gap.** Let us consider a function

$$w : \Omega \times [0, \infty] \longrightarrow R.$$

After multiplication of $\mathcal{A}(u)$ by $w$ and a series of integration by parts (again left to the reader as an exercise!), we obtain the following integral equation:

$$\int_0^\infty \int_F \left( [\![\partial_n u]\!] w - [\![u]\!] \partial_n w \right) ds\, dt = \int_0^\infty \int_{\Omega \setminus F} u \left( \partial_t \partial_t w - \Delta w \right) d\boldsymbol{x}\, dt$$
$$+ \int_{\Omega \setminus F} \left[ w\, \partial_t u - u\, \partial_t w \right]_0^\infty d\boldsymbol{x} + \int_0^\infty \int_{\partial\Omega} \left( w\, \partial_n u - u\, \partial_n w \right) ds\, dt. \tag{2.22}$$

In this case one will define the *adjoint problem* as:

$$\mathcal{A}^*(w) = \partial_t \partial_t w - \Delta w = 0 \tag{2.23}$$

together with a series of initial conditions at $t = \infty$, such that:

$$\begin{aligned} \int_0^\infty \int_{\Omega\setminus F} u\big(\partial_t\partial_t w - \Delta w\big)\, d\boldsymbol{x}dt = 0, \\ \int_{\Omega\setminus F} \big[w\,\partial_t u - u\,\partial_t w\big]_0^\infty\, d\boldsymbol{x} = 0, \end{aligned} \tag{2.24}$$

where the choice of the conditions on $w$ will be *dual* to the ones specified for $u$.

With $u$ solution of $\mathcal{A}(u) = 0$ and $w$ solution of $\mathcal{A}^*(w) = 0$ the preceding equation becomes:

$$-\int_0^\infty \int_F [\![u]\!]\, \partial_n w\, ds\, dt = \int_0^\infty \int_{\partial\Omega} \big(u\partial_n w - w\partial_n u\big)\, ds\, dt. \tag{2.25}$$

Therefore we shall define the *Betti reciprocity gap* $\mathcal{RB}$ as:

$$\mathcal{R}(w;\psi,\varphi) = \int_0^\infty \int_{\partial\Omega} \big(\psi\partial_n w - w\varphi\big)\, ds\, dt. \tag{2.26}$$

For a series of problems it will be interesting to reduce the time interval from $[0,\infty)$ to $[0,t]$ and to monitor the evolution of the reciprocity gap with growing $t$. Therefore we define the *instantaneous reciprocity gap*:

$$\mathcal{R}(w;\psi,\varphi)[t] = \int_{\partial\Omega} \big(\psi\partial_n w - w\varphi\big)\, ds. \tag{2.27}$$

**Identification of a planar crack.** As in the previous section, in order to identify the crack we assume that its position and shape are completely revealed by $[\![u]\!]$. The crack is assumed to be planar, i.e. completely included in a plane and as such it will be identified in three distinct steps using for each one a special family of adjoint functions:

- *Orientation of the plane*
  Let us define the following family of adjoint functions:

$$w_{\boldsymbol{k}}(\boldsymbol{x},t) = \begin{cases} f(\boldsymbol{k}\cdot\boldsymbol{x} + t) & \text{if} \quad t \in [0,T]\,, \\ 0 & \text{if} \quad t \in [T,\infty]\,. \end{cases}$$

A straightforward calculation shows that:

$$\nabla w_{\boldsymbol{k}} = \begin{cases} f'(\boldsymbol{k}\cdot\boldsymbol{x}+t)\boldsymbol{k} & \text{if} \quad t\in[0,T]\,, \\ 0 & \text{if} \quad t\in[T,\infty]\,, \end{cases}$$

$$\partial_{\boldsymbol{n}} w_{\boldsymbol{k}} = \begin{cases} f'(\boldsymbol{k}\cdot\boldsymbol{x}+t)(\boldsymbol{k}\cdot\boldsymbol{n}) & \text{if} \quad t\in[0,T]\,, \\ 0 & \text{if} \quad t\in[T,\infty]\,. \end{cases}$$

Therefore $\boldsymbol{k}$ is a solution of

$$\mathcal{RB}(w_{\boldsymbol{k}};\psi,\varphi) = 0$$

only if $\boldsymbol{k}\cdot\boldsymbol{n} = 0$. The normal to the plane of the crack is then given by:

$$\boldsymbol{n} = \boldsymbol{k}_1 \wedge \boldsymbol{k}_2$$

with $\boldsymbol{k}_1, \boldsymbol{k}_2$ such that their corresponding reciprocity gap is zero.

- *Position of the plane*
  In order to determine the position of the plane, once its normal $\boldsymbol{n}$ is known, let us consider the following family of adjoint functions:

$$w_b(\boldsymbol{x},t) = \begin{cases} \frac{1}{2}(\boldsymbol{x}\cdot\boldsymbol{n}-b)^2 + \frac{1}{2}(t-T)^2 & \text{if} \quad t\in[0,T]\,, \\ 0 & \text{if} \quad t\in[T,\infty]\,. \end{cases}$$

  The normal derivative of the adjoint function on the plane of the crack is:

$$\partial_{\boldsymbol{n}} w_b(\boldsymbol{x},t) = (\boldsymbol{x}\cdot\boldsymbol{n}-b),$$

  and the reciprocity gap is then expressed by

$$\mathcal{RB}(w_b;\psi,\varphi) = -\int_0^\infty \int_F [\![u]\!](\boldsymbol{x}\cdot\boldsymbol{n}-b)\,ds\,dt.$$

  The position of the plane is given by $b$, the solution of:

$$\mathcal{RB}(w_b;\psi,\varphi) = 0.$$

- *Extension of the crack in the plane*
  In order to identify the extension of the crack in the plane, let us recall the expression of the reciprocity gap:

$$\int_0^\infty \int_F [\![u]\!]\,\partial_n w\,ds\,dt = \mathcal{R}(w;\psi,\varphi).$$

As in the preceding section, where the elliptic case has been solved, we have to identify a family of adjoint functions such that the corresponding family of normal derivatives $\partial_n w$ forms a functional basis in $L^2$. More precisely, the technique developed by Bui et al. in [5] yields actually the planar Fourier transform of $[\![u]\!]$. Without proving their result, let us just remark that in order to find the solution they used a perturbed problem with a small viscosity term:

$$\partial_t \partial_t u - \Delta u + \varepsilon \partial_t u = 0,$$

and the family of adjoint fields had the following form:

$$w_{q\xi'}(\boldsymbol{x}, t) = \exp(iqt)\, \exp\big(-i(\boldsymbol{\xi}' \cdot \boldsymbol{x}')\big)\, \exp\big((|\boldsymbol{\xi}'|^2 - q^2 - i\varepsilon q)^{\frac{1}{2}} x_3\big),$$

where $\boldsymbol{\xi}' = (\xi_1, \xi_2) \in \mathbb{R}^2$ and $q \in \mathbb{R}$ and $\boldsymbol{x}' = (x_1, x_2) \in \mathbb{R}^2$.

### 2.2.3. Hyperbolic equation: elastodynamics

Next we will extend the Betti reciprocity gap to elastodynamics. In this case we present only some numerical results where the complete position and shape of a planar crack were identified using *only one* family of adjoint waves, see also [6]. Only planar waves are used as adjoint fields but different interpretations of the reciprocity enable us to reconstruct the crack.

Let us consider a homogenous elastic body $\Omega$ containing a crack $\Gamma_C$ in its interior (see Fig. 2.5). We assume that the crack $\Gamma_C$ is included in a plane $\Pi$. The exterior boundary of $\Omega$ will be denoted by $\partial\Gamma$.

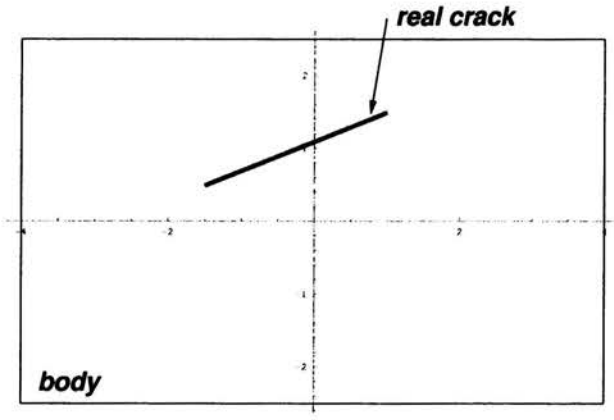


FIGURE 2.5. The geometry of the body and the position of the "real" crack.

For each $t \in [0,\infty)$ we consider that the vector field of displacement $\boldsymbol{u}$ and the tensor fields of strains and stresses $\boldsymbol{\epsilon}$, $\boldsymbol{\sigma}$, respectively, satisfy the following system of equations:

$$\operatorname{div}\boldsymbol{\sigma} = \rho\ddot{\boldsymbol{u}}, \qquad \boldsymbol{\sigma} = \boldsymbol{C}\boldsymbol{\varepsilon}, \qquad \boldsymbol{\varepsilon} = \frac{1}{2}(\nabla + \nabla^{\mathrm{T}})\boldsymbol{u}. \tag{2.28}$$

Hence we get:

$$\operatorname{div}\boldsymbol{C}\nabla\boldsymbol{u} = \rho\ddot{\boldsymbol{u}}, \tag{2.29}$$

where $\boldsymbol{C}$ denotes the fourth order tensor of elastic moduli.

We assume that both displacements and tractions are known on the exterior boundary $\partial\Omega$ for each $t \in [0,\infty)$:

$$\boldsymbol{u}|_{\partial\Omega} = \boldsymbol{\xi}, \qquad \boldsymbol{\sigma}\cdot\boldsymbol{n}|_{\partial\Omega} = \boldsymbol{\phi}. \tag{2.30}$$

In most practical case a free surface is considered $\boldsymbol{\phi} = \boldsymbol{0}$. The displacements $\boldsymbol{\xi}$ are then measured in a finite numbers of locations. The two faces of the crack are stress free:

$$\boldsymbol{\sigma}\cdot\boldsymbol{n}|_{\Gamma_C} = 0. \tag{2.31}$$

The variational principle associated with the equation (2.29) permits after a series of integrations by parts and application of the boundary condition for the solution to define the *adjoint problem*:

$$\operatorname{div}\boldsymbol{C}\nabla\boldsymbol{v} = \rho\ddot{\boldsymbol{v}}. \tag{2.32}$$

The *Betti reciprocity gap* takes the form

$$\mathcal{RB} = \int_0^\infty \int_{\Gamma_C} [\![\boldsymbol{u}^t]\!]\cdot\boldsymbol{\tau}[\boldsymbol{w}]\,ds\,dt = \int_0^\infty \int_{\Gamma} \{\boldsymbol{u}\cdot\boldsymbol{\sigma}[\boldsymbol{w}]\cdot\boldsymbol{n} - \boldsymbol{w}\cdot\boldsymbol{\sigma}[\boldsymbol{u}]\cdot\boldsymbol{n}\}\,ds\,dt + \int_{\Omega\setminus\Gamma_C} [\boldsymbol{u}\cdot\partial_t\boldsymbol{w} - \partial_t\boldsymbol{u}\cdot\boldsymbol{w}]_0^\infty\,dv. \tag{2.33}$$

In the definition of the reciprocity gap, $\boldsymbol{u}$ is a solution of the direct problem and $\boldsymbol{w}$ a solution of the adjoint problem.

The *instantaneous reciprocity gap* will be simply defined by the following expression:

$$\mathcal{RB}(t) = \int_{\Gamma_C} \{[\![\boldsymbol{u}^t]\!]\cdot\boldsymbol{\tau}[\boldsymbol{w}]\}\,ds = \int_{\Gamma} \{\boldsymbol{u}\cdot\boldsymbol{\sigma}[\boldsymbol{w}]\cdot\boldsymbol{n} - \boldsymbol{w}\cdot\boldsymbol{\sigma}[\boldsymbol{u}]\cdot\boldsymbol{n}\}\,ds. \tag{2.34}$$

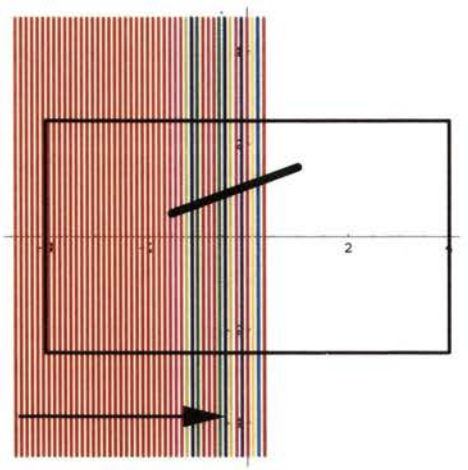


FIGURE 2.6. The evolution of the *instantaneous reciprocity gap* with the advancing adjoint wavefront (red corresponds to a zero value).

The instantaneous reciprocity gap measures the instantaneous virtual work done on the crack tips by the real displacements on the adjoint traction field. Its importance in the identification process will be illustrated by numerical example.

The example considered here corresponds to the body presented in Fig. 2.5. The numerical computations were done in two steps. In the first step we simulated the direct wave propagation problem and obtained a set of "artificial" displacement measurements. In the second step, these measurements were convoluted with a series of adjoint fields and the results were interpreted in order to identify the crack.

The direct computations and part of the identification procedure were programmed using the `Cast3M` finite element programming language. The complete mesh had 800 nodes and 1500 linear triangular elements. The crack faces were represented by 10 linear elements. A second order algorithm was used for the numerical integration of the direct wave propagation problem.

In the case of the direct problem a tangential shear vector was applied to the crack faces, next completely released after the initial moment $t = 0$, i.e.:

$$\boldsymbol{\tau}(t) = c\,\delta(t)\boldsymbol{t}, \tag{2.35}$$

where $\alpha$, $c$ are constants. All exterior surfaces are considered as stress free.

The boundary displacement has been collected in the direct problem and considered in the identification part as a measurement.

We notice that this loading opened the crack and no interpenetration of the material was observed during the considered time interval. As a consequence the real contact conditions on the crack tips, which would conduct to a nonlinear problem, can be neglected for this loading.

From a practical point of view this loading type describes an earthquake, but this case will not be discussed here.

The adjoint wave fields were constructed as 36 planar share wave fields. All directions of propagation of the wave fields were passing through the center of the body and where equally, spaced every $2\pi/36$ degrees.

Moreover, the initial time for the adjoined waves was chosen such that all reach the center of the body at the same instant.

$$\boldsymbol{w}(\boldsymbol{x},t) = \boldsymbol{k}Y(t - \frac{1}{c}\,\boldsymbol{x}\cdot\boldsymbol{p} - \tau)\,\boldsymbol{k}. \tag{2.36}$$

Here $\boldsymbol{x}$ and $t$ denote the space point and time instant when the displacement $\boldsymbol{w}$ is computed, while $\boldsymbol{p}$ and $\boldsymbol{k}$ are the direction of propagation of the wave and the direction of shear, respectively, and are for each wave orthogonal, i.e.: $\boldsymbol{p}\cdot\boldsymbol{k} = 0$; $\tau$ is the time parameter chosen such that the shear wave is outside the body at the initial instant $t = 0$, whereas $c$ denotes the velocity of the propagation of the shear waves and equals:

$$c = \sqrt{\frac{E}{\rho(1+\nu)}}$$

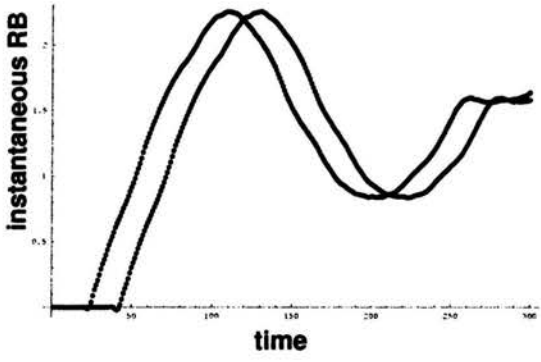


FIGURE 2.7. Time evolution of the reciprocity gap computed using two adjoint fields in opposite directions.

for an isotropic elastic body with Young modulus $E$, Poisson coefficient $\nu$ and a mass density $\rho$.

The stress state corresponding to the adjoined wave is a travelling Dirac impulse. It does therefore not produce any mechanical work with the displacement jump $[u]$ on the crack unless the adjoined wave field has "arrived" at the crack $\Gamma$ at time $t_p$. Therefore is instantaneous reciprocity gap vanishes for $t < t_p$ and has a non zero value after this instant (see Fig. 2.7).

Next using the previous observation on the interpretation of the instantaneous reciprocity gap and the fact that the waves are plane, certain characteristics of the crack can be identified:

- *Normal of the crack*
  From a simple geometric reasoning one can deduce that the adjoint wave having its wave front parallel to the crack tips will interact with the crack at a later instant when compared with the wave coming from the same half space with respect to the crack. Representing these time instants with respect to the angle of the incoming adjoint field defines by its two maxima the normal of the crack.
- *Position of the crack plane*
  Assuming that the normal of the plane is known, let us analyse the instantaneous reciprocity gap obtained from the adjoint waves propagating in the direction of the normal and denote $t_f$, $t_b$ the moments when the adjoint waves begin their interaction with the crack. If $R$ represents the distance from the starting point of the adjoint waves to

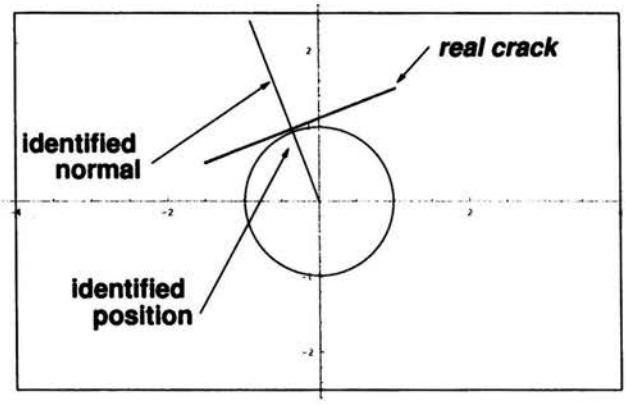


FIGURE 2.8. The real crack and its identified normal and position given by the intersection of the normal with the circle.

center of the body, we have:

$$v(t_f + t_b) = 2R,$$

where $v$ is the propagation speed of the wave. Then the distance of the crack to the center of the body is given by either:

$$d = R - t_f v \quad \text{or} \quad d = R + t_b v.$$

The results of this analysis are represented in Fig. 2.8 and compared with the initial position of the crack.

**Analysis of the numerical results.** Another way to analyse the results of the instantaneous reciprocity gap is the following one. On the rays, characterizing the direction of propagation of the adjoint waves, we represent at each time instant, in the real position of the wave front, the value of the instantaneous reciprocity gap by a color code. If the zero value is plotted in red, the colored domain, representing the start of non zero values, displays together with the wavefronts a convex hull of the crack. This representation is compared in Fig. 2.9 with the position of the real crack. Small errors at the end of the crack have the length order of one element and are justified by the fact that the crack tips do not open too much during the loading. As

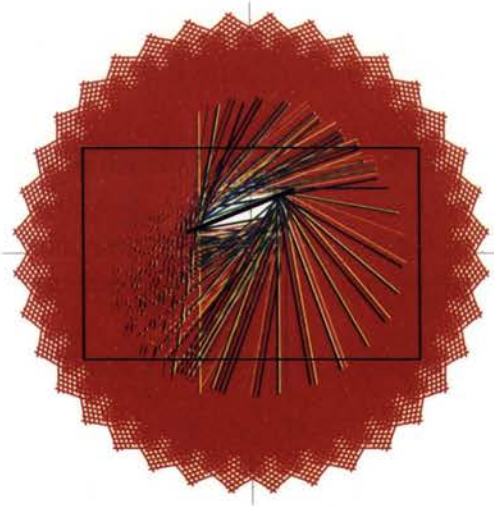

FIGURE 2.9. The real crack and the convex hull of null reciprocity obtained from the incoming adjoint waves with different directions.

such the virtual work measured by the reciprocity is nonzero only after an penetration of the adjoint wave of more than one element of the crack.

Note that both techniques give a very good match of the identified position and extension of the crack with the real crack.

## 2.3. Notes

**Other reciprocity results.** The reciprocity gap was also applied to crack identification in other problems which were not discussed here. Let us mention the following two domains:

- **Elastostatics**
  Ben Abda et al. [4] obtained a series of mathematical results for the idetification of a two-dimensional (2D) crack in an elastic body by means of static displacement and traction boundary measurements. These authors proved a uniqueness result in the general case, as well as the local Lipschitzian stability in the case of line segment emergent cracks. In last case, the search for the unique zero of the reciprocity gap functional related to the singular solution of the elasticity problem provides a fast algorithm to determine the unknown crack tip.
- **Heat equation**
  In the framework of the transient heat equation, A. Ben Adba and H. D. Bui [7] obtained a series of three families of adjoint solutions of the heat equation which permit to solve the crack identification problem.

**Other techniques for crack identification.** Before commenting a series of complementary techniques used in crack identification, let us just note that Bryan and Vogelius [8] provided a very interesting identifiability result, showing that $n + 1$ boundary measurements are sufficient to identify $n$ cracks in a body.

An overview of some practical methods for non-destructive crack evaluation are given in [9].

- **Scattering**
  Classical mathematical studies in the literature [10] within dynamics are subject to various limitations: unbounded domain, domain with known Green function, source in the interior of the body, source far away from the crack in order to consider plane waves, etc. In all these

investigations, a diffracted wave in an unbounded medium is examined to obtain the information on the crack. For recent results on the subject the reader is referred to [11] and references therein.

- **Complex functions**
  A series of crack identification techniques in the case of an electrostatic problem use the special representation formulas of the harmonic functions in the framework of complex analysis.
  Ban Abda et al. [12] dealt with non-destructive recovery of planar crack in a plane problem using approximation techniques in classes of analytic and mesomorphic functions. The localization algorithms are based on boundary computations of the reciprocity gap within this functional space.
  Elcrat et al. [13, 14] interpret the crack reconstruction problem as a parameter problem around the classical Schwarz–Christoffel formula.
- **Optimal control**
  After assuming that the crack at epicenter of an earthquake can be modeled as a time dependent concentrated force, Graselli and Yamamoto [15] provided an interesting optimal control formulation of the identification problem and showed that the identification problem has a solution.
- **Experiments**
  A recent paper by Lazarovitch et al. [16] presents a series of experiments performed on a network of resistors and a continuous medium containing one or two flaws. The identification method is based on the **minimization of least squares cost functional** and a gradient computed through direct differentiation. The results are interesting as they show that the method have a change to be applied in real engineering situation.

**Variational method for the identification of elastic moduli.** It is important to cite at this point a technique which is based only on the variational formulation (weak integral equation) of the elasticity equations in order to identify the values of elastic moduli. The technique was proposed by Grediac and Vautrin in early 1990 [17, 18, 19] and has been applied since then in a series of configurations (see for example [20]). On the one hand these authors performed measurements of surface distributions of displacements and strain by optical techniques and, on the other hand, they well chose

solutions of the elastic problem as test functions in the weak formulation in order to obtain a well-posed over-determined system of linear equations for the moduli.

## 2.4. References


1. S. ANDRIEUX and A. BEN ABDA, Identifications of planar cracks by complete over-determined data: inversion formulae, *Inverse Problems*, 12(3):553–563, 1996.
2. T. BANNOUR, A. BEN ABDA, and M. JAOUA, A semi-explicit algorithm for the reconstruction of 3d planar cracks, *Inverse Problems*, 13(4):899–917, 1997.
3. S. ANDRIEUX, A. BEN ABDA, and H. DUONG BUI, Reciprocity principle and crack identification, *Inverse Problems*, 15(1):59–65, 1999.
4. A. BEN ABDA, H. BEN AMEUR, and M. JAOUA, Identification of 2d cracks by elastic boundary measurements, *Inverse Problems*, 15(1):67–77, 1999.
5. H.D. BUI, A. CONSTANTINESCU, and H. MAIGRE, Diffraction acoustique inverse de fissure plane : solution explicite pour un solide borné, *C.R. Acad. Sci. Paris, série II*, 327:971–976, 1999.
6. H.D. BUI, A. CONSTANTINESCU, and H. MAIGRE, Numerical identification of planar cracks in elastodynamics using on the reciprocity gap, In INRIA, editor, *PICOF'02, Proceedings of the 2nd Conference on Inverse Problems Control and Shape Optimization*, pp.55–60, 2002.
7. A. BEN ABDA, and H.D. BUI, Reciprocity principle and crack identification in transient thermal problems, *J.Inverse Ill-Posed Problems*, 9(1):1–7, 2001.
8. K. BRYAN and M. VOGELIUS, A uniqueness result concerning the identification of a collection of cracks from finitely many electrostatic boundary measurments, *SIAM.J.Appl.Math*, 23(4):940–958, 1992.
9. R.S. ANDERSSEN Electromagnetic nondestructive evaluation (iii), *Inverse Problems*, 16(4):1081–1082, 2000.
10. D. COLTON and R. KRESS, *Inverse acoustic and electromagnetic scattering theory*, Springer Verlag, 1992.
11. C.J.S. ALVES AND T. HA-DUONG, Inverse scattering for elastic plane cracks, *Inverse Problems*, 15(1):91–97, 1999.
12. A. BEN ABDA, M. KALLEL, J. LEBLOND, and J.-P. MARMORAT, Line segment crack recovery from incomplete boundary data, *Inverse Problems*, 18(4):1057–1077, 2002.

13. A.R. ELCRAT, V. ISAKOV, and O. NECULOIU, On finding a surface crack from boundary measurements, *Inverse Problems*, 11(2):343–351, 1995.

14. B. BUNCK, A. ELCRAT, and T. HRYCAK, On detecting emerging surface cracks from boundary measurements, *Inverse Problems*, 17(5):1391–1400, 2001.

15. M. GRASSELLI and M. YAMAMOTO, Identifying a spatial body force in linear ealstodynamics via traction measurements, *SIAM J. Control Optim.*, 36(4):1190–1206, jul. 1998.

16. R. LAZAROVITCH, D. RITTEL, and I. BUCHER, Experimental crack identification using electrical impedance tomography, *NDT&E International*, 35:301–316, 2002.

17. M. GRÉDIAC and A. VAUTRIN, Mechanical characterization of anisotropic plates: experiments and results, *Eur.J. Mechanics A*, 12(6):819–838, 1993.

18. M. GRÉDIAC, On the direct determination of invariant parameters governing anisotropic plate bending problems, *Int.J. Solids Structures*, 1996.

19. M. GRÉDIAC and A. VAUTRIN, A new method for the determination of bending rigidities of thin anisotropic plates, *ASME J. Appl. Mech.*, 33(27):3969–3982, 1996.

20. F. PIERRON and M. GRÉDIAC, Identification of the through-thickness moduli of thick composites from whole-field measurements using the iosipescu fixture, *Composites Part A: Applied Science and Manufacturing*, 31(4):309–318, 2000.

# Chapter 3

# Identification of distributed fields

In this Chapter we shall not present applications of specific technique used for solving a series of inverse problems, but shall explore a series of problems related to one type of inverse problems, namely the *identification of distributed fields* from over-determined boundary conditions.

From a practical point of view problems of this type arise in practical applications like:

- the identification of stiff and soft areas in human body by palpation, the method doctors used from the antiquity to investigate patients;
- the identification of ground permeability from pressure and flow measurements in wells of interest for water management, oil recovery or tracing contaminants;
- medical electric tomographies, in order to identify pulmonary emboli, blood cloth in lungs, breast cancer, tracing of blood flow, understood as the identification of electric conductivities from boundary voltages and fluxes;
- identification of epilepsy disorder centers in brains, as an identification of electric sources from boundary measurements;
- identification of residual stresses.

## 3.1. Electricity

The identification problem of distributed electric conductivity can be formalized in the following mathematical structure.

Let us consider a body $\Omega$ with boundary $\partial\Omega$. The scalar field of the electric potential (voltage) $u$ is a solution of the following elliptic system of PDE's:

$$\operatorname{div}\left(\gamma(\boldsymbol{x})\operatorname{grad} u(\boldsymbol{x})\right) = 0, \quad \boldsymbol{x} \in \Omega, \tag{3.1}$$

where $\gamma(\boldsymbol{x})$ is the electric conductivity. We remark that $\gamma$ is considered a scalar field and corresponds as such to an isotropic conductor. In the case of anisotropy $\gamma$ would become a second-order tensor field.

The classical boundary conditions are:

- the Dirichlet boundary condition (i.e. given potential): $u|_{\partial\Omega} = \xi$,
- the Neumann boundary condition (i.e. given flux): $\gamma\partial_{\boldsymbol{n}} u|_{\partial\Omega} = \varphi$.

In the *direct* problem, one wants to recover the potential field $u$ from the given Dirichlet or Neumann boundary data, supposing that the field of the electric conductivity is known in advance. We shall just recall that this problem has a unique solution with Dirichlet boundary conditions and a unique solution up to a constant for Neumann boundary conditions.

The aim of the *inverse* problem is to recover the unknown field of electric conductivity $\gamma$ from pairs of over-specified boundary conditions $(\xi, \varphi)$. The data pair represents the results of an experiment where one would impose the voltage $\xi$ on the boundary and would measure the corresponding flux $\varphi$.

**The Dirichlet-to-Neumann data map.** If we disposed of *all* imaginable experiments, we would dispose of the *Dirichlet-to-Neumann data map*:

$$\Lambda_\gamma : \xi \longrightarrow \Lambda_\gamma(\xi) = \varphi \tag{3.2}$$

mapping each boundary voltage $\xi$ in the corresponding boundary flux $\varphi$ for the body with conductivity $\gamma$.

Using this definition, we can state the *inverse* problem as the identification of the conductivity $\gamma$ from the Dirichlet-to-Neumann data map $\Lambda_\gamma$.

**Important questions.** In analysing this inverse problem we must actually answer a series of questions like:

- what is the form of $\Lambda_\gamma$?

- is $\Lambda_\gamma \longrightarrow \gamma$ injective? (uniqueness)
- is $\Lambda_\gamma \longrightarrow \gamma$ continuous? (stability)
- effective reconstruction algorithms?
- ... can one define best measurements?

### 3.1.1. The difficulty with distributed coefficients

The difficulty of identifying distributed coefficients can be illustrated through some simple one-dimensional examples.

Let us consider the one-dimensional version of Eq. (3.2) on the interval $[0, \pi]$:

$$\partial_x(\gamma \partial_x u) = 0. \tag{3.3}$$

The measured boundary data (corresponding to the $\Lambda_\gamma$ map) are given by the two pairs of real numbers:

$$(u(0), \partial_x u(0)) \quad \text{and} \quad (u(\pi), \partial_x u(\pi)). \tag{3.4}$$

A simple integration of the equations gives the balance of fluxes as the following series of equalities:

$$\gamma(0)\partial_x u(0) = \gamma(x)\partial_x u(x) = \gamma(\pi)\partial_x u(\pi), \quad x \in [0, \pi]. \tag{3.5}$$

Intuitively one can understand that the measured boundary data carry just a small amount of information, and as such we would probably have difficulties in reconstructing the distribution of $\gamma(x)$ from the values at the end of the interval.

Let us consider a slightly modified equation:

$$\partial_x(\gamma \partial_x u) = 1 \tag{3.6}$$

corresponding to the heat equation with a constant source term. Suppose now that the real, measured data, correspond to the following solution:

$$\gamma(x) = \frac{1}{2}, \qquad u(x) = x^2. \tag{3.7}$$

We can construct the following series of perturbed solutions:

$$\gamma_N(x) = \frac{1}{2 + \cos Nx}, \qquad u_N(x) = x^2 + \frac{x}{N}\sin Nx + \frac{1}{N^2}\cos Nx, \tag{3.8}$$

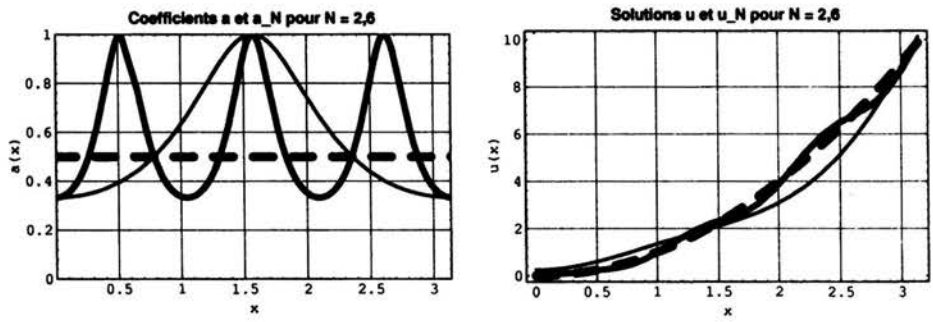


FIGURE 3.1. Variations of the conductivity coefficient $\gamma$ (left) and of the potential $u$ (right).

which have the property that the boundary data, as well as the potential $u$, can be brought as close as desired to the real solution, provided that the conductivity begins to oscillate with a constant amplitude (see Fig. 3.1).

W note that in the one-dimensional example we have actually tried to identify a real function from the knowledge of its boundary values which are actually just a pair of real numbers. In higher dimensions the information gets richer as we shall try to identify a function from boundary data which are also functions.

**Exercise:** *[1] Consider the following system:*

$$\partial_x(\gamma\partial_x u) = f(x), \quad -k(0)u'(0) = A, \quad k(1)u'(1) = B.$$

*Show that a differentiable function $k$ exists only if:*

$$\int_0^1 f(x)dx = A - B.$$

*Interpret this result in term of balance!*

**Exercise:** *[1] Show that $u(x) = x$ and $k(x) = x$ are solutions of the equation:*

$$\partial_x(\gamma\partial_x u) = 1, \quad x \in [0,1].$$

*Then show that for $\eta > 0$ the following functions are also solutions:*

$$k_\eta(x) = \frac{\eta x}{\eta + \cos(x/\eta^2)} \quad \text{and} \quad u_\eta(x) = \eta\sin(x/\eta^2) + x.$$

*What can be stated about the following limits:*

$$\lim_{\eta \to \eta} k_\eta(x) \quad \lim_{\eta \to \eta} u_\eta(x) \quad \forall x.$$

### 3.1.2. Variational formulations

In this Section we shall recall the technique presented in the preceding Chapter and apply it to the identification of distributed coefficients.

**The Dirichlet-to-Neumann data map and the energy functional.** In order to characterize the physical interpretation of the Dirichlet-to-Neumann data map we show it is a directly related with the "electric work" of fluxes and potential on the boundary $\partial\Omega$, which depends also essentially on the function $\gamma$:

$$\Lambda_\gamma \quad \longleftrightarrow \quad W_\gamma(u) = \int_{\partial\Gamma} u\Lambda_\gamma(u)\, ds. \tag{3.9}$$

Let us introduce the energy function, defined for each $\gamma$:

$$\gamma \longrightarrow Q_\gamma \tag{3.10}$$

as a map on the voltage functions:

$$Q_\gamma(u) = \frac{1}{2}\int_\Omega \nabla u\, \gamma\, \nabla u\, dv. \tag{3.11}$$

The next exercises permit to show that the knowledge of the Dirichlet-to-Neumann data map $\Lambda_\gamma$ is equivalent to the knowledge of the energy function $Q_\gamma$. This reflects the well-known physical relations between work and energy in linear materials.

**Exercise:** *Polarization $Q_\gamma \longrightarrow \Lambda_\gamma$. Show that*

$$4\int_{\partial\Omega} v\Lambda_\gamma(u)ds = Q_\gamma(u+v) - Q_\gamma(u-v).$$

**Exercise:** *Clapeyron Energy Theorem $\Lambda_\gamma \longrightarrow Q_\gamma$. Show that*

$$Q_\gamma(u) = \frac{1}{2}\int_{\partial\Omega} u\Lambda_\gamma(u)ds.$$

The foregoing relations hold even if we pass to anisotropic conductivities, that means that the scalar conductivity field $\gamma$ becomes a symmetric second-order tensor field $\boldsymbol{\gamma}$. In this case Kohn and Vogelius [2] showned that we can construct two conductivity matrices $\boldsymbol{\gamma}$, $\boldsymbol{\kappa}$ related through a diffeomorphism $\boldsymbol{\psi}$ such that the two bodies have the same Dirichlet-to-Neumann data map:

$$\Lambda_{\boldsymbol{\gamma}} = \Lambda_{\boldsymbol{\kappa}}. \tag{3.12}$$

**Exercise:** *Find the relation between the two conductivities using the equality of the two energies $Q_{\boldsymbol{\gamma}} = Q_{\boldsymbol{\kappa}}$ and the fact that the solution should be related through*

$$u_{\boldsymbol{\gamma}} = v_{\boldsymbol{\kappa}} \circ \boldsymbol{\psi}.$$

*Hint: Use the formula for change of variables.*

**The Betti reciprocity gap $\mathcal{RB}$.** Let us apply the Betti reciprocity relations, as presented in the last Chapter, to two problems:

- $u$ solution of $\operatorname{div}(\gamma \nabla u) = 0$ in $\Omega$,
- $w$ solution of $\operatorname{div}(\kappa \nabla w) = 0$ in $\Omega$.

In this case we obtain:

$$\int_{\partial\Omega} [u\Lambda_{\kappa}(w) - w\Lambda_{\gamma}\nabla(u)]\, ds = \int_{\Omega} \nabla u(\kappa - \gamma)\nabla w\, dv. \tag{3.13}$$

If $\kappa$ is only a perturbation of $\gamma$ (see Fig. 3.2), i.e.,

$$\kappa = \gamma + \delta\gamma \tag{3.14}$$

the last relation becomes:

$$\mathcal{RB}(\delta\gamma; u, w) = \int_{\partial\Omega} [u\Lambda_{\gamma+\delta\gamma}(w) - w\Lambda_{\gamma}(u)]\, ds = \int_{\Omega} \nabla u(\delta\gamma)\nabla w\, dv. \tag{3.15}$$

**Exercise:** *Prove the two preceding relations using the Stokes formulas.*

With the preceding notations, assuming the following linearisation hypothesis with $\eta$ as a small parameter:

- $\gamma = \gamma_0 + \eta\gamma_1 + \wr(\eta^2)$,
- $u = u_0 + \eta u_1 + \wr(\eta^2)$,
- $w = w_0$,

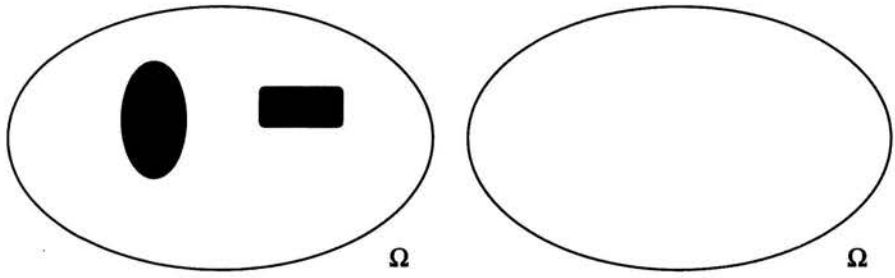


FIGURE 3.2. Body with perturbed (left) and unperturbed (right) conductivity.

we obtain the following linearized reciprocity gap:

$$\mathcal{RB}(\Lambda_{\gamma_0}; u_0, w_0) = \int_{\partial\Omega} [\Lambda_{\gamma_0}(u_0)w_0 - \Lambda_{\gamma_0}(w_0)u_0]\, ds = \int_{\Omega} \nabla u_0\, (\eta\gamma_1)\, \nabla w_0\, dv. \quad (3.16)$$

**Exercise:** *Find the preceding reciprocity relations directly by using polarization and series expansions of* $Q_\gamma$, $\Lambda_\gamma$.

**Calderon's uniqueness theorem.** Calderon [3] was the first to propose the foregoing linearization of the reciprocity relation. Moreover he proposed a choice of the unperturbed field $u_0$ and the adjoint field $w_0$ showing that $\gamma_1$ can be identified from this relation. He chose the harmonic functions:

$$u_0 = \exp(-i\boldsymbol{\zeta}\cdot\boldsymbol{x}), \qquad w_0 = \exp(-i\bar{\boldsymbol{\zeta}}\cdot\boldsymbol{x}), \quad (3.17)$$

where:

$$\boldsymbol{\zeta} = \frac{1}{2}(\boldsymbol{m} + i\boldsymbol{m}^{\perp}), \qquad \bar{\boldsymbol{\zeta}} = \frac{1}{2}(\boldsymbol{m} - i\boldsymbol{m}^{\perp}),$$
$$|\boldsymbol{m}| = |\boldsymbol{m}^{\perp}|, \qquad \boldsymbol{m}\cdot\boldsymbol{m}^{\perp} = 0.$$

This choice transforms Eq. (3.16) into:

$$\int_{\Omega} (\eta\gamma_1)\, \exp(-i\boldsymbol{m}\cdot\boldsymbol{x})\, dv = \mathcal{RB}(u_0, w_0, \Lambda_\gamma), \quad (3.18)$$

showing that the spatial Fourier transform of the conductivity perturbation $(\eta\gamma_1)$ is completely determined by the Dirichlet-to-Neumann data map.

In the last decade this method was exploited by many authors [4, 5, 2, 6, 7] to obtain various properties in the identification procedure.

### 3.1.3. The error on constitutive law

Up to now, we discussed various techniques stemming from the variational form of the equations of the problem using a series of privileged solutions to be used as test functions. These considerations apply to the reciprocity principles but also to the technique developed by Calderon.

At this point let us pass to another class of techniques, in which the problem is reformulated as a minimization problem for a well chosen cost functional. Without getting into the details we can already state that it is generally a constrained minimization problem and that a series of questions and answers for this general form problem statement will be discussed in the next two Chapters.

In this framework the identification problem of an inhomogeneous conductivity can be stated in the following form:

*Find $\gamma$ minimizing $ECL(\epsilon, \sigma, \gamma)$ under the constraints $\epsilon \in KA(\xi)$ and $\sigma \in SA(\varphi)$, where the error on the constitutive law is defined by*

$$ECL(\epsilon, \sigma, C) = \int_{\Omega} \left(\sigma\gamma^{-1}\sigma - 2\sigma\epsilon + \epsilon\gamma\epsilon\right) dv.$$

$\operatorname{div}\boldsymbol{\sigma} = 0 \quad \boldsymbol{\sigma}\cdot\boldsymbol{n}|_{\partial\Omega} = \varphi$

$\downarrow$

$\boldsymbol{\sigma}$ $\qquad\qquad$ $\boldsymbol{\sigma} = \gamma\nabla u$ $\qquad\qquad$ $\epsilon = \nabla u$

$\uparrow$

$u \quad u|_{\partial\Omega} = \xi$

*statically admissible* $\qquad$ *kinematically admissible*

$$\left|\frac{1}{\gamma^{\frac{1}{2}}}\sigma - \gamma^{\frac{1}{2}}\nabla u\right|^2$$

FIGURE 3.3. The Tonti diagram in electrostatics [9].

In Fig. 3.3 we have plotted a scheme with the equations and boundary conditions forming the final electric conductivity problem. On the left hand side we have the equilibrium equations relating fluxes and on the right hand side we have the equations defining the potential.

From a historical point of view, this error functional was first defined by Wexler around 1985 to determine the permeability distribution of aquifers. Second, numerical applications in the electric case were discussed by Kohn and McKenney [8]. More theoretical results, like convexity of the error functional and existence and uniqueness of the minimum procedures were discussed in [2]. Similar error functionals were proposed for elasticity and other problems and will be discussed in the next Sections.

## 3.2. Elasticity

We shall explore the next identification problem of distribution of elastic coefficients using a similar framework as in the case of electric coefficients.

Let us consider an elastic body $\Omega$ with the boundary $\partial\Omega$ under the hypothesis of small strains and in the absence of initial stress field. The vector field of the displacements $\boldsymbol{u}$ is a solution of the following elliptic system of PDE's:

$$\operatorname{div} \boldsymbol{C}(\boldsymbol{x}) \nabla \boldsymbol{u} = 0, \quad \boldsymbol{x} \in \Omega, \tag{3.19}$$

with $\boldsymbol{C}$ the positive definite fourth-order tensor of elastic moduli. This tensor has the following symmetries in the Cartesian coordinate system:

$$C_{ijkl} = C_{klij} = C_{jikl} \tag{3.20}$$

which assure the existence of the energy potential functional and, respectively, the symmetry of the stress tensor.

In the case of elastic identification problem, we shall describe most of the properties of the general anisotropic $\boldsymbol{C}$; and specific cases, like isotrpy:

$$C_{ijkl} = \lambda \delta_{ij} \delta_{kl} + \mu(\delta_{ij}\delta_{kl} + \delta_{ik}\delta_{jl}), \tag{3.21}$$

will be mentioned, when needed. The classical boundary conditions are similar to the ones in electricity:

- the Dirichlet boundary condition, i.e. the displacements $\boldsymbol{u} = \boldsymbol{\xi}$ are prescribed on the boundary,

- the Neumann boundary condition, i.e. the boundary tractions $\sigma \cdot n = \varphi$ are prescribed on $\partial\Omega$.

Regarding contact boundary conditions, one can remark that they introduce a nonlinearity in the system and will therefore be discussed in the next Chapter.

In the *direct* problem, one wants to recover the displacement field $u$ from the given Dirichlet or Neumann boundary data, assuming that the tensor field of the elastic moduli $C$ is known in advance. Recall that this problem has a unique solution with the Dirichlet boundary condition and a unique solution up to a rigid displacement for the Neumann boundary condition.

As we already know, the *inverse* problem proposes to recover the unknown field of electric conductivity $C$ from pairs of over-specified boundary conditions $(\xi, \varphi)$. The data pair represents the results of an experiment where one would impose the displacement $\xi$ on the boundary and measure the corresponding boundary traction $\varphi$.

The general character of the elasticity problem is similar to the preceding electricity problem. However, the complexity is increased as we pass from scalar fields to tensor fields.

**The Dirichlet-to-Neumann data map.** Exactly as before we can imagine that we dispose of *all* imaginable experiments and define the *Dirichlet-to-Neumann data map*:

$$\Lambda_\gamma : \xi \longrightarrow \Lambda_C(\xi) = \varphi, \tag{3.22}$$

mapping each boundary displacement $\xi$ in the corresponding boundary traction $\varphi$ for the body with elasticity tensor $C$.

Using this definition, the *inverse* problem leads to the identification of $C$ from the Dirichlet-to-Neumann data map $\Lambda_C$.

Of course one would like to answer the same questions about $\Lambda_C$ as in the electric case.

### 3.2.1. The difficulty with distributed coefficients

In the electric case, we have shown that a non-uniqueness problem arises in a one-dimensional example when one tries to identify the conductivity from the Dirichlet-to-Neuman data map. Let us consider a similar example in elasticity: an elastic ball of radius $R$ under the conditions of radial symmetry

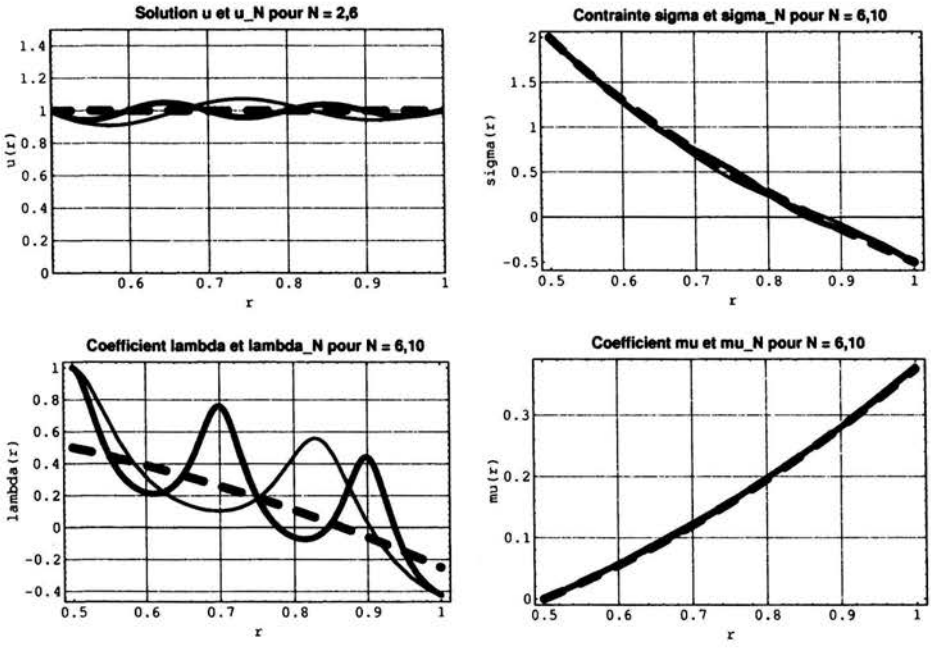


FIGURE 3.4. The perturbed and unperturbed distributions of the radial displacement (upper left), radial stress (upper right) and of the elastic moduli $\lambda$ (lower left) and respectively $\mu$ (lower right) in the case of an elastic ball.

(see Fig. 3.4). In this case, the equations of elasticity are reduced to:

$$\frac{\partial}{\partial r}\left(\frac{\lambda+2\mu}{r^2}\frac{\partial}{\partial r}(r^2 u_r)\right) - \frac{\mu'}{r}u_r = 0, \qquad r \in [0, R]. \tag{3.23}$$

On the one hand, we have the *unperturbed solution* corresponding to the radial displacement:

$$u_r(r) = 1 \tag{3.24}$$

and the elastic moduli:

$$\mu(r) = \mu_0 + r^2, \qquad \lambda(r) = \frac{1}{2} - 2\mu(r). \tag{3.25}$$

On the other hand we can construct a family of *perturbed solutions* ($N \in \mathbb{N}$) with radial displacements:

$$u_r^N(r) = 1 + \frac{1}{Nr}\sin Nr + \frac{1}{N^2 r^2}\cos Nr \tag{3.26}$$

and the elastic moduli:

$$\mu^N(r) = \mu_0 + \int_{r_1}^{r_2} \frac{r\,dr}{1 + \frac{1}{Nr}\sin Nr + \frac{1}{N^2r^2}\cos Nr},$$
$$\lambda^N(r) = \frac{1}{2 + \cos Nr} - 2\mu^N(r). \tag{3.27}$$

We note that similarly to the electric case there is no convergence of the perturbed moduli $\lambda_N$ toward $\lambda$ in spite of the convergence of the perturbed boundary displacements and stresses toward the unperturbed ones.

This actually shows that the uniqueness and stability problems can be encountered in solving inverse problems. More precisely, we can speak of a weak continuity, because small errors in the input data can lead to large errors in the final solution.

**Exercise:** *Prove the relations of this Section.*

### 3.2.2. Variational formulations

**The Dirichlet-to-Neumann data map and the energy functional.** Similar to the reasoning done in the electric case, one can directly relate the Dirichlet-to-Neumann data map to the mechanical work done on the surface of the body:

$$\Lambda_{\boldsymbol{C}} \quad \longleftrightarrow \quad W_{\boldsymbol{C}}(\boldsymbol{u},\boldsymbol{v}) = \int_{\partial\Omega} \boldsymbol{u}\cdot\Lambda_{\boldsymbol{C}}(\boldsymbol{v})\,ds. \tag{3.28}$$

We can also introduce the energy functional $Q_{\boldsymbol{C}}$ for each fourth-order tensor:

$$\boldsymbol{C} \quad \longrightarrow \quad Q_{\boldsymbol{C}} \tag{3.29}$$

as a functional defined on displacement fields:

$$Q_{\boldsymbol{C}} = \frac{1}{2}\int_{\Omega} \nabla\boldsymbol{u} : \boldsymbol{C} : \nabla\boldsymbol{v}. \tag{3.30}$$

**Exercise:** *Polarization* $Q_\gamma \longrightarrow \Lambda_\gamma$. *Show that*

$$4\int_{\partial\Omega} \boldsymbol{v}\cdot\Lambda_{\boldsymbol{C}}(\boldsymbol{v})\,ds = Q_\gamma(\boldsymbol{u}+\boldsymbol{v}) - Q_\gamma(\boldsymbol{u}-\boldsymbol{v}).$$

**Exercise:** *Clapeyron Energy Theorem* $\Lambda_\gamma \longrightarrow Q_\gamma$. *Show that*

$$Q_\gamma(u) = \frac{1}{2}\int_{\partial\Omega} \boldsymbol{u} \cdot \Lambda_{\boldsymbol{C}}(\boldsymbol{u})\, ds.$$

**Non-uniqueness in the anisotropic case.** In the foregoing relations between $\Lambda_{\boldsymbol{C}}$ and $Q_{\boldsymbol{C}}$ we have not used any information involving the material symmetries of $\boldsymbol{C}$, meaning that they hold for any entropy.

As in the electric case, where Kohn and Vogelius [2] showed that we can construct two conductivity matrices which will correspond to the same Dirichlet-to-Neumann data map, it was shown in [10] that one can construct two different fields of elastic moduli $\boldsymbol{L}$ and $\boldsymbol{C}$, equally related through a diffeomorphism $\boldsymbol{\psi}$, such that the two bodies have the same Dirichlet-to-Neumann data map:

$$\Lambda_{\boldsymbol{C}} = \Lambda_{\boldsymbol{L}}. \tag{3.31}$$

**Exercise:** *Find the relation between the two conductivities using the equality of the two energies* $Q_{\boldsymbol{C}} = Q_{\boldsymbol{L}}$ *and the fact that the solution should be related through*

$$\boldsymbol{u_\gamma} = v_{\boldsymbol{\kappa}} \circ \boldsymbol{\psi}.$$

*Hint: Use the formula for change of variables.*

However the complete discussion is more complicated here as both tensor $\boldsymbol{L}$ and $\boldsymbol{C}$ have to respect the symmetry relations (3.20).

**Betti reciprocity gap.** If one applies the Betti reciprocity relations for two different bodies occupying the same volume $\Omega$ and having two different fields of elastic moduli:

- $\boldsymbol{u}$ solution of $\operatorname{div} \boldsymbol{C}\nabla\boldsymbol{u} = 0$ in $\Omega$,
- $\boldsymbol{w}$ solution of $\operatorname{div} \boldsymbol{L}\nabla\boldsymbol{w} = 0$ in $\Omega$,

one obtains the following reciprocity gap:

$$\int_{\partial\Omega} [\boldsymbol{u} \cdot \Lambda_{\boldsymbol{C}}(\boldsymbol{w})\, ds - \boldsymbol{w} \cdot \Lambda_{\boldsymbol{L}}(\boldsymbol{u})]\, ds = \int_{\Omega} \nabla\boldsymbol{u} : (\boldsymbol{L} - \boldsymbol{C}) : \nabla\boldsymbol{w}\, dx. \tag{3.32}$$

If $\boldsymbol{L}$ differes from $\boldsymbol{C}$ by a small perturbation, i.e. $\boldsymbol{L} = \boldsymbol{C} + \delta\boldsymbol{C}$, we can write the reciprocity gap in the following form:

$$\mathcal{RB}(\delta\boldsymbol{C}; \boldsymbol{u}, \boldsymbol{w}) = \int_{\partial\Omega} [\boldsymbol{u}\, \Lambda_{\boldsymbol{C}+\delta\boldsymbol{C}}(\boldsymbol{w})\, ds - \boldsymbol{w}\, \Lambda_{\boldsymbol{C}}(\boldsymbol{u})]\, ds = \int_{\Omega} \nabla\boldsymbol{u} : \delta\boldsymbol{C} : \nabla\boldsymbol{v}_0\, dv. \quad (3.33)$$

With the preceding notations, assuming the following linearisation hypothesis with $\eta$ a small parameter:

- $\boldsymbol{C} = \boldsymbol{C}_0 + \eta\boldsymbol{C}_1 + \wr(\eta^2)$,
- $\boldsymbol{u} = \boldsymbol{u}_0 + \eta\boldsymbol{u}_1 + \wr(\eta^2)$,
- $\boldsymbol{w} = \boldsymbol{w}_0$,

one obtains the following linearized reciprocity relation:

$$\mathcal{RB}(\delta\boldsymbol{C}; \boldsymbol{u}_0, \boldsymbol{w}_0) = \int_{\partial\Omega} [\boldsymbol{u}_0\, \Lambda_{\boldsymbol{C}+\delta\boldsymbol{C}}(\boldsymbol{w}_0)\, ds - \boldsymbol{w}\, \Lambda_{\boldsymbol{C}}(\boldsymbol{u})]\, ds = \int_{\Omega} \nabla\boldsymbol{u}_0 : \eta\boldsymbol{C}_1 : \nabla\boldsymbol{w}_0\, dv. \quad (3.34)$$

**Exercise:** *Prove the preceding relation using Stokes formulas, directly by using polarization and series expansions of* $Q_{\boldsymbol{C}}$, $\Lambda_{\boldsymbol{C}}$.

**Exercise:** *Prove similar relations in the case of a elastodynamic problem:*

$$\operatorname{div} \boldsymbol{C}\nabla\boldsymbol{u} = \rho\ddot{\boldsymbol{u}}$$

*under the assumption that both* $\boldsymbol{C}$ *and* $\rho$ *can vary between the two bodies.*

**Ikehata's uniqueness theorem.** Ikehata [11] used the linearized reciprocity relation (3.34) for an isotropic elastic body. The elastic moduli are represented by $(\lambda + \delta\lambda, \mu + \delta\mu)$, the Lamé moduli.

The technique of the proof was the one given by Calderon [3] in electricity, i.e. constructing special solutions of the unperturbed equations, such that the first order term of the deformation energy of the body will provide a spatial Fourier transform of the perturbed moduli $(\delta\lambda, \delta\mu)$.

In order to introduce the fields proposed by Ikehata, let us introduce the following notations:

$$\begin{aligned} \zeta &= \frac{1}{2}(m + im^{\perp}), \qquad \bar{\zeta} = \frac{1}{2}(m - im^{\perp}), \\ \zeta_1 &= \frac{1}{2}(m + im^{\perp}), \qquad \zeta_2 = -\bar{\zeta}_1, \\ |m| &= |m^{\perp}|, \qquad m \cdot m^{\perp} = 0. \end{aligned} \tag{3.35}$$

The first family of test functions $(u_0, v_0)$ is then defined as:

$$u_i = \nabla\big(\exp(-x \cdot \zeta_i)\big), \quad i = 1, 2, \tag{3.36}$$

and the second family of test functions $(u_0, v_0)$ has the form:

$$u_{ij} = (\lambda_0 + 2\mu_0) \triangle g_{ij} - (\lambda_0 + \mu_0)\nabla(\div g_{ij}) \tag{3.37}$$

with $g_{ij}$ biharmonic:

$$g_{ij} = -\frac{1}{2}|\zeta_i|^{-2}(x \cdot \overline{\zeta_i}) \exp(-x \cdot \zeta_i)\zeta_j. \tag{3.38}$$

If $\xi_1 = u_1|_{\partial\Omega}$ and $\xi_2 = u_2|_{\partial\Omega}$ then the linearized reciprocity relations is written for the first family of test functions as:

$$\int_{\partial\Omega} \xi_1 \, d\Lambda_{(\lambda_0,\mu_0)}[(\delta\lambda, \delta\mu)](\xi_2) \, ds = \frac{|m|^4}{4} \int_{\Omega} 2\delta\mu \exp(-\sqrt{-1}x \cdot m) \, dx. \tag{3.39}$$

If $\xi_3 = u_{12}|_{\partial\Omega}$ and $\xi_4 = u_{21}|_{\partial\Omega}$ then the linearized reciprocity relations is written for the second family of test functions as:

$$\begin{aligned} &\int_{\partial\Omega} \xi_3 \, d\Lambda_{(\lambda_0,\mu_0)}[(\delta\lambda, \delta\mu)](\xi_4) \, ds \\ &\quad = \mu_0^2 \frac{|m|^4}{4} \int_{\Omega} 2\,\delta\lambda \ \exp(-\sqrt{-1}x \cdot m) \, dx \\ &\quad + \mu_0^2 \frac{|m|^4}{4} \int_{\Omega} 2\,\delta\mu \ \exp(-\sqrt{-1}x \cdot m) \, dx \\ &\quad + (\lambda_0 + \mu_0)^2 \frac{|m|^4}{8} \zeta_1^T \zeta_2 \int_{\Omega} 2x^T x \, \delta\lambda \ \exp(-\sqrt{-1}x \cdot m) \, dx. \end{aligned} \tag{3.40}$$

These relations prove that $\delta\mu$ $\delta\lambda$ are obtained as an inverse Fourier transform of the measured boundary values and as a consequence we conclude that the measured boundary values expressed as the Dirichlet-to-Neumann boundary data map determine uniquely the perturbation of the elastic moduli. A sketch of the passage to a more general uniqueness theorem is given in [9].

From a practical point of view, we note that the inverse Fourier transform is not appropriate for simple inversions as a series of numerical oscillation problems might be encountered on the boundary of the perturbation. We will therefore explore some other numerical techniques to compute unknown perturbation from boundary measurements.

### 3.2.3. The error on constitutive law

Let us discuss now a practical approach to the elastic inverse problem defined in an ideal case as:

> *Identify the distribution of elastic moduli $\boldsymbol{C}$ from the knowledge of the Dirichlet-to-Neumann data map.*

One of the convenient techniques for a numerical reconstruction algorithm is a minimization approach, which is based on two choices: one regarding the cost functional to be minimized and the second pertains to the descent algorithm.

In this Section, we shall explore an extension to elasticity of the *error on constitutive law* presented in the last Section for the electric case. We shall leave the discussion on more classical least square cost functionals as well as on the direct differentiation and the adjoint state method to the next Chapter. We shall start the discussion from a global point of view analysing the structure of the elasticity equations as presented by Tonti [9] (see Fig. 3.5). In this diagram, one can remark that on the left hand side we find the *statically admissible fields* ($SA$) defined by the given boundary traction $\boldsymbol{\varphi}$ and on the right hand side, the *kinematically admissible fields* ($KA$) defined by the boundary displacement $\boldsymbol{\xi}$. As such, only the constitutive relation:

$$\boldsymbol{\sigma} = \boldsymbol{C}\boldsymbol{\varepsilon} \tag{3.41}$$

relates the two sets. It seems therefore natural to define a distance on the constitutive relation and then to try to match using a field of elastic moduli $\boldsymbol{C}$ preserving the symmetry relations (3.20), a displacement field $\boldsymbol{u} \in KA(\boldsymbol{\xi})$ and a stress field $\boldsymbol{\sigma} \in SA(\boldsymbol{\varphi})$.

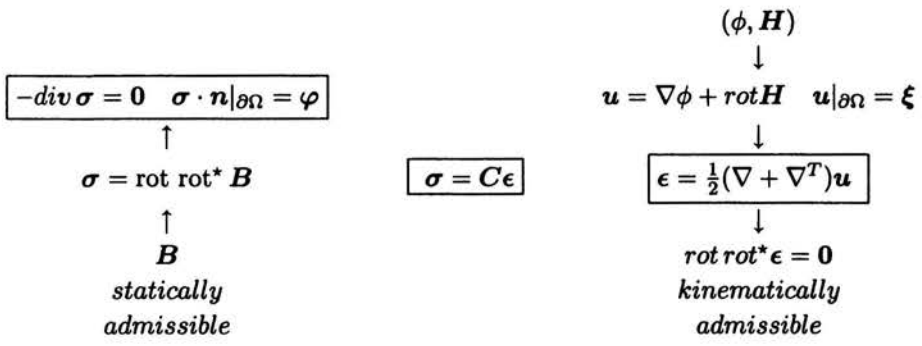


FIGURE 3.5. Tonti's diagram in elasticity [9].

The *error on constitutive law* is defined as:

$$ECL(\epsilon, \boldsymbol{\sigma}, \boldsymbol{C}) = \int_{\Omega} |\boldsymbol{C}^{-\frac{1}{2}}\boldsymbol{\sigma} - \boldsymbol{C}^{\frac{1}{2}}\epsilon|^2\, dv \tag{3.42}$$

which is also equivalent to:

$$ECL(\epsilon, \boldsymbol{\sigma}, \boldsymbol{C}) = \int_{\Omega} \left(\boldsymbol{\sigma} : \boldsymbol{C}^{-1} : \boldsymbol{\sigma} - 2\boldsymbol{\sigma}\epsilon + \epsilon : \boldsymbol{C} : \epsilon\right) dv. \tag{3.43}$$

In the last formula we note that the physical dimension of the $ECL$ is the energy, and that actually it is measures a distance between strain energy and stress energy taking into account the work of the boundary conditions.

This error functional can be first retrieved in the works of Ladevèze and Leguillon [12] as a measure of the error of finite element computations. The second time it has been used as a cost functional for identifying spatially distributed electric conductivities by Kohn et al. [2, 8] (see Sec. 3.1.3). Therefore the *Inverse Problem* can be stated as:

> *Find* $\boldsymbol{C}$ *minimizing* $ECL(\epsilon, \boldsymbol{\sigma}, \boldsymbol{C})$ *under the constrains* $\epsilon \in KA(\boldsymbol{\xi})$ *and* $\boldsymbol{\sigma} \in SA(\boldsymbol{\varphi})$.

The expression of the $ECL$ conducts straightforward to an alternating direction minimization algorithm, where at each iterations one minimizes the strain, respectively the stress energy, which are equivalent to $ELC$ in these directions and the updates of the elastic moduli by minimizing the $ELC$ with given strain and stresses. This will be discussed in the next Section.

**The algorithm.** In a practical case one can suppose that we dispose of a finite number of displacement-traction boundary data pairs: $(\boldsymbol{\xi}_i, \boldsymbol{\varphi}_i)_{i=1}^N$. For each data pair $(\boldsymbol{\xi}_i, \boldsymbol{\varphi}_i)$ we shall have a strain and a stress field $(\boldsymbol{\epsilon}_i, \boldsymbol{\sigma}_i)$ and as such we shall define the *ELC* for the all the measurements as:

$$ECL(\boldsymbol{\epsilon}_1, \ldots, \boldsymbol{\epsilon}_N, \boldsymbol{\sigma}_1, \ldots, \boldsymbol{\sigma}_N, \boldsymbol{C}) = \sum_{i=1}^{N} \int_{\Omega} |\boldsymbol{C}^{-\frac{1}{2}} \boldsymbol{\sigma}_i - \boldsymbol{C}^{\frac{1}{2}} \boldsymbol{\epsilon}_i|^2 \, dv. \tag{3.44}$$

An integration by parts yields the following expression:

$$\begin{aligned} &ECL(\boldsymbol{\epsilon}_1, \ldots, \boldsymbol{\epsilon}_N, \boldsymbol{\sigma}_1, \ldots, \boldsymbol{\sigma}_N, \boldsymbol{C}) \\ &\quad = \sum_{i=1}^{N} \int_{\Omega} \left( \boldsymbol{\sigma}_i : \boldsymbol{C}^{-1} : \boldsymbol{\sigma}_i - 2\boldsymbol{\sigma}_i \boldsymbol{\epsilon}_i + \boldsymbol{\epsilon}_i : \boldsymbol{C} : \boldsymbol{\epsilon}_i \right) dv \\ &\quad = \sum_{i=1}^{N} \int_{\Omega} \left( \boldsymbol{\sigma}_i : \boldsymbol{C}^{-1} : \boldsymbol{\sigma}_i + \boldsymbol{\epsilon}_i : \boldsymbol{C} : \boldsymbol{\epsilon}_i \right) dv - 2 \sum_{i=1}^{N} \int \boldsymbol{\xi}_i \cdot \boldsymbol{\varphi}_i \, ds. \end{aligned} \tag{3.45}$$

As $(\boldsymbol{\xi}_i, \boldsymbol{\varphi}_i)$ are known quantities, one can reduce the minimization of the *ELC* to the minimization of sum of strain and stress energies.

Each iteration of the algorithm consists of the following steps:

1. *with $\boldsymbol{C}$ fixed (as determined by the previous step) minimize the strain energies*, i.e. solve the $N$ Dirichlet problems (imposed displacements):

$$\begin{aligned} \operatorname{div}(\boldsymbol{C} \nabla \boldsymbol{u}_i) &= \boldsymbol{0} \quad \text{in} \quad \Omega, \\ \boldsymbol{u}_i|_{\partial\Omega} &= \boldsymbol{\xi}_i \quad \text{on} \quad \partial\Omega, \end{aligned} \tag{3.46}$$

2. *with $\boldsymbol{C}$ fixed (as determined by the previous step) minimize the stress energies*, i.e. solve the $N$ Neumann problems (imposed forces):

$$\begin{aligned} \operatorname{div}(\boldsymbol{C} \nabla \boldsymbol{u}_i) &= \boldsymbol{0} \quad \text{in} \quad \Omega, \\ \boldsymbol{C} \nabla \boldsymbol{u}_i|_{\partial\Omega} &= \boldsymbol{\varphi}_i \quad \text{on} \quad \partial\Omega, \end{aligned} \tag{3.47}$$

3. with $(\boldsymbol{\varepsilon}_i)_{i=1}^N$ determined by 1 and $(\boldsymbol{\sigma}_i)_{i=1}^N$ determined by 2, update $\boldsymbol{C}$, by minimizing:

$$G(\boldsymbol{C}) = ELC(\boldsymbol{C}, \boldsymbol{\varepsilon}_1, \ldots, \boldsymbol{\varepsilon}_N, \boldsymbol{\sigma}_1, \ldots, \boldsymbol{\sigma}_N). \tag{3.48}$$

The last step is simplified if one uses the spectral decomposition of the elasticity tensor $\boldsymbol{C}$. For detailed presentation of different classes of anisotropy,

see [13, 14, 15]. Let us simply remark that in the isotropic case, the eigenvalues are the bulk and the shear moduli:

$$K = \frac{3\lambda + 2\mu}{3}, \qquad G = 2\mu, \tag{3.49}$$

and they correspond to the spherical and deviatoric part of the strain and stress fields which play the role of eigenvectors:

$$\boldsymbol{\varepsilon} = \frac{1}{3} \operatorname{tr} \boldsymbol{\varepsilon} \mathbf{1} + \operatorname{dev} \boldsymbol{\varepsilon}, \tag{3.50}$$

$$\boldsymbol{\sigma} = \frac{1}{3} \operatorname{tr} \boldsymbol{\sigma} \mathbf{1} + \operatorname{dev} \boldsymbol{\sigma}. \tag{3.51}$$

The minimization of the $ELC$ with respect to $K$ and $G$ with fixed $(\boldsymbol{\varepsilon}_i, \boldsymbol{\sigma}_i)_{i=1}^N$ gives:

$$K(\boldsymbol{x})^2 = \frac{\sum_{i=1}^N (\operatorname{tr} \boldsymbol{\sigma}_i)^2}{\sum_{i=1}^N (\operatorname{tr} \boldsymbol{\varepsilon}_i)^2}, \qquad G(\boldsymbol{x})^2 = \frac{\sum_{i=1}^N \operatorname{dev} \boldsymbol{\sigma}_i \cdot \operatorname{dev} \boldsymbol{\sigma}_i}{\sum_{i=1}^N \operatorname{dev} \boldsymbol{\varepsilon}_i \cdot \operatorname{dev} \boldsymbol{\varepsilon}_i}. \tag{3.52}$$

This method has the advantage of decreasing the value of $I$ at every iteration, even if the convergence rate proves to be small as we approach to the minimum.

**Numerical results in 2D Elasticity.** In Figs. 3.6 and 3.7, we present (for a detailed description see [15]) the real and the reconstructed distribution of different elastic moduli obtained with the algorithm presented before. The

real | 2 iterations 10% noise | 14 iterations 0% noise

FIGURE 3.6. Copper corner inclusion in aluminum matrix, real distribution of the Poisson coefficient (left) and reconstruction with noise (middle) and without noise (right).

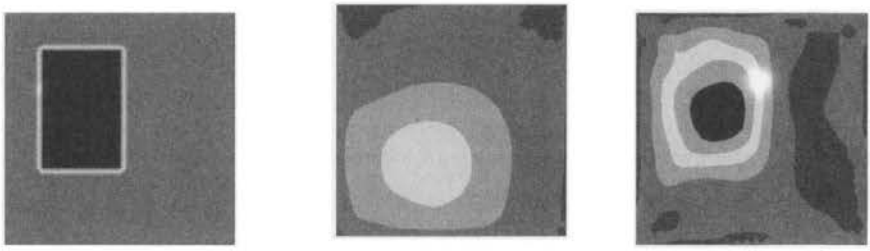

real | 5 iterations moments 0% noise | 32 iterations moments 0% noise

FIGURE 3.7. Copper corner inclusion in aluminum matrix, real distribution of the Young moduli (left) and reconstruction with noise (middle) and without noise (right).

considered material symmetry was cubic symmetry and the values of the moduli correspond to aluminum and copper.

$$E_{\mathrm{Al}} = 66 \cdot 10^9\,\mathrm{Pa}, \quad \nu_{\mathrm{Al}} = 0.32, \quad G_{\mathrm{Al}} = \frac{E_{\mathrm{Al}}}{2(1+\nu_{\mathrm{Al}})} = 25.10^9\,\mathrm{Pa},$$
$$E_{\mathrm{Cu}} = 66 \cdot 10^9\,\mathrm{Pa}, \quad \nu_{\mathrm{Cu}} = 0.42, \quad G_{\mathrm{Cu}} = 75.10^9\,\mathrm{Pa}.$$

The measurements correspond to parabolic and concentrated force distributions as well as localized moment distributions. They have been simulated by direct computations and eventually distorted by white noise.

**Spatial localization property.** An intriguing result of the numerical reconstruction using the ELC has been the good spatial localization of the defects or perturbations of the elastic moduli through the error on constitutive law. The good spatial localization of defects of the error on constitutive law have been reported in a series of papers [16, 17, 10, 15, 18].

In order to explain the spatial localization property of the ECL functional we shall examine o series of differences between solutions of perturbed and unperturbed problems and express them as boundary integral equations (for a complete discussion, see [19].

In the sequel we shall consider the following series expansion of the fields depending on a small parameter $\eta \in \mathbb{R}$:

- $\boldsymbol{C} = \boldsymbol{C}_0 + \eta \boldsymbol{C}_1$,

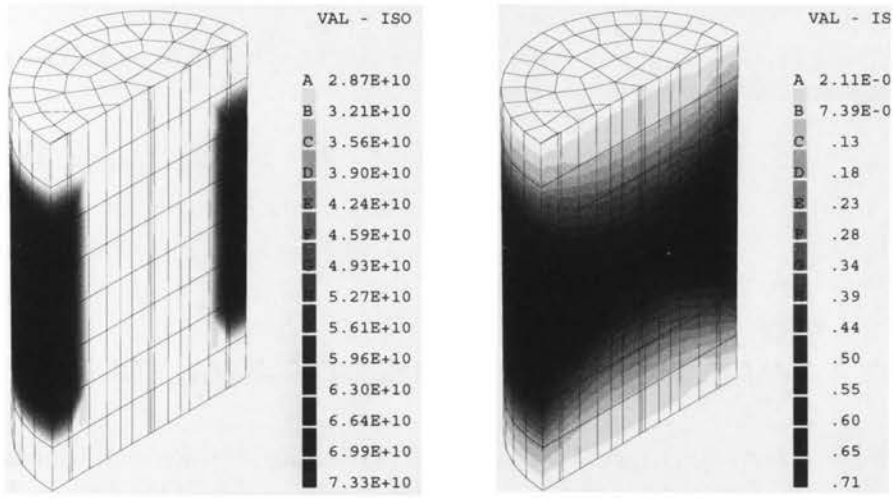


FIGURE 3.8. Spatial localization property during a torsion experiment: spatial localization of the inclusion (left) and spatial distribution of the error in constitutive law (right).

- $\boldsymbol{u} = \boldsymbol{u}_0 + \eta \boldsymbol{u}_1 + o(\eta^2)$,
- $\boldsymbol{\sigma} = \boldsymbol{\sigma}_0 + \eta \boldsymbol{\sigma}_1 + o(\eta^2)$,

where the support of $\boldsymbol{C}_1$ is strictly included in the interior of $\Omega$.

The *zero order* displacement $\boldsymbol{u}_0$ is solution of the following equation:

$$\operatorname{div}(\boldsymbol{C}_0 : \nabla \boldsymbol{u}_0) = \boldsymbol{0}, \tag{3.53}$$

with boundary conditions:

$$\boldsymbol{u}_0|_{\partial\Omega} = \boldsymbol{w} \quad \text{or} \quad \boldsymbol{\sigma}_0 \boldsymbol{n}|_{\partial\Omega} = \boldsymbol{t}. \tag{3.54}$$

The stress field $\boldsymbol{\sigma}_0$ can be expressed using a classical integral representation:

$$\boldsymbol{\sigma}_0(\boldsymbol{x}) = -\int_{\partial\Omega} \boldsymbol{P}_{\boldsymbol{C}_0}(\boldsymbol{x}, \boldsymbol{y}) \cdot \boldsymbol{u}_0(\boldsymbol{y})\, dS_{\boldsymbol{y}} + \int_{\partial\Omega} \boldsymbol{Q}_{\boldsymbol{C}_0}(\boldsymbol{x}, \boldsymbol{y}) \cdot (\boldsymbol{\sigma}_0(\boldsymbol{y}) \cdot \boldsymbol{n}(\boldsymbol{y}))\, dS_{\boldsymbol{y}}, \tag{3.55}$$

with $\boldsymbol{P}_{\boldsymbol{C}_0}$ and $\boldsymbol{Q}_{\boldsymbol{C}_0}$ vectors fields computed from the Green function of the domain.

*Integral representation formulas [20]*

The fundamental solution or the Green function $\boldsymbol{G}_{\boldsymbol{C}_0}$ is defined on an open set $E$ compatible with $\Omega$ by the equations:

$$\operatorname{div} \boldsymbol{L}_0 \nabla_{\boldsymbol{y}} \boldsymbol{G}^k_{\boldsymbol{C}_0}(\boldsymbol{x}, \boldsymbol{y}) + \delta(\boldsymbol{x} - \boldsymbol{y}) \boldsymbol{e}_k = \boldsymbol{0}. \tag{3.56}$$

For $\boldsymbol{x} \in \Omega$ it can shown that the elastic stress field can be expressed as:

$$\sigma_{ij}(\boldsymbol{x}) = \int_{\partial\Omega} \boldsymbol{C}_0 : \nabla_{\boldsymbol{x}} \boldsymbol{G}_{\boldsymbol{C}_0}(\boldsymbol{x}, \boldsymbol{y}) \cdot \boldsymbol{t}\, dS_{\boldsymbol{y}} - \int_{\partial\Omega} \boldsymbol{n} \cdot \boldsymbol{C}_0 : \nabla_{\boldsymbol{x}} \boldsymbol{G}_{\boldsymbol{C}_0}(\boldsymbol{x}, \boldsymbol{y}) \cdot \boldsymbol{w}\, dS_{\boldsymbol{y}} + \int_{\Omega} \boldsymbol{C}_0 : \nabla_{\boldsymbol{x}} \boldsymbol{G}_{\boldsymbol{C}_0} \cdot \boldsymbol{b}\, dV_{\boldsymbol{y}}, \tag{3.57}$$

where $\boldsymbol{w}$, $\boldsymbol{t}$, $\boldsymbol{b}$ denote, respectively, the vector of boundary displacement, boundary traction and body forces. $\boldsymbol{n}$ represents the unit outward normal of the domain. The following notations will be used for the third order tensor fields:

$$\boldsymbol{Q}_{\boldsymbol{C}_0}(\boldsymbol{x}, \boldsymbol{y}) = \boldsymbol{C}_0 : \nabla_{\boldsymbol{x}} \boldsymbol{G}_{\boldsymbol{C}_0}(\boldsymbol{x}, \boldsymbol{y}), \tag{3.58}$$

$$\boldsymbol{P}_{\boldsymbol{C}_0}(\boldsymbol{x}, \boldsymbol{y}) = \boldsymbol{n} \cdot \boldsymbol{C}_0 : \nabla_{\boldsymbol{x}} \boldsymbol{G}_{\boldsymbol{C}_0}(\boldsymbol{x}, \boldsymbol{y}) = \boldsymbol{n} \cdot \boldsymbol{C}_0 : \nabla_{\boldsymbol{x}} \boldsymbol{Q}_{\boldsymbol{C}_0}(\boldsymbol{x}, \boldsymbol{y}). \tag{3.59}$$

If $\boldsymbol{\sigma}_0$ has been determined with the imposed displacement $\boldsymbol{w}$ we can further write:

$$\boldsymbol{\sigma}_0[\boldsymbol{w}](\boldsymbol{x}) = -\int_{\partial\Omega} \boldsymbol{P}_{\boldsymbol{C}_0}(\boldsymbol{x}, \boldsymbol{y}) \cdot \boldsymbol{w}(\boldsymbol{y})\, dS_{\boldsymbol{y}} + \int_{\partial\Omega} \boldsymbol{Q}_{\boldsymbol{C}_0}(\boldsymbol{x}, \boldsymbol{y}) \cdot \Lambda_{\boldsymbol{C}_0}(\boldsymbol{w})(\boldsymbol{y})\, dS_{\boldsymbol{y}}. \tag{3.60}$$

The *first order* displacement $\boldsymbol{u}_1$ is solution of the following equation:

$$\operatorname{div}(\boldsymbol{C}_0 : \nabla \boldsymbol{u}_1) = -\operatorname{div}(\boldsymbol{C}_1 : \nabla \boldsymbol{u}_0), \tag{3.61}$$

with boundary conditions:

$$\boldsymbol{u}_1|_{\partial\Omega} = \boldsymbol{0} \quad \text{or} \quad \boldsymbol{\sigma}_1 \boldsymbol{n}|_{\partial\Omega} = \boldsymbol{0}. \tag{3.62}$$

The first order perturbation displacement is therefore generated by the body force term corresponding to stresses created by the zero displacement and the perturbation of the elastic moduli.

The Dirichlet-to-Neuman data map corresponding to this problem will be denoted by $\Lambda_{\boldsymbol{C}_0, \boldsymbol{C}_1}$.

Similarly, we can rewrite the *perturbed* system of equations:

$$\operatorname{div}(\boldsymbol{C} : \nabla \boldsymbol{u}) = 0 \tag{3.63}$$

under the following equivalent form:

$$\operatorname{div}(\boldsymbol{C}_0 : \nabla \boldsymbol{u}) = -\operatorname{div}(\eta \boldsymbol{C}_1 : \nabla \boldsymbol{u}), \tag{3.64}$$

which yields the following integral representation of the stress field:

$$\begin{aligned}\boldsymbol{\sigma}(\boldsymbol{x}) = &\int_\Omega \boldsymbol{C}_0 : \nabla_{\boldsymbol{x}} \boldsymbol{G}_{\boldsymbol{C}_0}(\boldsymbol{x}, \boldsymbol{y}) \cdot \operatorname{div}_{\boldsymbol{y}}(\eta \boldsymbol{C}_1 : \nabla \boldsymbol{u}(\boldsymbol{y}))\, dV_{\boldsymbol{y}} \\ &- \int_{\partial\Omega} \boldsymbol{P}_{\boldsymbol{C}_0}(\boldsymbol{x}, \boldsymbol{y}) \cdot \boldsymbol{u}(\boldsymbol{y})\, dS_{\boldsymbol{y}} + \int_{\partial\Omega} \boldsymbol{Q}_{\boldsymbol{C}_0}(\boldsymbol{x}, \boldsymbol{y}) \cdot (\boldsymbol{\sigma}(\boldsymbol{y}) \cdot \boldsymbol{n}(\boldsymbol{y}))\, dS_{\boldsymbol{y}}. \end{aligned} \tag{3.65}$$

The difference between the *nonlinear* and the *zero order* solution, $\boldsymbol{\sigma}[\boldsymbol{w}]$ and $\boldsymbol{\sigma}_0[\boldsymbol{w}]$, can be written after an integration by parts as:

$$\begin{aligned}&\boldsymbol{\sigma}[\boldsymbol{w}](\boldsymbol{x}) - \boldsymbol{\sigma}_0[\boldsymbol{w}](\boldsymbol{x}) \\ &\quad = (fp) \int_\Omega \left( \boldsymbol{C}_0 : \nabla_{\boldsymbol{x}} \nabla_{\boldsymbol{y}} \boldsymbol{G}_{\boldsymbol{C}_0}(\boldsymbol{x}, \boldsymbol{y}) \right) \cdot (\boldsymbol{C}_1 : \nabla \boldsymbol{u}(\boldsymbol{y}))) \, dV_{\boldsymbol{y}} \\ &\qquad + \int_{\partial\Omega} \boldsymbol{Q}_{\boldsymbol{C}_0}(\boldsymbol{x}, \boldsymbol{y}) \cdot (\Lambda_{\boldsymbol{C}}(\boldsymbol{w}) - \Lambda_{\boldsymbol{C}_0}(\boldsymbol{w}))\, dS_{\boldsymbol{y}}, \end{aligned} \tag{3.66}$$

where $(fp)$ denotes that the finite part of the integral.

A close inspection of the integrals shows their behaviour for $\boldsymbol{x} \in \Omega \setminus \operatorname{supp} \boldsymbol{C}_1$. For a three dimensional problem:

- the first term behaves as $|\boldsymbol{x} - \boldsymbol{y}|^{-3}$. As the inclusion lies in the interior of the body, $\operatorname{supp} \boldsymbol{C}_1 \subset \Omega$, it follows that the integral decreases as $r^{-3}$ where $r = d(\boldsymbol{x}, \operatorname{supp} \boldsymbol{C})$,
- the second term behaves as $|\boldsymbol{x} - \boldsymbol{y}|^{-2}$, it then follows that the integral decreases as $r^{-2}$ with $r = d(\boldsymbol{x}, \partial\Omega)$.

For two dimensional problems, the decrease is in $r^{-2}$ from the inclusion $(r = d(\boldsymbol{x}, \operatorname{supp} \boldsymbol{C}))$ and in $r^{-1}$ from the boundary $(r = d(\boldsymbol{x}, \partial\Omega))$.

A direct consequence of this behaviour, whether in two or three dimensions, is that the stress difference $\boldsymbol{\sigma}[\boldsymbol{w}] - \boldsymbol{\sigma}_0[\boldsymbol{w}]$ is negligible outside the support of the perturbation of the elastic moduli $\boldsymbol{C}_1$ and far from the boundaries.

The error on constitutive law can also be expressed in one of the following equivalent forms:

$$\begin{aligned}\mathcal{J}(\boldsymbol{C},\boldsymbol{\epsilon},\boldsymbol{\sigma}) &= \int_{\Omega} (\boldsymbol{\sigma}-\boldsymbol{C}:\boldsymbol{\epsilon}) : \boldsymbol{C}^{-1} : (\boldsymbol{\sigma}-\boldsymbol{C}:\boldsymbol{\epsilon})\, dV \\ &= \int_{\Omega} (\boldsymbol{C}^{-1}:\boldsymbol{\sigma}-\boldsymbol{\epsilon}) : \boldsymbol{C} : (\boldsymbol{C}^{-1}:\boldsymbol{\sigma}-\boldsymbol{\epsilon})\, dV.\end{aligned} \tag{3.67}$$

For these fields one can write the error on constitutive law from (3.67) as:

$$\begin{aligned}\mathcal{J}(\boldsymbol{C},\boldsymbol{\epsilon}_{\boldsymbol{C}}[\boldsymbol{w}],\boldsymbol{\sigma}_{\boldsymbol{C}}[\boldsymbol{t}]) &= \int_{\partial\Omega} (\boldsymbol{u}_{\boldsymbol{C}}[\boldsymbol{w}]-\boldsymbol{u}_{\boldsymbol{C}}[\boldsymbol{t}]) : (\boldsymbol{\sigma}_{\boldsymbol{C}}[\boldsymbol{w}]\cdot\boldsymbol{n}-\boldsymbol{\sigma}_{\boldsymbol{C}}[\boldsymbol{t}]\cdot\boldsymbol{n})\, dS \\ &= \int_{\partial\Omega} (\boldsymbol{w}-\boldsymbol{u}_{\boldsymbol{C}}[\boldsymbol{t}])\cdot(\boldsymbol{\sigma}_{\boldsymbol{C}}[\boldsymbol{w}]\boldsymbol{n}-\boldsymbol{t})\, dS.\end{aligned} \tag{3.68}$$

**Exercise:** *Show using integration by parts and the exact boundary conditions that the preceding equations hold.*

We note that if $(\boldsymbol{w},\boldsymbol{t})$ is a measurement pair, i.e. $\boldsymbol{t}=\boldsymbol{\Lambda}_{\boldsymbol{C}}(\boldsymbol{w})$, then $\boldsymbol{u}_{\boldsymbol{C}}[\boldsymbol{w}]=\boldsymbol{u}_{\boldsymbol{C}}[\boldsymbol{t}]$, consequently the ECL vanishes as expected:

$$\mathcal{J}(\boldsymbol{C},\boldsymbol{\epsilon}_{\boldsymbol{C}}[\boldsymbol{w}],\boldsymbol{\sigma}_{\boldsymbol{C}}[\boldsymbol{t}])=0. \tag{3.69}$$

The last boundary integral provides another physical interpretation for the ELC as the mechanical work provided by the error in displacements on the error on forces.

Let us now assume that $(\boldsymbol{w},\boldsymbol{t})$ is a measurement pair, i.e. $\boldsymbol{t}=\boldsymbol{\Lambda}_{\boldsymbol{C}}(\boldsymbol{w})$ and compute the zero order approximations $\boldsymbol{u}_0[\boldsymbol{w}]$ and $\boldsymbol{u}_0[\boldsymbol{t}]$.

Using the solution of the unperturbed problem $\boldsymbol{u}[\boldsymbol{w}]=\boldsymbol{u}[\boldsymbol{t}]$ we obtain the following expressions of the error on constitutive law computed for the zero order fields:

$$\begin{aligned}\mathcal{J}(\boldsymbol{C}_0,\boldsymbol{\epsilon}_0[\boldsymbol{w}],\boldsymbol{\sigma}_0[\boldsymbol{t}]) &= \int_{\Omega} (\boldsymbol{\epsilon}_0[\boldsymbol{w}]-\boldsymbol{\epsilon}_0[\boldsymbol{t}]) : \boldsymbol{C}_0 : (\boldsymbol{\epsilon}_0[\boldsymbol{w}]-\boldsymbol{\epsilon}_0[\boldsymbol{t}])\, dV \\ &= \int_{\Omega} (\boldsymbol{\epsilon}_0[\boldsymbol{w}]-\boldsymbol{\epsilon}[\boldsymbol{w}]) : \boldsymbol{C}_0 : (\boldsymbol{\epsilon}_0[\boldsymbol{w}]-\boldsymbol{\epsilon}[\boldsymbol{w}])\, dV \\ &+ \int_{\Omega} (\boldsymbol{\epsilon}[\boldsymbol{t}]-\boldsymbol{\epsilon}_0[\boldsymbol{t}]) : \boldsymbol{C}_0 : (\boldsymbol{\epsilon}[\boldsymbol{t}]-\boldsymbol{\epsilon}_0[\boldsymbol{t}])\, dV.\end{aligned} \tag{3.70}$$

The ELC is now expressed in terms of the difference between the perturbed and the zero order solution of the direct problem which have been previously computed.

The integrand in the ECL is therefore negligible far from the support of the inclusion and the boundary. More precisely, in the three dimensional problem they behave like:

- $r^{-6}$ as a function of the distance to the support of the inclusion $r = d(\boldsymbol{x}, \operatorname{supp} \boldsymbol{C})$, and as
- $r^{-4}$ as a function of with the distance to the boundary $r = d(\boldsymbol{x}, \partial\Omega)$.

For two dimensional problems, the decrease is in $r^{-4}$ from the inclusion ($r = d(\boldsymbol{x}, \operatorname{supp} \boldsymbol{C})$) and in $r^{-2}$ from the boundary ($r = d(\boldsymbol{x}, \partial\Omega)$).

### 3.2.4. ECL for Love–Kirchhoff Plates

Let us consider a thin elastic plate in the classical framework of the Love–Kirchhoff plate theory occupying in the reference configuration a regular domain $\Omega$ with boundary $\partial\Omega$. $\mathbf{n}$ and $\mathbf{t}$ will denote the normal and tangent unit vector on the $\partial\Omega$.

Let $w$, $\mathbf{k}$ , $\mathbf{M}$ stand respectively for the deflection field of the plate, the second-order tensor of generalized strain, corresponding to curvature, and the second-order tensor of generalized stress, corresponding to bending moments. Considering a stress-free initial state and no body forces, the governing equations on $\Omega$ are:

$$\mathbf{k} = \nabla\nabla w, \qquad \mathbf{M} = \mathbf{D}\mathbf{k}, \qquad \operatorname{div}\operatorname{div} M = 0, \tag{3.71}$$

where $\mathbf{D}$ is the fourth-rank tensor of the bending rigidities, related to the Hooke elasticity tensor in the classical way. $\mathbf{D}$ is positive definite and for which the classical symmetry relations:

$$M_{\alpha\beta\gamma\phi} = M_{\beta\alpha\gamma\phi} = M_{\gamma\phi\alpha\beta}, \qquad \alpha, \beta, \gamma, \phi = 1, 2. \tag{3.72}$$

$\mathbf{D}$ is supposed to be inhomogeneous, i.e. $\mathbf{D} = \mathbf{D}(\mathbf{x})$, $\mathbf{x} \in \Omega$, unless specified otherwise.

The above equations and the prescription of two of the following quantities on the boundary:

- deflection: $w = \phi$,
- normal derivative of the deflection: $\dfrac{\partial w}{\partial \mathbf{n}} = \psi$,

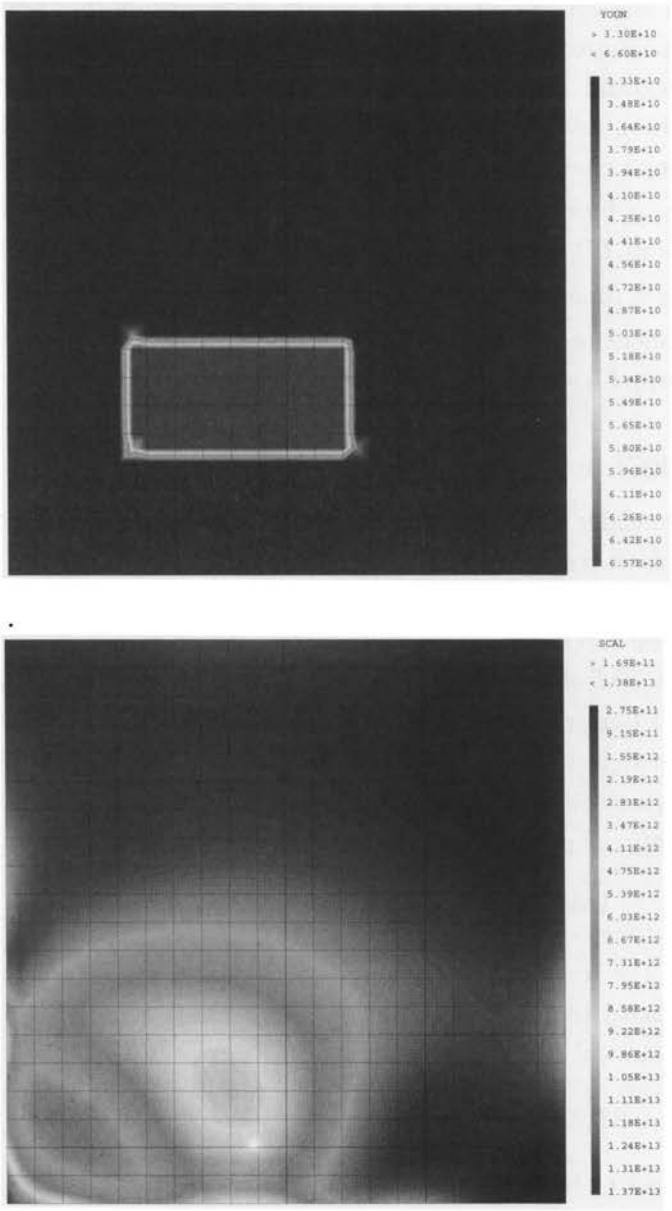


FIGURE 3.9. Inclusion (top) and spatial distribution (bottom) of the error on constitutive law obtained for a parabolic pressure distribution on the boundary located on the lower side of the square.

- moment: $\mathbf{nMn} = \Phi$,
- forces: $\frac{\partial}{\partial \mathbf{t}} (\mathbf{nMt}) + (\operatorname{div} \mathbf{M})\, \mathbf{n} = \Psi$,

describe completely the classical *direct problem* for elastic plates. For this problem uniqueness of the solution as well as continuous dependence of the boundary values and elastic moduli are assured.

The mathematical *inverse problem for plates* (see [21, 22]), supposes that the tensor of the bending rigidities $D$ is not known and that it has to be recovered from the knowledge of the Dirichlet-to-Neumann data map:

$$\Pi_{\mathbf{M}} : \begin{pmatrix} w \\ \frac{\partial w}{\partial \mathbf{n}} \end{pmatrix} \longrightarrow \begin{pmatrix} \mathbf{nMn} \\ \frac{\partial}{\partial \mathbf{t}} (\mathbf{nMt}) + (\operatorname{div} \mathbf{M})\, \mathbf{n} \end{pmatrix}. \tag{3.73}$$

This idealized problem of non-destructive testing and its electrical analogue have extensively been discussed in the mathematical literature. One of the important addressed questions is uniqueness, stated in the context of plates as follows: *If two two plates having bending rigidities* $\mathbf{D}$ *and* $\mathbf{D}'$ *give the same response to measurements, are necessary* $\mathbf{D}$ *and* $\mathbf{D}'$ *equal ?*. This problem is more difficult than the global elastic one as explained in [22].

For the isotropic elastic plates a uniqueness result for the linearized problem has been given by Ikehata [11]. He has showed that the Young modulus and the Poisson ratio can be identified from the Dirichlet-to-Neumann data map if their boundary values and their derivatives are known and if they are close enough to a constant.

For anisotropic elastic plates general uniqueness can not be expected as in the case of three dimensional elasticity [10], as explained by Ikehata in [22]. The uniqueness of the linearized problem is related to two classes of homogeneous elasticity tensors which coincide with the ones defined by Lehnitskii [23] for the study of the general solution of the plate equation. The global uniqueness questions remains to our knowledge still an open problem.

From an engineering point of view, one can remark that problems are stated in a slightly different manner. One has to recover the bending rigidities $D$ from a series of simultaneous displacement and force measurements and generally a series of additional information is given. In a certain number of cases one can accept that bending rigidities are homogeneous or deflection can be measured on a portion of the surface of the plate. A series of experiments and and different methods for determining homogeneous bending rigidities have already been described in a series of papers [24, 25, 26]. However, as it will be shown in the sequel, these information are sufficient under a certain

number of assumptions to obtain some informations about a inhomogeneous distribution of bending rigidities. The measured data will be represented by a series of simultaneous measured boundary fields $\{\phi_i, \psi_i, \Phi_i, \Psi_i\}_{i=1,\dots,N}$ and eventually the corresponding series of measured deflections and concentrated forces $\{v_i, f_i\}_{i=1,\dots,N}$ on a certain number of interior points.

Considering the constitutive equation apart, it is natural to form the space of kinematically and statically admissible fields, $\mathbf{KA}(\phi, \psi, v)$ and respectively $\mathbf{SA}(\Phi, \Psi, f)$. This permits to uncoupling the general laws of dynamics and kinematics from the general problem and to state the inverse problem as a constrained minimization problem:

*Find the distribution of bending rigidities* $\mathbf{D}$ *and deflections*

$$w_i \in \mathbf{KA}(\phi_i, \psi_i, v_i), \quad (i = 1, \dots, N),$$

*and the bending moments*

$$\mathbf{M}_i \in \mathbf{SA}(\Phi, \Psi, f), \quad (i = 1, \dots, N),$$

*minimizing the error on the constitutive law (ECL):*

$$I(\mathbf{D}, \{w_i\}_{i=1,\dots,N}, \{\mathbf{M}_i\}_{i=1,\dots,N}) = \sum_{i=1,\dots,N} \int_\Omega \|\mathbf{D}^{-1/2}\mathbf{M}_i - \mathbf{D}^{1/2}\mathbf{k}_i\|^2 dv.$$

The numerical results present the identification of an inclusion in case of an isotropic elastic plate. The tensor of bending rigidities has in this case the form in the Cartesian coordinate system presented in Fig. 3.10.

### 3.2.5. Notes

A series of other identification problems have equally been studied using the error on constitutive law, we shall just briefly cite next some of main directions of research:

**Elastodynamics.** A complete definition of the error on constitutive law in the case of elastodynamics as well as a short discussion in terms of the Tonti's diagram is presented in Bui [27]. A more applied discussion involving also nonlinear material behaviour is done in [27] (see also the last note).

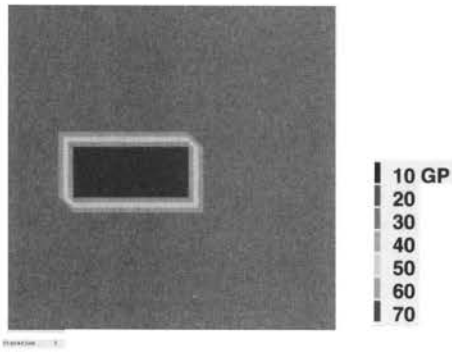


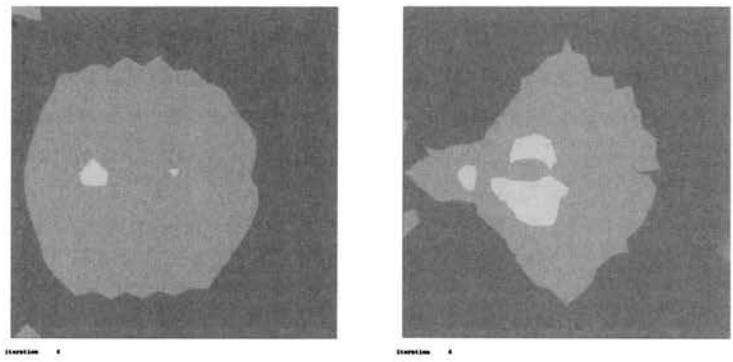

Reconstruction after 5 iterations

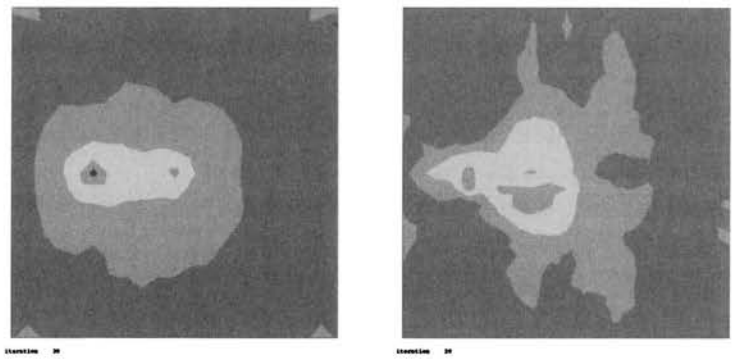

Reconstruction after 20 iterations

FIGURE 3.10. Real and reconstructed values of the Young modulus using $d_{(1)} = 2a + b = \frac{M_{11}+M_{22}}{k_{11}+k_{22}}$ (left column) and $d_{(2)} = 2b = \frac{M_{12}}{k_{12}}$ (right column) eigenelastic moduli.

**Vibrations.** The error on the constitutive law has been defined for vibration problems by M.Reynier in her Ph.D. thesis [28]. The method was developed to update stiffness and mass matrices of finite element models with respect to measurements. This approach has later been developed in the same direction and some recent results can be found in [29, 30]. An overview and review of the error on constitutive law with applications to model updating is presented in [31]. This reference is interesting as it also discusses the extension of this error functional for nonlinear constitutive behaviour.

**Nonlinear constitutive behaviour.** A first attempt to generalize the idea of error on constitutive law was proposed by L. Rota in his Ph.D. thesis [27]. He showed that using notions of energy, and complementary energy in the general framework of standard generalized materials, one can define a generalized error on constitutive law. He also tested this theoretical construction in a series of identifications of constitutive parameters from dynamic impact experiments obtained on Hopkinsons bars.

## 3.3. References

1. C.W. GROETSCH, *Inverse Problems*, The Mathematical Society of America, 1999.

2. R.V. KOHN and M. VOGELIUS, Relaxation of a variational method for impedance computed tomography, *Comm.Pure.Appl.Math.*, 40:745–777, 1987.

3. A. CALDERON, On an inverse boundary value problem, in: Rio de Janeiro Soc. Brasiliera de Matématica (Ed.), *Seminar on Numerical analysis and its Application to Continuum Physics*, pp.65–73, 1980.

4. R.V. KOHN and M. VOGELIUS, Determining conductivity by boundary measurments, *Comm.Pure.Appl.Math.*, 37:289–298, 1984.

5. R.V. KOHN and M. VOGELIUS, Determining conductivity by boundary measurments ii interior results, *Comm.Pure.Appl.Math.*, 37:643–667, 1985.

6. Z SUN and G. UHLMANN, Generic uniqueness for determined inverse problems in 2 dimensions, in: M. Yamaguti (Ed.), *Inverse Problems in Engineering Sciences*, ICM-90 Satellite Conference Proceedings, Springer Verlag , Tokyo, 1991.

7. G. NAKAMURA and G. UHLMANN, Inverse problems at the boundary for an elastic medium, *SIAM J. Math. Anal.*, 26:263–279, March 1995.

8. R.V. KOHN and A. MCKENNEY, Numerical implementation of a variational method for electric impedance tomography, *Inverse Problems*, 1(6):389–414, 1990.

9. H.D. BUI, *Introduction aux Problèmes Inverses en Mécanique des Matériaux*, Eyrolles, Paris / CRC Roca Baton, 1993.

10. A. CONSTANTINESCU, *Sur l'identification des modules élastiques*, Ph.D. thesis, Ecole Polytechnique, France, 1994.

11. M. IKEHATA, Inversion formulas for the linearized problem for an inverse boundary value problem in elastic prospection, *SIAM J. Math. Anal.*, 50:1635–1644, December 1990.

12. P. LADEVÈZE and D. LEGUILLON, Error estimates procedures in the finite element methoid and applications, *SIAM J. Numer. Anal.*, 20(3), 1983.

13. S.C. COWIN and M. MEHRABADI, Eigentenors of linear elastic materials, *Q.J.Mech.Appl.Math*, 43, 1990.

14. S.C. COWIN and M. MEHRABADI, The structure of the linear anisotropic symetries, *J.Mech.Phys.Solids*, 40(7):1459–1471, 1992.

15. A. CONSTANTINESCU, On the identification of elastic moduli from displacement-force boundary measurements, *International Journal of Inverse Problems in Engineering*, 1:293–315, 1995.

16. J. BEN ABDALLAH, *Inversion gaussienne appliquée à la correction paramétrique de modèles structuraux*, Ph.D. thesis, Ecole Polytechnique, France, 1995.

17. J. BEN ABDALLAH, M. BONNET, and M. REYNIER, Analyse de la localisation par l'erreur en relation de comportement, private communication, 1998.

18. A. CONSTANTINESCU, On the identification of elastic moduli in plates, in: G. S. Dulikravich, M. Tanaka (Eds.), *Inverse problems in engineering mechanics (Proceedings of the ISIP'98 Conference, Nagano, Japan, march 1998)*, pp.205–214, Elsevier, 1998.

19. H.D. BUI AND A. CONSTANTINESCU, Spatial localization of the error on constitutive law for the identification of defects in elastic bodies, *Archive of Mechanics*, 52(4-5):511–522, 2000.

20. M. BONNET, *Boundary Integral Equations*, CNRS Editions / Eyrolles, 1995.

21. M. IKEHATA, An inverse problem for the plate in the Love–Kirchhoff theory, *SIAM J. Appl. Math.*, 53:942–970, August 1993.

22. M. IKEHATA, The linearization of the Dirichlet to Neumannn data map in anisotropic plate theory. *Inverse Problems*, 11:165–181, August 1995.

23. S.G. LEKHNITSKII, *Theory of Elasticity of an Anisotropic Elastic Body*, Holden Day series in Mathematical Physics, 1963.

24. M. GREDIAC and A. VAUTRIN, Mechanical characterization of anisotropic plates: experiments and results, *Eur.J. Mechanics A*, 12(6):819–838, 1993.

25. M. GREDIAC, On the direct determination of invariant parameters governing anisotropic plate bending problems, *Int. J. Solids Structures*, 33(27):3969–3982, 1996.

26. M. GREDIAC and A. VAUTRIN, A new method for the determination of bending rigidities of thin anisotropic plates, *ASME J. Appl. Mech.*, 57:964–968, 1990.

27. ROTA LAURENT, *Application de Méthodes Inverse au Dépouillement de l'Essai aux Barres de Hopkinson*, Ph.D. thesis, Ecole Polytechnique, France, 1997.

28. M. REYNIER *Sur le contrôle des modélisations éléments finis: recalage à partir des essais dynamiques*, Ph.D. thesis, Université Pierre et Marie Curie, Paris, France, 1990.

29. P. LADEVÈZE and A. CHOUAKI, Application of a posteriori error estimation for structural model updating, *Inverse Problems*, 15(1):49–58, 1999.

30. A. DERAEMAEKER, P. LADEVÈZE, and PH. LECONTE, Reduced bases for model updating in structural dynamics based on constitutive relation error, *Computer Methods in Applied Mechanics and Engineering*, 191(21–22):2427–2444, 2002.

31. P. LADEVÈZE, M. REYNIER, and D. NEDJAR, Parametric corrections of finite element models using modal tests, in: H.D. Bui and M. Tanaka (Eds.), *IUTAM Symposium on Inverse problems in engineering mechanics*. Springer Verlag, Tokyo, 1993.

# Chapter 4

# Sensitivity computations: linear case

## 4.1. Introduction

In the preceding Chapters we have been studied inverse problems by trying to exploit the intimate properties of the problem formulation and we have shown that in this way a series of spectacular results can be obtained. However, it is not always possible to do this fine analysis and therefore in a certain number of cases inverse problems are reformulated as an optimization problem, i.e. as the minimization of a certain cost functional. The solution obtained by the minimization procedure is in such cases only an approximate solution in the sense of the cost functional, sometimes called a *quasi*–solution.

If the inverse problem is defined as a minimization problem two main questions arise:

- *what is the choice of the cost functional?*
- *what is the choice of the minimization algorithm?*

### 4.1.1. The choice of cost functional

In order to exemplify the importance of the choice of the cost functional in an inverse problem, let us analyse the identification of a square inclusion in an elastic domain using boundary displacement and force measurement $\boldsymbol{\xi}^{\text{real}}, \boldsymbol{\phi}^{\text{real}}$.

The numerical experiment performed consisted in moving a mock inclusion in a similar domain and measuring the distance between the real and mock measurements for different positions of the mock inclusion using two error (cost) functionals, the error on displacements being defined by:

$$EU(\boldsymbol{C}^{\text{mock}}, \boldsymbol{\varphi}^{\text{real}}, \boldsymbol{\xi}^{\text{real}}) = \frac{1}{2} \int_{\Omega} [\![ \boldsymbol{u}[\boldsymbol{C}^{\text{mock}}, \boldsymbol{\varphi}^{\text{real}}] - \boldsymbol{\xi}^{\text{real}} ]\!]^2 \, ds. \tag{4.1}$$

Here $\boldsymbol{u}[\boldsymbol{C}^{\text{mock}}, \boldsymbol{\varphi}]$ is the displacement obtained from the imposed force $\boldsymbol{\varphi}^{\text{real}}$ on the body with the mock inclusion $\boldsymbol{C}^{\text{mock}}$ and the error on constitutive law, defined in the previous Chapter by:

$$ELC(\boldsymbol{C}^{\text{mock}}, \boldsymbol{\varphi}^{\text{real}}, \boldsymbol{\xi}^{\text{real}}) = \frac{1}{2} \int_{\Omega} [\![ \boldsymbol{C}^{\text{mock}\,-1/2} \boldsymbol{\sigma}[\boldsymbol{\varphi}^{\text{real}}] - \boldsymbol{C}^{\text{mock}\,-1/2} \boldsymbol{\varepsilon}[\boldsymbol{\xi}^{\text{real}}] ]\!]^2 \, dv. \tag{4.2}$$

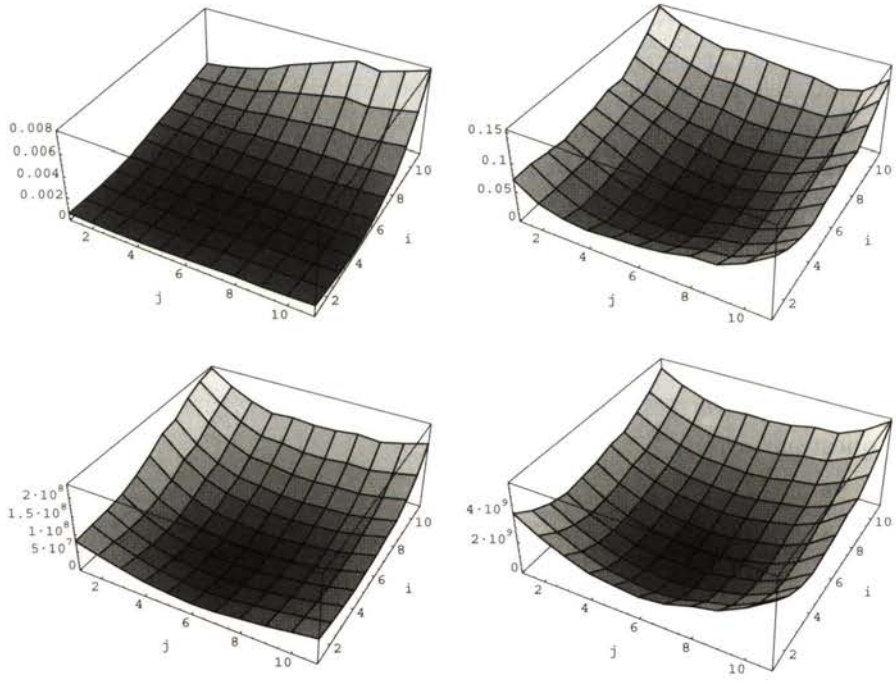


FIGURE 4.1. Comparison between the shapes of the least square distance in displacement (upper row) and the error on constitutive law (lower row) for 2 measurements on the boundary (left column) and 72 measurements on the boundary (right column) [1, 2].

The mock measurements consisted of a series of imposed parabolic distributions of pressure on the boundary. On each side of the square body we have imposed 18 distribution and as a consequence we have disposed of 72 measurements.

For comparison, in Fig. 4.1 we have displayed the shapes of the error on displacement $EU$ and the error on constitutive law $ELC$ with respect to the position of the mock inclusion. In each case we have displayed on the left the error functional computed for two measurements and on the right row the error functional computed with the complete series of 72 measurements. We note that the minimum indicating the correct position of inclusion is found in all cases. However, in the case of the error in displacements and for a small number of measurements the shape of the error functional is more flat. This would probably impose more difficulties in a numerical identification method.

### 4.1.2. The choice of the minimization algorithm

They are two large classes of minimization algorithms, the first class uses only estimations of the cost functional and the second class uses estimation of the cost functional as well the estimations of its derivatives.

In the no-gradient class, we can cite the dichotomy, the simplex method, the Monte-Carlo methods, more generally stochastic minimization techniques, or the modern class of genetic algorithms and refer the reader to more specialized literature like [3, 4]. We observe that these methods have the advantage of exploring in an extensive manner the parameter space, but are as such extremely expensive from the computational point of view.

The class of gradient based algorithms, was extensively studied in the last decades and a series of excellent textbook exist on this subject [5, 6, 7, 8]. Without getting in the heart of these algorithms we shall only explore next various methods of computing the gradient of the cost functional.

Let us specify a certain number of important points that should be taken into account when choosing a cost functional and an appropriate minimization technique:

- *existence of local and global minima*,
- *stability*, understood as the "rate" of continuity with respect to parameters and the engineering interesting scale of the same parameters,

- usage of *a priori information* about the parameter state and the underlying engineering problem.

Without giving a precise answer to these questions we shall try to emphasize their importance during the discussion of various examples in the sequel.

Let us nest focus on the techniques for the gradient computation of a cost functional and let us start the discussion from a basic idea: the *first order Taylor series expansion* of the cost function:

$$\mathcal{J}(\boldsymbol{c}+\Delta\boldsymbol{c}) = \mathcal{J}(\boldsymbol{c}) + \nabla_{\boldsymbol{c}}\mathcal{J}(\boldsymbol{c})\cdot\Delta\boldsymbol{c} + o(|\Delta\boldsymbol{c}|^2). \tag{4.3}$$

## 4.2. Linear elliptic systems

### 4.2.1. The finite dimensional case

Let us consider the following simple formulation of the problem:

*Minimize the cost functional $\mathcal{J}(\boldsymbol{c},\boldsymbol{u}(\boldsymbol{c}))$ with respect to $\boldsymbol{c}$, under the constraint that $\boldsymbol{u}(\boldsymbol{c})$ is a solution of the linear problem depending on the parameter $\boldsymbol{c}$:*

$$\boldsymbol{K}(\boldsymbol{c})\boldsymbol{u}(\boldsymbol{c}) = \boldsymbol{f}(\boldsymbol{c}). \tag{4.4}$$

In the case of an elastic discretized problem using the finite element method: $\boldsymbol{K}$, $\boldsymbol{u}$ and $\boldsymbol{f}$ would typically stand for the stiffness matrix, the displacement vector, and the force vector. The parameter $\boldsymbol{c}$ could express the elastic properties of structures, a control parameter of the load, etc.

**Finite Difference Method.** One can simple rewrite the *first order Taylor series expansion* and obtain a *forward difference approximation* for the gradient:

$$\nabla_{\boldsymbol{c}}\mathcal{F}(\boldsymbol{c})\cdot\Delta\boldsymbol{c} = \mathcal{F}(\boldsymbol{c}+\Delta\boldsymbol{c}) - \mathcal{F}(\boldsymbol{c}) + o(|\Delta\boldsymbol{c}|^2). \tag{4.5}$$

As such we can estimate the value of the gradient of the cost functional $\nabla_{\boldsymbol{c}}\mathcal{J}$ in the point $\mathcal{J}(\boldsymbol{c},\boldsymbol{u})$ from the values of the cost functional itself for given small changes of the parameter $\Delta\boldsymbol{c}$, i.e. $\mathcal{J}(\boldsymbol{c}+\Delta\boldsymbol{c},\boldsymbol{u}(\boldsymbol{c}+\Delta\boldsymbol{c}))$, where: $\boldsymbol{u}(\boldsymbol{c}+\Delta\boldsymbol{c})$ is obtained by solving the equation:

$$\boldsymbol{K}(\boldsymbol{c}+\Delta\boldsymbol{c})\boldsymbol{u}(\boldsymbol{c}+\Delta\boldsymbol{c}) = \boldsymbol{f}(\boldsymbol{c}+\Delta\boldsymbol{c}). \tag{4.6}$$

If the parameter is a $n$-dimensional vector $\boldsymbol{c} = (c_1, c_2, \ldots, c_n)$, computation of the gradient with the preceding first order formula will then

require $n+1$ direct computations, corresponding to $\boldsymbol{c}$ and the directions $\Delta \boldsymbol{c}_i = (0, \ldots, 0, c_i, 0, \ldots, 0)$, $i = 1, \ldots, n$. In this we use the following formula:

$$\nabla_{c_i} \mathcal{J}(\boldsymbol{c}) \cdot \Delta \boldsymbol{c} = \frac{\mathcal{J}(\boldsymbol{c} + \Delta \boldsymbol{c}_i) - \mathcal{J}(\boldsymbol{c})}{\Delta \boldsymbol{c}_i} + o(|\Delta \boldsymbol{c}_i|^2) \tag{4.7}$$

for the computation of $i$-th component of the gradient. Let us note that other approximation formulas are equally available. The *backward difference approximation* is given by:

$$\nabla_{c_i} \mathcal{J}(\boldsymbol{c}) \cdot \Delta \boldsymbol{c} = \frac{\mathcal{J}(\boldsymbol{c}) - \mathcal{J}(\boldsymbol{c} - \Delta \boldsymbol{c}_i)}{\Delta \boldsymbol{c}_i} + o(|\Delta \boldsymbol{c}_i|^2), \tag{4.8}$$

whereas the second-order accurate *central difference approximation* is expressed as follows:

$$\nabla_{c_i} \mathcal{J}(\boldsymbol{c}) \cdot \Delta \boldsymbol{c} = \frac{\mathcal{J}(\boldsymbol{c} + \Delta \boldsymbol{c}_i) - \mathcal{J}(\boldsymbol{c} - \Delta \boldsymbol{c}_i)}{2\Delta \boldsymbol{c}_i} + o(|\Delta \boldsymbol{c}_i|^2). \tag{4.9}$$

The finite difference method is very simple to implement as it depends solely on computations of the direct problem but is has two major drawbacks:

- The truncation error in the gradient estimation is of the order of $\Delta \boldsymbol{c}_i$. The smaller $\Delta \boldsymbol{c}_i$, the smaller the error should be, if we were not to approach numerical round off errors in the computations.
  In relation with this phenomenon we could also point out, that more generally, numerical differentiation of data is a generally ill-posed problem [10, 15].
- The $n$ different additional problems (4.6) need to compute and inverse the stiffness matrix $\boldsymbol{K}(\boldsymbol{c} + \Delta \boldsymbol{c})$. And these are expensive numerical operations.

Therefore one should, if possible, replace the *finite difference technique* by more precise and efficient method for computing the gradient based on analytical estimations of the gradient as presented below.

**Direct Differentiation Method.** The differentiation of the cost functional $\mathcal{J}$ with respect to $\boldsymbol{c}$ is given by:

$$\nabla_{\boldsymbol{c}} \mathcal{J}(\boldsymbol{c}, \boldsymbol{u}(\boldsymbol{c})) = \frac{\partial \mathcal{J}}{\partial \boldsymbol{c}}(\boldsymbol{c}, \boldsymbol{u}(\boldsymbol{c})) + \frac{\partial \mathcal{J}}{\partial \boldsymbol{u}}(\boldsymbol{c}, \boldsymbol{u}(\boldsymbol{c})) \cdot \frac{d\boldsymbol{u}}{d\boldsymbol{c}}, \tag{4.10}$$

or for each component $c_i$ $(i = 1, \ldots, n)$ of $\boldsymbol{c}$:

$$\nabla_{c_i} \mathcal{J}(\boldsymbol{c}, \boldsymbol{u}(c_i)) = \frac{\partial \mathcal{J}}{\partial c_i}(\boldsymbol{c}, \boldsymbol{u}(\boldsymbol{c})) + \frac{\partial \mathcal{J}}{\partial \boldsymbol{u}}(\boldsymbol{c}, \boldsymbol{u}(\boldsymbol{c})) \cdot \frac{d\boldsymbol{u}}{dc_i}. \tag{4.11}$$

The objective is to compute:

$$\frac{d\boldsymbol{u}}{d\boldsymbol{c}} = \left(\frac{d\boldsymbol{u}}{dc_1}, \frac{d\boldsymbol{u}}{dc_2}, \ldots, \frac{d\boldsymbol{u}}{dc_n}\right).$$

Toward this purpose let us differentiate equation (4.4) with respect to $\boldsymbol{c}$ in considering each component $c_i$:

$$\boldsymbol{K}(\boldsymbol{c})\frac{d\boldsymbol{u}}{dc_i}(\boldsymbol{c}) + \frac{d\boldsymbol{K}}{dc_i}(\boldsymbol{c})\boldsymbol{u}(\boldsymbol{c}) = \frac{d\boldsymbol{f}}{dc_i}(\boldsymbol{c}). \tag{4.12}$$

As the unknown is $\frac{d\boldsymbol{u}}{dc_i}$ and as $\boldsymbol{u}(\boldsymbol{c})$ can be considered as known from the initial analysis (4.4) we can rearrange the preceding equation in the following form:

$$\boldsymbol{K}(\boldsymbol{c})\frac{d\boldsymbol{u}}{dc_i}(\boldsymbol{c}) = \frac{d\boldsymbol{f}}{dc_i}(\boldsymbol{c}) - \frac{d\boldsymbol{K}}{dc_i}(\boldsymbol{c})\boldsymbol{u}(\boldsymbol{c}), \tag{4.13}$$

which yields the solution:

$$\frac{d\boldsymbol{u}}{dc_i}(\boldsymbol{c}) = \boldsymbol{K}^{-1}(\boldsymbol{c})\left(\frac{d\boldsymbol{f}}{dc_i}(\boldsymbol{c}) - \frac{d\boldsymbol{K}}{dc_i}(\boldsymbol{c})\boldsymbol{u}(\boldsymbol{c})\right). \tag{4.14}$$

Substituting now in equation (4.11) we obtain the composed expression for the gradient $\nabla_{\boldsymbol{c}}\mathcal{J}$:

$$\nabla_{c_i}\mathcal{J}(\boldsymbol{c}, \boldsymbol{u}(c_i)) = \frac{\partial\mathcal{J}}{\partial c_i}(\boldsymbol{c}, \boldsymbol{u}(\boldsymbol{c})) + \frac{\partial\mathcal{J}}{\partial\boldsymbol{u}}(\boldsymbol{c}, \boldsymbol{u}(\boldsymbol{c})) \cdot \boldsymbol{K}^{-1}(\boldsymbol{c})\left(\frac{d\boldsymbol{f}}{dc_i}(\boldsymbol{c}) - \frac{d\boldsymbol{K}}{dc_i}(\boldsymbol{c})\boldsymbol{u}(\boldsymbol{c})\right). \tag{4.15}$$

Defining this procedure as the *direct differentiation method* we can conclude that:

- Exactly as in the finite difference method, the direct differentiation method is based on solving $n + 1$ additional problems. However, the direct differentiation method provides a mathematical exact gradient and eliminates all truncation problems of the latter.
- The additional equations (4.13) have the same stiffness matrix $\boldsymbol{K}(\boldsymbol{c})$ as the equation of the initial problem (4.4). If the inverse stiffness matrixes $\boldsymbol{K}^{-1}(\boldsymbol{c})$ have been stored it implies that derivatives $\frac{d\boldsymbol{u}}{dc_i}(\boldsymbol{c})$ can be efficiently computed by forming the right hand side of the equation and a backsubstitution.
- The additional computational cost is therefore small after solving the initial analysis, compared to the additional cost in the case of the direct differentiation method.

**Adjoint State Method.** The adjoint state method starts from the remark that finding the minimum of a constrained functional is equivalent with finding the saddle point of an augmented (Lagrangian) functional. In our case we can define the Lagrangian as:

$$\mathcal{L}(\boldsymbol{c}, \boldsymbol{u}, \boldsymbol{u}^*) = \mathcal{J}(\boldsymbol{c}, \boldsymbol{u}) - \boldsymbol{u}^{*T} \cdot (\boldsymbol{K}(\boldsymbol{c})\boldsymbol{u} - \boldsymbol{f}(\boldsymbol{c}))\,, \tag{4.16}$$

where the field $\boldsymbol{u}^*$ acts as a Lagrange multiplier for the constraint. It is important to note that in our analysis we shall suppose that the variables $(\boldsymbol{c}, \boldsymbol{u}, \boldsymbol{u}^*)$ are independent.

The saddle point of the Lagrangian $\mathcal{L}$ is characterized by a vanishing gradient:

$$\langle \frac{\partial \mathcal{L}}{\partial \boldsymbol{u}^*}, \boldsymbol{v}^* \rangle = -\boldsymbol{v}^* \cdot (\boldsymbol{K}(\boldsymbol{c})\boldsymbol{u} - \boldsymbol{f}(\boldsymbol{c}) \qquad \forall \boldsymbol{v}^* = 0, \quad \forall \boldsymbol{v}^*, \tag{4.17}$$

$$\langle \frac{\partial \mathcal{L}}{\partial \boldsymbol{u}}, \boldsymbol{v} \rangle = \frac{\partial J}{\partial \boldsymbol{u}}(\boldsymbol{c}, \boldsymbol{u}) \cdot \boldsymbol{v} - \boldsymbol{u}^* \cdot \boldsymbol{K}(\boldsymbol{c})\boldsymbol{v} = 0 \qquad \forall \boldsymbol{v}, \tag{4.18}$$

$$\langle \frac{\partial \mathcal{L}}{\partial \boldsymbol{c}}, \boldsymbol{d} \rangle = \frac{\partial J}{\partial \boldsymbol{c}}(\boldsymbol{c}, \boldsymbol{u}) \cdot \boldsymbol{v} - \boldsymbol{u}^* \cdot \left( \frac{\partial \boldsymbol{K}}{\partial \boldsymbol{c}}(\boldsymbol{c})\boldsymbol{v} - \frac{\partial \boldsymbol{f}}{\partial \boldsymbol{c}}(\boldsymbol{c} \right) = 0 \qquad \forall \boldsymbol{d}. \tag{4.19}$$

The notation of the gradient used before, introduces actually the Fréchet differential of a functional and has been just used in this case in order to introduce the notations in the next paragraphs. $(\boldsymbol{d}, \boldsymbol{v}, \boldsymbol{v}^*)$ are varying in the corresponding vector spaces of different fields which will not be specified here for the sake of simplicity.

The first equations have $\boldsymbol{u}$ as unknown and expresses that the constraint should be satisfied:

$$\boldsymbol{K}(\boldsymbol{c})\boldsymbol{u} - \boldsymbol{f}(\boldsymbol{c} = 0. \tag{4.20}$$

It will also be called the *direct problem.*

The next equation has $\boldsymbol{u}^*$ as an unknown:

$$\frac{\partial J}{\partial \boldsymbol{u}}(\boldsymbol{c}, \boldsymbol{u}) - \boldsymbol{u}^{*T} \cdot \boldsymbol{K}(\boldsymbol{c}) = 0, \tag{4.21}$$

and is called the *adjoint problem.* Its solution is:

$$\boldsymbol{u}^* = \boldsymbol{K}^{-T}(\boldsymbol{c}) \frac{\partial J}{\partial \boldsymbol{u}}(\boldsymbol{c}, \boldsymbol{u}). \tag{4.22}$$

Let us note that the solution of the three equations provides the optimal solution of the inverse problem. This technique has been implemented in a

thermal inverse problem by Delattre, Ivaldi and Stolz [9]. Usually one will only try to estimate the gradient of the cost functional $\nabla_c \mathcal{J}$ and find the complete solution only through a minimization procedure.

If $\boldsymbol{u}$ is a solution of the direct problem, i.e. it satisfies the constraint, then the value of Lagrangian equals the value of the cost functional:

$$\mathcal{J}(\boldsymbol{c}, \boldsymbol{u}) = \mathcal{L}(\boldsymbol{c}, \boldsymbol{u}, \boldsymbol{u}^*).$$

If we differentiate both hand sides with respect to $\boldsymbol{c}$ and take into account that $\boldsymbol{u}^*$ is a solution of the adjoint problem, we obtain:

$$\langle \nabla_{\boldsymbol{c}} \mathcal{J}, \boldsymbol{d} \rangle = \langle \frac{\partial \mathcal{L}}{\partial \boldsymbol{c}}, \boldsymbol{d} \rangle = \frac{\partial J}{\partial \boldsymbol{c}}(\boldsymbol{c}, \boldsymbol{u}) \cdot \boldsymbol{v} - \boldsymbol{u}^* \cdot \left( \frac{\partial \boldsymbol{K}}{\partial \boldsymbol{c}}(\boldsymbol{c})\boldsymbol{v} - \frac{\partial \boldsymbol{f}}{\partial \boldsymbol{c}}(\boldsymbol{c}) \right). \quad (4.23)$$

As expected, the last equation corresponds to the solution obtained by the direct differentiation method.

For the *adjoint state method* we conclude that:

- The gradient computed through the adjoint state method is exact.
- The gradient computation requires the solution of a *single additional equation*
- The adjoint problem is defined by the adjoint stiffness matrix $\boldsymbol{K}^T$. If $\boldsymbol{K}$ is symmetric, as in the case of electricity or elasticity, finite element problems, and its inverse, can be stored and the computation of the adjoint field is very fast.
- The complete solution of the saddle point of the Lagrangian provides directly, i.e. without any minimization procedure, the solution of the optimization problem.

**Exercise:** *[10] Compute the gradient of the following cost functional:*

$$\mathcal{J} = \frac{1}{2} [\boldsymbol{C}(\boldsymbol{u} - \boldsymbol{w})]^2,$$

*where the $\boldsymbol{u} = (u_1, u_2)$ is the displacement solution of the spring system of Fig. 4.2, using the direct differentiation and the adjoint state method. $\boldsymbol{C}$ is a symmetric $2 \times 2$ matrix and $\boldsymbol{w}$ is a measured displacement vector.*

*Hint: Recall that the stiffness matrix and the force vector are written as:*

$$\boldsymbol{K} = \begin{pmatrix} k_1 + k_2 & k_2 \\ k_2 & k_2 \end{pmatrix}, \qquad \boldsymbol{f} = \begin{pmatrix} f_1 \\ f_2 \end{pmatrix}.$$

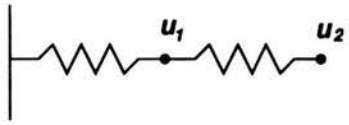


FIGURE 4.2. A simple system of springs.

### 4.2.2. The infinite dimensional case – the continuous problem

We shall now extend the techniques developed in the preceding subsection for the finite dimensional case to the continuous problem which represents an infinite dimensional case.

We shall consider that the following problem formulation of the problem:

*Minimize the cost functional $\mathcal{J}(\boldsymbol{c}, \boldsymbol{u}(\boldsymbol{c}))$ with respect to $\boldsymbol{c}$, under the constraint that $\boldsymbol{u}(\boldsymbol{c})$ is a solution of the linear elastic problem depending on the parameter $\boldsymbol{c}$:*

$$\operatorname{div} \boldsymbol{C}(\boldsymbol{c})\nabla \boldsymbol{u}(\boldsymbol{c}) + \boldsymbol{f}(\boldsymbol{c}) = 0 \qquad \forall \boldsymbol{x} \in \Omega, \tag{4.24}$$

$$\boldsymbol{\sigma}(\boldsymbol{c}) \cdot \boldsymbol{n} = (\boldsymbol{C}(\boldsymbol{c})\nabla \boldsymbol{u}(\boldsymbol{c})) \cdot \boldsymbol{n} = \boldsymbol{\varphi} \qquad \forall \boldsymbol{x} \in \partial\Omega, \tag{4.25}$$

*where $\boldsymbol{C}$ is the fourth-order tensor of the elastic moduli, $\boldsymbol{\sigma}$ is the second-order tensor of stresses, $\boldsymbol{n}$ the outward unit normal on the boundary and $\boldsymbol{\varphi}$ is the measured traction vector on the boundary.*

In the case of the identification of distributed elastic moduli, we have: $\boldsymbol{c} = \boldsymbol{C}$. A classical "least square" cost functional would take in this case the following form:

$$\mathcal{J}(\boldsymbol{c}, \boldsymbol{u}(\boldsymbol{c})) = \frac{1}{2} \int_{\partial\Omega} \|\boldsymbol{\xi} - \boldsymbol{u}(\boldsymbol{c})\|^2 \, ds, \tag{4.26}$$

where the norm is to be chosen either as a $L^2$-norm or a higher order norm like $H^2, \ldots$ including also the derivatives of functions. We recall that $\boldsymbol{\xi}$ is the measured boundary value of the displacement which we would like to attain in the solution of the minimization problem.

A more general expression for the cost functional could be:

$$\mathcal{J}(\boldsymbol{c}, \boldsymbol{u}) = \int_{\Omega} \mathrm{j}_{\Omega}(\boldsymbol{c}, \boldsymbol{u}) \, dv + \int_{\partial\Omega} \mathrm{j}_{\partial\Omega}(\boldsymbol{c}, \boldsymbol{u}) \, ds. \tag{4.27}$$

The functions $|_\Omega$ and $|_{\partial\Omega}$ express similarly to the earlier example a distance between measurements and predictions:

$$\mathrm{j}_\Omega(\boldsymbol{c}, \boldsymbol{u}) = 0, \qquad \mathrm{j}_{\partial\Omega}(\boldsymbol{c}, \boldsymbol{u}) = \frac{1}{2}\|\boldsymbol{\xi} - \boldsymbol{u}\|^2. \tag{4.28}$$

Moreover, they can also include regularisation terms, imposing a minimal norm of parameters to be identified, i.e.,

$$\frac{1}{2}\|\boldsymbol{c}\|^2, \quad \frac{1}{2}\|\boldsymbol{u}\|^2, \quad \frac{1}{2}\|\nabla\boldsymbol{u}\|^2, \quad \ldots .$$

As in the finite dimensional case, we can define a Finite Difference Method to solve this optimization problem. Its details and subsequent advantages and inconveniences are similar in both cases and we shall not develop this method again in the continuous case.

Let us however discuss in more detail the Direct Differentiation and the Adjoint Method.

**Direct Differentiation Method.** We had previously started this method by differentiation of the cost functional for each component $c_i$ $(i = 1, \ldots, n)$ of $\boldsymbol{c}$:

$$\nabla_{c_i}\mathcal{J}(\boldsymbol{c}, \boldsymbol{u}(c_i)) = \frac{\partial\mathcal{J}}{\partial c_i}(\boldsymbol{c}, \boldsymbol{u}(\boldsymbol{c})) + \frac{\partial\mathcal{J}}{\partial\boldsymbol{u}}(\boldsymbol{c}, \boldsymbol{u}(\boldsymbol{c})) \cdot \frac{d\boldsymbol{u}}{dc_i}, \tag{4.29}$$

and the objective was to compute:

$$\frac{d\boldsymbol{u}}{d\boldsymbol{c}} = \left(\frac{d\boldsymbol{u}}{dc_1}, \frac{d\boldsymbol{u}}{dc_2}, \ldots, \frac{d\boldsymbol{u}}{dc_n}\right). \tag{4.30}$$

Exactly as in the discrete case, one can differentiate the direct problem, and obtain a series of $n$ problems defining the displacement fields $\dfrac{d\boldsymbol{u}}{dc_i}(\boldsymbol{c})$:

$$\mathrm{div}\left(\boldsymbol{C}(\boldsymbol{c}) : \nabla\frac{d\boldsymbol{u}}{dc_i}(\boldsymbol{c})\right) + \mathrm{div}\,\frac{d\boldsymbol{C}}{dc_i}(\boldsymbol{c})\nabla\boldsymbol{u}(\boldsymbol{c}) + \frac{d\boldsymbol{f}}{dc_i}(\boldsymbol{c}) = 0 \quad \forall\boldsymbol{x} \in \Omega, \tag{4.31}$$

$$\frac{d\boldsymbol{\sigma}}{dc_i}(\boldsymbol{c}) \cdot \boldsymbol{n} = \left(\boldsymbol{C}(\boldsymbol{c}) : \nabla\frac{d\boldsymbol{u}}{dc_i}(\boldsymbol{c})\right) \cdot \boldsymbol{n} = \frac{d\boldsymbol{\varphi}}{dc_i}(\boldsymbol{c}) \quad \forall\boldsymbol{x} \in \partial\Omega, \tag{4.32}$$

where $\boldsymbol{u}(\boldsymbol{c})$ is still the solution of the direct problem with parameters $\boldsymbol{c}$ which are supposed to be known in the differentiated problems. Therefore

we consider the term:

$$\operatorname{div} \frac{d\boldsymbol{C}}{dc_i}(\boldsymbol{c})\nabla \boldsymbol{u}(\boldsymbol{c})$$

as a given additional force term, acting as another force.

We conclude about the *Direct Differentiation Method* in the infinite dimensional case by noting that:

- The method is based on solving $n+1$ additional problems and yields a mathematical exact gradient of all the fields.
- One of the additional equations (4.31) is defined by the same elastic moduli as the direct problem and will conduct after discretization to equations with the same stiffness matrix, confirming the results obtained before.

**Exercise:** *Derive the variational formulation for the differentiated equations first by:*

- *direct integration of equations (4.31) and (4.32),*
- *differentiation of the variational formulation of the direct problem.*

**Adjoint State Method.** We stated in the finite dimensional case that the adjoint state method starts from the remark that finding the minimum of constrained functional is equivalent to finding the saddle point of an augmented (Lagrangian) functional. In the continuous case the Lagrangian is given by:

$$\mathcal{L}(\boldsymbol{c}, \boldsymbol{u}, \boldsymbol{u}^*) = \mathcal{J}(\boldsymbol{c}, \boldsymbol{u}) + \int_\Omega \nabla \boldsymbol{u} : \boldsymbol{C}(\boldsymbol{c})\nabla \boldsymbol{u}^* \, dv - \int_\Omega \boldsymbol{f}(\boldsymbol{c}) \cdot \boldsymbol{u}^* \, dv - \int_\Omega \boldsymbol{\varphi}(\boldsymbol{c}) \cdot \boldsymbol{u}^* \, ds. \quad (4.33)$$

The Lagrangian is actually formed by adding to the cost functional the expression of the variational formulation of direct problem. The field $\boldsymbol{u}^*$ acts therefore as a Lagrange multiplier for the constraint and is actually a test function associated with the variational formulation of the direct problem. Similarly to the finite dimensional case we assume that the variables $(\boldsymbol{c}, \boldsymbol{u}, \boldsymbol{u}^*)$ are independent.

If we use the general integral form of the cost functional we obtain the following expression:

$$\mathcal{L}(\boldsymbol{c},\boldsymbol{u},\boldsymbol{u}^*) = \int_\Omega \mathrm{j}_\Omega(\boldsymbol{c},\boldsymbol{u})\,dv + \int_{\partial\Omega} \mathrm{j}_{\partial\Omega}(\boldsymbol{c},\boldsymbol{u})\,ds + \int_\Omega \nabla\boldsymbol{u} : \boldsymbol{C}(\boldsymbol{c})\nabla\boldsymbol{u}^*\,dv - \int_\Omega \boldsymbol{f}(\boldsymbol{c})\cdot\boldsymbol{u}^*\,dv - \int_\Omega \boldsymbol{\varphi}(\boldsymbol{c})\cdot\boldsymbol{u}^*\,ds. \quad (4.34)$$

The saddle point of the Lagrangian $\mathcal{L}$ is characterized by vanishing of the gradient:

$$\langle\frac{\partial\mathcal{L}}{\partial\boldsymbol{u}^*},\boldsymbol{v}^*\rangle = 0 \qquad \forall\boldsymbol{v}^*, \quad (4.35)$$

$$\langle\frac{\partial\mathcal{L}}{\partial\boldsymbol{u}},\boldsymbol{v}\rangle = 0 \qquad \forall\boldsymbol{v}, \quad (4.36)$$

$$\langle\frac{\partial\mathcal{L}}{\partial\boldsymbol{c}},\boldsymbol{d}\rangle = 0 \qquad \forall\boldsymbol{d}. \quad (4.37)$$

Computing the derivatives of the Lagrangian we obtain consequently the following problems.

For the derivation with respect to $\boldsymbol{u}^*$:

$$\langle\frac{\partial\mathcal{L}}{\partial\boldsymbol{u}^*},\boldsymbol{v}^*\rangle = \int_\Omega \nabla\boldsymbol{u} : \boldsymbol{C}(\boldsymbol{c})\nabla\boldsymbol{v}^*\,dv - \int_\Omega \boldsymbol{f}(\boldsymbol{c})\cdot\boldsymbol{v}^*\,dv - \int_\Omega \boldsymbol{\varphi}(\boldsymbol{c})\cdot\boldsymbol{v}^*\,ds \qquad \forall\boldsymbol{v}^*, \quad (4.38)$$

which is actually the variational formulation of the direct problem having $\boldsymbol{v}^*$ as a test function.

For the derivation with respect to $\boldsymbol{u}$:

$$\langle\frac{\partial\mathcal{L}}{\partial\boldsymbol{u}},\boldsymbol{v}\rangle = \langle\frac{\partial\mathcal{J}}{\partial\boldsymbol{u}},\boldsymbol{v}\rangle + \int_\Omega \nabla\boldsymbol{v} : \boldsymbol{C}(\boldsymbol{c}) : \nabla\boldsymbol{u}^*\,dv = 0 \qquad \forall\boldsymbol{v}. \quad (4.39)$$

Using the general form of the cost functional we obtain the following variational equation:

$$\int_\Omega \frac{\partial\mathrm{j}_\Omega}{\partial\boldsymbol{u}}(\boldsymbol{c},\boldsymbol{u})\cdot\boldsymbol{v}\,dv + \int_{\partial\Omega} \frac{\partial\mathrm{j}_{\partial\Omega}}{\partial\boldsymbol{u}}(\boldsymbol{c},\boldsymbol{u})\cdot\boldsymbol{v}\,ds + \int_\Omega \nabla\boldsymbol{v} : \boldsymbol{C}(\boldsymbol{c}) : \nabla\boldsymbol{u}^*\,dv = 0 \qquad \forall\boldsymbol{v}. \quad (4.40)$$

After integration by parts of the last expression we obtain the following problem for the adjoint field $\boldsymbol{u}^*$, denoted as the *adjoint problem*:

$$\operatorname{div} \boldsymbol{C}(\boldsymbol{c})\nabla \boldsymbol{u}^* - \frac{\partial \mathrm{j}_\Omega}{\partial \boldsymbol{u}}(\boldsymbol{c}, \boldsymbol{u}) = 0, \tag{4.41}$$

$$\boldsymbol{\sigma}^* \cdot \boldsymbol{n} = (\boldsymbol{C}(\boldsymbol{c}) : \nabla \boldsymbol{u}^*) \cdot \boldsymbol{n} = \frac{\partial \mathrm{j}_{\partial\Omega}}{\partial \boldsymbol{u}}(\boldsymbol{c}, \boldsymbol{u}). \tag{4.42}$$

We observe that the adjoint field is defined by body forces and surface tractions equal to the derivatives of the cost functional. In the case of least square cost functional, these terms represent actually the distance between the measurement and the solution of the direct problem.

The derivation of the Lagrangian with respect to the parameters $\boldsymbol{c}$ gives:

$$\langle \frac{\partial \mathcal{L}}{\partial \boldsymbol{c}}, \boldsymbol{d} \rangle = \langle \frac{\partial \mathcal{J}}{\partial \boldsymbol{c}}, \boldsymbol{d} \rangle + \int_\Omega \nabla \boldsymbol{u} : [\frac{\partial \boldsymbol{C}}{\partial \boldsymbol{c}}(\boldsymbol{c}) \cdot \boldsymbol{d}] : \nabla \boldsymbol{u}^* \, dv$$
$$- \int_\Omega [\frac{\partial \boldsymbol{f}}{\partial \boldsymbol{c}}(\boldsymbol{c}) \cdot \boldsymbol{d}] \cdot \boldsymbol{u}^* \, dv - \int_\Omega [\frac{\partial \boldsymbol{\varphi}}{\partial \boldsymbol{c}}(\boldsymbol{c}) \cdot \boldsymbol{d}] \cdot \boldsymbol{u}^* \, ds = 0 \qquad \forall \boldsymbol{d}. \tag{4.43}$$

Using the general form of the cost functional $\mathcal{J}$ we get

$$\langle \frac{\partial \mathcal{L}}{\partial \boldsymbol{c}}, \boldsymbol{d} \rangle = \int_\Omega \frac{\partial \mathrm{j}_\Omega}{\partial \boldsymbol{c}}(\boldsymbol{c}, \boldsymbol{u}) \cdot \boldsymbol{d} \, dv + \int_{\partial\Omega} \frac{\partial \mathrm{j}_{\partial\Omega}}{\partial \boldsymbol{c}}(\boldsymbol{c}, \boldsymbol{u}) \cdot \boldsymbol{d} \, ds + \int_\Omega \nabla \boldsymbol{u} : [\frac{\partial \boldsymbol{C}}{\partial \boldsymbol{c}}(\boldsymbol{c}) \cdot \boldsymbol{d}] : \nabla \boldsymbol{u}^* \, dv$$
$$- \int_\Omega [\frac{\partial \boldsymbol{f}}{\partial \boldsymbol{c}}(\boldsymbol{c}) \cdot \boldsymbol{d}] \cdot \boldsymbol{u}^* dv - \int_\Omega [\frac{\partial \boldsymbol{\varphi}}{\partial \boldsymbol{c}}(\boldsymbol{c}) \cdot \boldsymbol{d}] \cdot \boldsymbol{u}^* \, ds = 0 \qquad \forall \boldsymbol{d}. \tag{4.44}$$

If $\boldsymbol{u}$ is the solution of the *direct problem* and $\boldsymbol{u}^*$ is the solution of the *adjoint problem*, the last equation expresses the total variation of the cost functional $\mathcal{J}$ in the direction $\boldsymbol{d}$, i.e.,

$$\langle \nabla_{\boldsymbol{c}} \mathcal{J}(\boldsymbol{c}), \boldsymbol{d} \rangle = \langle \frac{\partial \mathcal{L}}{\partial \boldsymbol{c}}, \boldsymbol{d} \rangle. \tag{4.45}$$

We see that it provides the explicit computation of the gradient $\nabla_{\boldsymbol{c}} \mathcal{J}(\boldsymbol{c})$ from $\boldsymbol{u}$ and $\boldsymbol{u}^*$. The practical interest of this formula comes from its complete independence of the number of parameters $\boldsymbol{c}$.

As in the finite dimensional case we conclude that:

- The gradient computed through the adjoint state method is exact.
- The gradient computation requires the solution of a *single additional equation.*

- The adjoint problem is defined by the same elastic moduli. This means that for solving the adjoint problem we consider the same system as in the direct problem with only different loading parameters.
- The *complete* solution of the saddle point of the Lagrangian provides directly, i.e. without any minimization procedure, the solution of the optimization problem. A solution of this type in the case of the steady state heat equation is presented in [9].

**Exercise:** *Compute the Lagrangian and the corresponding adjoint problem for the a steady state heat equation for:*

- $\partial\Omega = \partial\Omega_m \bigcup \partial\Omega_u$ *and* $\partial\Omega_m \bigcap \partial\Omega_u = \emptyset$,
- *overdetermined (measured) boundary conditions on* $\partial\Omega_m$*:*

$$\theta|_{\partial\Omega_m} = \theta^m \qquad \boldsymbol{q}|_{\partial\Omega_m} = -k\frac{\partial\theta}{\partial\boldsymbol{n}} = \boldsymbol{q}^m,$$

- *unknown boundary conditions on* $\partial\Omega_u$,
- *consider the following cost functional including a regulatisation term*

$$\mathcal{J}(\theta) = \frac{1}{2}\int\limits_{\partial\Omega_m} \|\theta - \theta^m\|^2\, dv + \frac{1}{2}\int\limits_{\partial\Omega_u} \|\theta\|^2\, dv.$$

**Exercise:** *Generalize the preceding problem to the case of an transient heat equation.*
*Remark: The terms of the cost functional and of variational formulation will also contain a time integration.*
*Hint: The resulting adjoint problem is a backward heat equation!*

### 4.2.3. Contact boundary conditions

In a series of practical problems, like the indentation problem, one has to consider contact boundary conditions. In such a case the variational formulation of the direct problem does not conduct to a variational equality, but to a variational inequality and therefore the direct differentiation and the adjoint state method cannot be applied directly similarly to the preceding Section in solving various inverse problems.

Now we present the indentation of an elastic body with a rigid indentor and discuss the identification of elastic parameters from the measured indentation depth and force. The solution method used is the adjoint state method and we shall present the main steps and results, indicating that a complete presentation is given in [11, 12].

**The direct contact problem.** Let us consider an axisymmetric body, with its section occupying in its reference configuration an open subset $\Omega \subset \mathbb{R}^2$ with smooth boundary $\Gamma$ (see Fig. 4.3). The boundary is partitioned into three parts: $\Gamma = \Gamma_D \cup \Gamma_F \cup \Gamma_C$; on $\Gamma_D$ displacements are imposed, $\Gamma_F$ is the free surface, and $\Gamma_C$ is the surface of potential contact. $\Gamma_C^{\text{eff}} \subset \Gamma_C$ denotes the effective contact area for a given indentation depth.

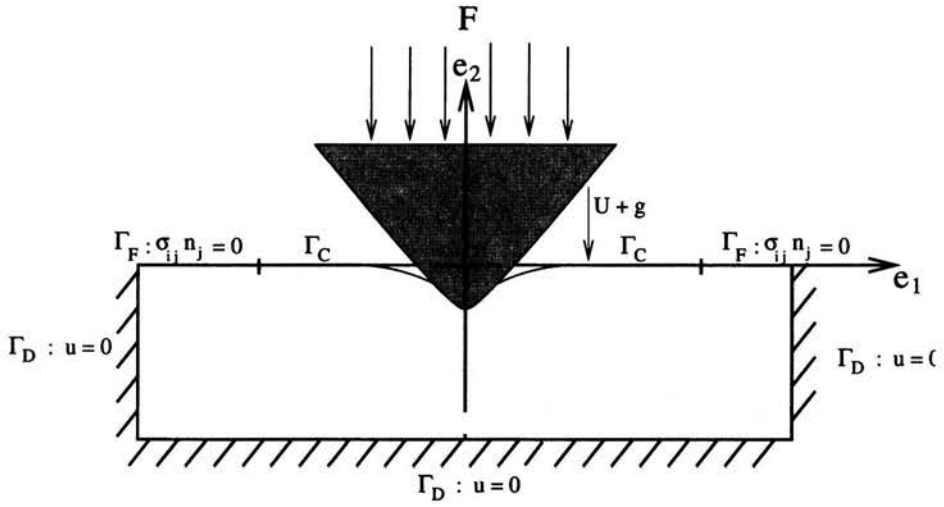


FIGURE 4.3. Indentation test (direct problem ($\mathcal{P}$)).

The problem considered in the sequel is the frictionless indentation of $\Omega$ by a rigid punch with a profile characterized by the gap $g$ (i.e. the distance between the punch and the surface $\Gamma_C$). The difficulties of the contact problem are given by the fact that the effective contact region $\Gamma_C^{\text{eff}}$ is not known in advance. For a complete mathematical presentation of the contact problems see [13].

We shall consider the real and the virtual displacement fields $\boldsymbol{u}$, $\boldsymbol{v}$ in the following functional space:

$$\boldsymbol{V} = \{\boldsymbol{v} \in (H^1(\Omega))^2 \mid \boldsymbol{u} = \boldsymbol{0} \text{ on } \Gamma_D\}. \tag{4.46}$$

Under the assumptions of small strains and of an elastic constitutive law, the displacement vector, the second-order strain and stress tensors satisfy

the following set of equations:

$$\boldsymbol{\varepsilon}(\boldsymbol{u}) = \frac{1}{2}(\nabla \boldsymbol{u} + \nabla^T \boldsymbol{u}), \tag{4.47}$$

$$\boldsymbol{\sigma}(\boldsymbol{u}) = \boldsymbol{A}(\boldsymbol{c}) : \boldsymbol{\varepsilon}(\boldsymbol{u}), \tag{4.48}$$

where $\boldsymbol{C}(\boldsymbol{c})$ is the fourth-order tensor of elastic moduli depending on a vector of material parameters $\boldsymbol{c} \in \boldsymbol{L}$, a closed subset of $\mathbb{R}^n$ ($n \geq 1$). The stress tensor $\boldsymbol{\sigma}$ satisfies the equilibrium equation:

$$\operatorname{div} \boldsymbol{\sigma}(\boldsymbol{u}) = \boldsymbol{0}. \tag{4.49}$$

In the *direct Problem* $(\mathcal{P})$ one will determine the complete solution $(\boldsymbol{u}, \boldsymbol{\varepsilon}, \boldsymbol{\sigma})$ from a given indentation depth $U$ or the corresponding resultant indentation force $F$. The resultant indentation force can be directly calculated as the sum of the contact pressure:

$$F = \int_{\Gamma_C} \boldsymbol{n} \cdot \boldsymbol{\sigma}(\boldsymbol{u}) \cdot \boldsymbol{n} \, d\Gamma. \tag{4.50}$$

**The inverse problem.** The inverse problem, corresponds to the identification of the material properties $\boldsymbol{c}$ from a displacement-force measurement curve $(U^{\exp}(t), F^{\exp}(t))$ pertaining to the indenter.

The identification problem will be considered in the form:

$$\textit{Find } \boldsymbol{c} \textit{ minimising the cost functional } \mathcal{J}(\boldsymbol{c}), \tag{4.51}$$

where $\mathcal{J}$ represents the cost functional involving measured and calculated quantities. Different cost functionals can be imagined:

- difference between measured and calculated forces $F^{\exp}$, $F$ for given material parameter $\boldsymbol{c}$ and prescribed indentation depth $U^{\exp}$:

$$\mathcal{J}(\boldsymbol{c}) = \frac{1}{2}(F - F^{\exp})^2, \tag{4.52}$$

- difference between measured and calculated displacements $U^{\exp}$, $U$ for imposed indentation force $F^{\exp}$:

$$\mathcal{J}(\boldsymbol{c}) = \frac{1}{2}(U - U^{\exp})^2, \tag{4.53}$$

- reciprocity gap, i.e, crossed difference between calculated and measured forces and displacements:

$$\mathcal{J}(\boldsymbol{c}) = (U^{\text{exp}} - U)(F - F^{\text{exp}}). \tag{4.54}$$

If the preceding cost functionals have been defined for a single definite indentation depth, one can imagine also cost functionals as sums or time integrals of these quantities. Next we shall consider simple cost functionals based on the least square difference between calculated and experimental forces (4.52).

In order to apply the adjoint state method to solve the constrained minimization problem associated with the identification problem defined before we recall three classical variational formulations of the frictionless contact problem between a rigid punch of arbitrary shape and an elastic foundation. This mathematical problem is known as the Signorini problem and for a detailed presentation the reader is referred to the monography by Kikuchi and Oden [13]).

**Primal formulation ($\mathcal{P}$).** This problem is driven by the indentation depth $U^{\text{exp}}$ and is written as follows:

$$\begin{aligned} &\textit{Find } \boldsymbol{u} \in \boldsymbol{K} \textit{ such that } \int_{\Omega} \boldsymbol{\sigma}(\boldsymbol{u}) : \boldsymbol{\varepsilon}(\boldsymbol{v} - \boldsymbol{u})\, d\Omega \geq 0 \\ &\qquad \forall \boldsymbol{v} \in \boldsymbol{K} = \{\boldsymbol{v} \in \boldsymbol{V} \mid v_2 \leq g + U^{\text{exp}} \textit{ on } \Gamma_C\}. \end{aligned} \tag{4.55}$$

The resultant force $F$ on the indenter is calculated from the solution $\boldsymbol{u}$ of the contact problem by:

$$F = \int_{\Gamma_C} \sigma_{22}(\boldsymbol{u})\, d\Gamma. \tag{4.56}$$

Within this formulation, the contact conditions are directly imposed on the solution $\boldsymbol{u}$ by searching it in the closed convex set $\boldsymbol{K}$. This causes a certain number of difficulties from a numerical point of view and therefore equivalent formulations on vector spaces are preferred.

**Penalized formulation ($\mathcal{P}_\epsilon$).** For an arbitrary small $\epsilon > 0$, we consider the problem:

*Find $\boldsymbol{u}_\epsilon \in \boldsymbol{V}$ such that*

$$\int_\Omega \boldsymbol{\sigma}(\boldsymbol{u}_\epsilon) : \boldsymbol{\varepsilon}(\boldsymbol{v})\, d\Omega + \frac{1}{2\epsilon} \int_{\Gamma_C} \langle u_{\epsilon 2} - g - U^{\exp} \rangle_+^2 v_2\, d\Gamma = 0 \quad \forall \boldsymbol{v} \in \boldsymbol{V}, \quad (4.57)$$

where $\langle\, . \,\rangle_+$ denotes the positive part.

The reaction force $F_\epsilon$ on the punch is determined by:

$$F_\epsilon = -\frac{1}{2\epsilon} \int_{\Gamma_C} \langle u_{\epsilon 2} - U^{\exp} - g \rangle_+^2\, d\Gamma. \quad (4.58)$$

In this case one can consider, in a rough interpretation, that the contact conditions are replaced by a nonlinear contact force proportional to the allowed interpenetration and inverse proportional to $\epsilon$. Some convergence properties are proven: $\boldsymbol{u}_\epsilon$ converges strongly to $\boldsymbol{u}$ in $\boldsymbol{V}$ and $F_\epsilon$ converges to $F$ in $\mathbb{R}$. Formally, this means that, as $\epsilon \to 0$, the solution to the penalized problem $(\mathcal{P}_\epsilon)$ converges to the solution to the primal problem $(\mathcal{P})$.

**Mixed formulation ($\mathcal{P}_m$).** This formulation has the following form:

*Find $(\boldsymbol{u}, p) \in \boldsymbol{V} \times \boldsymbol{N}$ such that:*

$$\begin{aligned} &\int_\Omega \boldsymbol{\sigma}(\boldsymbol{u}) : \boldsymbol{\epsilon}(\boldsymbol{v})\, d\Omega - \int_{\Gamma_C} p \cdot v_2\, d\Gamma = 0 \qquad \forall \boldsymbol{v} \in \boldsymbol{V}, \\ &\int_{\Gamma_C} (q - p) \cdot (u_2 - U - g)\, d\Gamma \geq 0 \qquad \forall q \in \boldsymbol{N}. \end{aligned} \quad (4.59)$$

In this case the contact condition have been relaxed by the introduction of the Lagrange multiplier $p$. The displacement field $\boldsymbol{u}$ is now supposed to belong to the vector space $\boldsymbol{V}$ and the Lagrange multipliers $p$ to the convex cone $\boldsymbol{N} = \{q \in (H^{1/2}(\Gamma_C))' \mid q \leq 0\}$, where $(\, . \,)'$ denotes the dual space.

The Lagrange multiplier $p \in \boldsymbol{N}$ shows up to be the pressure distribution under the punch. Therefore, the resultant force $F$ is determined by:

$$F = \int_{\Gamma_C} p\, d\Gamma. \quad (4.60)$$

**The adjoint state method based on the penalized formulation** $(\mathcal{P}_\epsilon^{-1})$. For a small $\epsilon > 0$, the inverse problem is expressed by:

> *Minimize* $\mathcal{J}_\epsilon = \frac{1}{2}(F_\epsilon - F^{\exp})^2$ *with respect to* $\boldsymbol{c} \in \boldsymbol{L}$, *where* $F_\epsilon$ *is calculated from the solution of* $(\mathcal{P}_\epsilon)$.

As we handle a constrained minimization problem, it is natural to introduce a Lagrangian $\mathcal{L}_\epsilon$, by adjoining to the penalized cost functional $\mathcal{J}_\epsilon$ the variational equality of the penalized direct problem $(\mathcal{P}_\epsilon)$:

$$\mathcal{L}_\epsilon(\boldsymbol{u}_\epsilon, \boldsymbol{v}_\epsilon, \boldsymbol{c}) = \frac{1}{2}(F_\epsilon - F^{\exp})^2 + \int_\Omega \boldsymbol{\sigma}(\boldsymbol{u}_\epsilon) : \boldsymbol{\varepsilon}(\boldsymbol{v}_\epsilon)\, d\Omega + \frac{1}{2\epsilon}\int_{\Gamma_C} \langle u_{\epsilon 2} - g - U^{\exp}\rangle_+^2 v_{\epsilon 2}\, d\Gamma, \quad (4.61)$$

where $F_\epsilon$ is given by (4.58) and $(\boldsymbol{u}_\epsilon, \boldsymbol{v}_\epsilon, \boldsymbol{c}) \in \boldsymbol{V}^2 \times \boldsymbol{L}$.

All variables are assumed to be mutually independent, the virtual displacement field $\boldsymbol{v}_\epsilon$ plays the role of a Lagrange multiplier. The construction of the Lagrangian ensures that the saddle point of $\mathcal{L}_\epsilon$ gives the minimum of $\mathcal{J}_\epsilon$ and that $\mathcal{L}_\epsilon \equiv \mathcal{J}_\epsilon$ if $\boldsymbol{u}_\epsilon$ is a solution to the direct problem $(\mathcal{P}_\epsilon)$.

The necessary conditions of stationarity of $\mathcal{L}$ can be formally written as:

$$(\frac{\partial \mathcal{L}_\epsilon}{\partial \boldsymbol{v}_\epsilon}, \boldsymbol{w}) = \int_\Omega \boldsymbol{\sigma}(\boldsymbol{u}_\epsilon) : \boldsymbol{\varepsilon}(\boldsymbol{w})\, d\Omega + \frac{1}{2\epsilon}\int_{\Gamma_C} \langle u_{\epsilon 2} - g - U^{\exp}\rangle_+^2 w_2\, d\Gamma = 0 \qquad \forall \boldsymbol{w} \in \boldsymbol{V}, \quad (4.62)$$

$$(\frac{\partial \mathcal{L}_\epsilon}{\partial \boldsymbol{u}_\epsilon}, \boldsymbol{w}) = \int_\Omega \boldsymbol{\sigma}(\boldsymbol{v}_\epsilon) : \boldsymbol{\varepsilon}(\boldsymbol{w})\, d\Omega + \frac{1}{\epsilon}\int_{\Gamma_C} \langle u_{\epsilon 2} - g - U^{\exp}\rangle_+ w_2 (v_{\epsilon 2} - (F_\epsilon - F^{\exp}))\, d\Gamma = 0 \qquad \forall \boldsymbol{w} \in \boldsymbol{V}, \quad (4.63)$$

$$[\frac{\partial \mathcal{L}_\epsilon}{\partial \boldsymbol{c}}, \boldsymbol{d} - \boldsymbol{c}] = \int_\Omega \boldsymbol{\varepsilon}(\boldsymbol{u}_\epsilon) : \frac{\partial \boldsymbol{A}}{\partial \boldsymbol{c}} : \boldsymbol{\varepsilon}(\boldsymbol{v}_\epsilon) \cdot (\boldsymbol{d} - \boldsymbol{c})\, d\Omega \geq 0 \qquad \forall \boldsymbol{d} \in \boldsymbol{L}, \quad (4.64)$$

where $(.,.)$ and $[.,.]$ are, respectively, the duality pairing on $\boldsymbol{V}' \times \boldsymbol{V}$ and $\boldsymbol{L}' \times \boldsymbol{L}$.

As expected, the derivation of the Lagrangian with respect to the adjoint variable $\boldsymbol{v}_\epsilon$ (4.62) yields the variational formulation of the penalized direct problem. The derivation of the Lagrangian with respect to the direct variable $\boldsymbol{u}_\epsilon$ (4.63) yields the weak formulation of elastic problem, called the penalized adjoint problem $(\boldsymbol{\mathcal{P}}_\epsilon^{\text{adj}})$.

Let us choose a point $(\boldsymbol{u}_\epsilon, \boldsymbol{v}_\epsilon, \boldsymbol{c})$. If $\boldsymbol{u}_\epsilon$ is solution of $(\boldsymbol{\mathcal{P}}_\epsilon)$, by definition of $\mathcal{L}_\epsilon$, we have $\mathcal{L}_\epsilon \equiv \mathcal{J}_\epsilon$. Moreover, if $\boldsymbol{v}_\epsilon$ is solution of $(\boldsymbol{\mathcal{P}}_\epsilon^{\text{adj}})$ it follows that:

$$\nabla_{\boldsymbol{c}} \mathcal{J}_\epsilon = \frac{\partial \mathcal{L}_\epsilon}{\partial \boldsymbol{c}} = \int_\Omega \boldsymbol{\varepsilon}(\boldsymbol{u}_\epsilon) : \frac{\partial \boldsymbol{A}}{\partial \boldsymbol{c}} : \boldsymbol{\varepsilon}(\boldsymbol{v}_\epsilon)\, d\Omega. \tag{4.65}$$

Thus the explicit expression of the gradient of $\mathcal{J}_\epsilon$ has been obtained using the solution to the direct and the adjoint penalized problems.

The previous result has been established by applying the penalized formulation. It is interesting to know how it evolves as $\epsilon \to 0$. Without giving a precise mathematical proof, the following results can be conjectured:

- The solution $\boldsymbol{v}_\epsilon$ to the penalized adjoint problem $(\boldsymbol{\mathcal{P}}_\epsilon^{\text{adj}})$ converges to the solution $\boldsymbol{v}$ to the adjoint problem $(\boldsymbol{\mathcal{P}}^{\text{adj}})$ driven by the imposed displacements $(F - F^{\text{exp}})$ on the effective contact surface $\Gamma_C^{\text{eff}}$:

$$\begin{aligned} &\textit{Find } \boldsymbol{v} \in \boldsymbol{V}^{\text{adj}} \textit{ such that } \int_\Omega \boldsymbol{\sigma}(\boldsymbol{v}) : \boldsymbol{\varepsilon}(\boldsymbol{w})\, d\Omega = 0 \\ &\qquad \forall \boldsymbol{w} \in \boldsymbol{V}^{\text{adj}} = \{\boldsymbol{w} \in \boldsymbol{V} \;\mid\; w_2 = (F - F^{\text{exp}}) \textit{ on } \Gamma_C^{\text{eff}}\}. \end{aligned} \tag{4.66}$$

  Here $F$, $\Gamma_C{}^{\text{eff}}$ are, respectively, the force on the indenter and the effective contact surface, found in the direct contact problem $(\boldsymbol{\mathcal{P}})$.

- The limits and the gradient operations are commutative, i.e.,

$$\lim_{\epsilon \to 0} \nabla_{\boldsymbol{c}} \mathcal{J}_\epsilon = \nabla_{\boldsymbol{c}} (\lim_{\epsilon \to 0} \mathcal{J}_\epsilon) = \nabla_{\boldsymbol{c}} \mathcal{J}. \tag{4.67}$$

Consequently the gradient of the cost functional can be calculated using the following formula:

$$\nabla_{\boldsymbol{c}} \mathcal{J} = \int_\Omega \boldsymbol{\varepsilon}(\boldsymbol{u}) : \frac{\partial \boldsymbol{A}}{\partial \boldsymbol{c}} : \boldsymbol{\varepsilon}(\boldsymbol{v})\, d\Omega, \tag{4.68}$$

where $\boldsymbol{u}$ and $\boldsymbol{v}$ are the solutions to the direct problem $(\boldsymbol{\mathcal{P}})$ and the adjoint problem $(\boldsymbol{\mathcal{P}}^{\text{adj}})$, respectively.

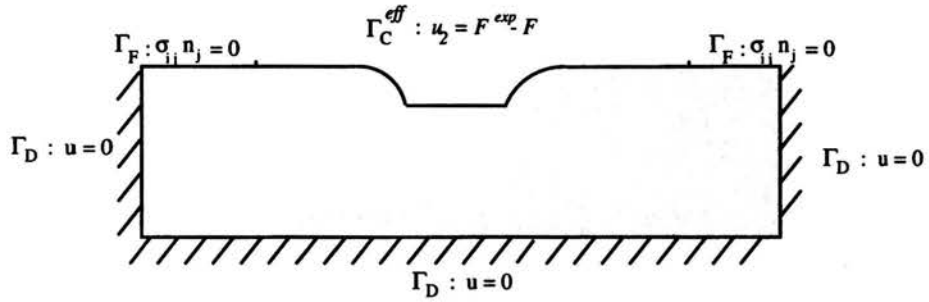


FIGURE 4.4. Adjoint problem ($\mathcal{P}^{adj}$).

**The adjoint state method based on the mixed formulation ($\mathcal{P}_m^{-1}$).** This problem reads:

> *Minimize* $\mathcal{J} = \frac{1}{2}(F - F^{exp})^2$ *with respect to* $\boldsymbol{c} \in \boldsymbol{L}$, *where* $F$ *is calculated from the solution to* $(\mathcal{P}_m)$.

The corresponding Lagrangian is expressed by:

$$\mathcal{L}(\boldsymbol{u}, \boldsymbol{v}, p, q, \boldsymbol{c}) = \frac{1}{2}(F - F^{exp})^2 - \int_\Omega \boldsymbol{\sigma}(\boldsymbol{u}) : \boldsymbol{\varepsilon}(\boldsymbol{v})\, d\Omega + \int_{\Gamma_C} p \cdot v_2\, d\Gamma + \int_{\Gamma_C} q \cdot (u_2 - U - g)\, d\Gamma, \quad (4.69)$$

where $F$ is given by (4.60), $(\boldsymbol{u}, \boldsymbol{v}, p, q, \boldsymbol{c}) \in \boldsymbol{V}^2 \times \boldsymbol{Q}^2 \times \boldsymbol{L}$ and $\boldsymbol{Q} = \{q \in (H^{1/2}(\Gamma_C))' \mid q = 0 \text{ on } \Gamma_C/\Gamma_C^{eff}\}$.

Let us note that, in contrast to the classical application of the adjoint state method, $q$ has not been sought in the closed convex $\boldsymbol{N}$. If $q$ was in $\boldsymbol{N}$, the stationarity conditions would turn out to be a set of coupled variational inequalities, which are ineffective for practical search of the adjoint state.

With $q \in \boldsymbol{Q}$, the necessary conditions of stationarity of $\mathcal{L}$ can be formally written as follows:

$$(\frac{\partial \mathcal{L}}{\partial \boldsymbol{v}}, \boldsymbol{w}) = \int_\Omega \boldsymbol{\sigma}(\boldsymbol{u}) : \boldsymbol{\varepsilon}(\boldsymbol{w})\, d\Omega - \int_{\Gamma_C} p \cdot w_2\, d\Gamma = 0 \qquad \forall \boldsymbol{w} \in \boldsymbol{V}, \quad (4.70)$$

$$(\frac{\partial \mathcal{L}}{\partial \boldsymbol{u}}, \boldsymbol{w}) = \int_\Omega \boldsymbol{\sigma}(\boldsymbol{v}) : \boldsymbol{\varepsilon}(\boldsymbol{w})\, d\Omega - \int_{\Gamma_C} q \cdot w_2\, d\Gamma = 0 \qquad \forall \boldsymbol{w} \in \boldsymbol{V}, \quad (4.71)$$

$$\{\frac{\partial \mathcal{L}}{\partial q}, s\} = \int_{\Gamma_C} s \cdot (u_2 - U - g)\, d\Gamma = 0 \qquad \forall s \in \boldsymbol{Q}, \qquad (4.72)$$

$$\{\frac{\partial \mathcal{L}}{\partial p}, s\} = \int_{\Gamma_C} s \cdot (v_2 - F^{\text{exp}} + F)\, d\Gamma = 0 \qquad \forall s \in \boldsymbol{Q}, \qquad (4.73)$$

$$[\frac{\partial \mathcal{L}}{\partial \boldsymbol{c}}, \boldsymbol{d} - \boldsymbol{c}] = \int_{\Omega} \boldsymbol{\varepsilon}(\boldsymbol{u}) : \frac{\partial \boldsymbol{A}}{\partial \boldsymbol{c}} : \boldsymbol{\varepsilon}(\boldsymbol{v}) \cdot (\boldsymbol{d} - \boldsymbol{c})\, d\Omega \geq 0 \qquad \forall \boldsymbol{d} \in \boldsymbol{L}, \qquad (4.74)$$

where $\{\,.\,,\,.\,\}$ denotes the duality pairing on $\boldsymbol{Q}' \times \boldsymbol{Q}$.

In this case, the derivation of the Lagrangian with respect to the adjoint variables $\boldsymbol{v}$ (4.70) and $q$ (4.72) does not yield the mixed formulation $(\boldsymbol{\mathcal{P}}_m)$ of the direct problem. Nevertheless, the solutions to $(\boldsymbol{\mathcal{P}}_m)$ are also solutions to (4.70) and (4.72).

The derivation of the Lagrangian with respect to the direct variables $\boldsymbol{u}$ (4.71) and $p$ (4.73) yields an equivalent formulation of the adjoint problem $(\boldsymbol{\mathcal{P}}^{\text{adj}})$ (4.66).

Therefore if $(\boldsymbol{u}, p)$ is solution to the direct problem $(\boldsymbol{\mathcal{P}})$ and $(\boldsymbol{v}, q)$ is a solution to the adjoint problem $(\boldsymbol{\mathcal{P}}^{\text{adj}})$, then (4.70)-(4.73) are satisfied. Consequently in the penalized case the gradient can be expressed by:

$$\nabla_{\boldsymbol{c}} \mathcal{J} = \frac{\partial \mathcal{L}}{\partial \boldsymbol{c}} = \int_{\Omega} \boldsymbol{\varepsilon}(\boldsymbol{u}) : \frac{\partial \boldsymbol{A}}{\partial \boldsymbol{c}} : \boldsymbol{\varepsilon}(\boldsymbol{v})\, d\Omega. \qquad (4.75)$$

**Remarks on the adjoint problem** $(\boldsymbol{\mathcal{P}}^{\text{adj}})$. For problems with Dirichlet or Neumann boundary conditions described by variational equalities, the application of the adjoint state method leads to a linear adjoint problem described by variational equalities [14, 15].

It is important to point out that, for problems described by variational inequalities, the obtained adjoint problem $(\boldsymbol{\mathcal{P}}^{\text{adj}})$ is linear with Dirichlet boundary conditions (see Fig. 4.4), and therefore described by a variational equality (4.66).

From a practical point of view, this implies that the overburden of computing the adjoint problem, and implicitly the gradient of the cost functional, is very small.

**Numerical results.** In order to asses the presented adjoint state method we shall present briefly some numerical results:

- A comparison of gradient evaluations of the cost functional $\mathcal{J}$ using the adjoint state method (ASM) and the finite difference method (FDM) is presented in Table 4.1.

TABLE 4.1. Comparison of gradients between finite difference method (FDM) and adjoint state method (ASM).

| $E^{\exp}$ | $E$ | $\nabla\mathcal{J}(E)$ | $\nabla\mathcal{J}(E)$ |
|---|---|---|---|
| GPa | GPa | ASM | FDM |
| 200 | 100 | −34.609 | −34.607 |
| 200 | 170 | −10.383 | −10.380 |
| 200 | 300 | 34.609 | 34.614 |
| 200 | 230 | 10.383 | 10.387 |
| 20 | 10 | −3.461 | −3.461 |
| 20 | 30 | 3.461 | 3.461 |

- Identifications have been performed in the case of a cylinder composed of two perfectly bonded elastic coatings. The thickness of the coating has been considered as a priori known and only the values of the two Young's moduli, i.e. $\boldsymbol{c} = (E_1, E_2)$, have been identified from simulated measurements. Two cost functionals were defined as follows:

$$\mathcal{J}_1(c_1, c_2) = \frac{1}{2}(F - F_1^{\exp})^2, \qquad \mathcal{J}_2(c_1, c_2) = \frac{1}{2}(F - F_2^{\exp})^2,$$

and the minimization has been done by alternating the minimization between the two cost functionals. As such, we have directly used the different sensitivities of the cost functionals with respect to the two parameters (see Fig. 4.5).
The real, starting and final identified values of the parameters are presented in Table 4.2.

TABLE 4.2. Identification results for the bimaterial.

| Starting | Final | Reference |
|---|---|---|
| $(E_1, E_2)$ | $(E_1, E_2)$ | $(E_1, E_2)$ |
| ($10^5$ MPa) | ($10^5$ MPa) | ($10^5$ MPa) |
| (0.4, 0.4) | (1.200, 2.801) | (1.200, 2.800) |
| (0.4, 4.0) | (1.200, 2.801) | (1.200, 2.800) |
| (4.0, 0.4) | (1.200, 2.799) | (1.200, 2.800) |
| (4.0, 4.0) | (1.200, 2.799) | (1.200, 2.800) |

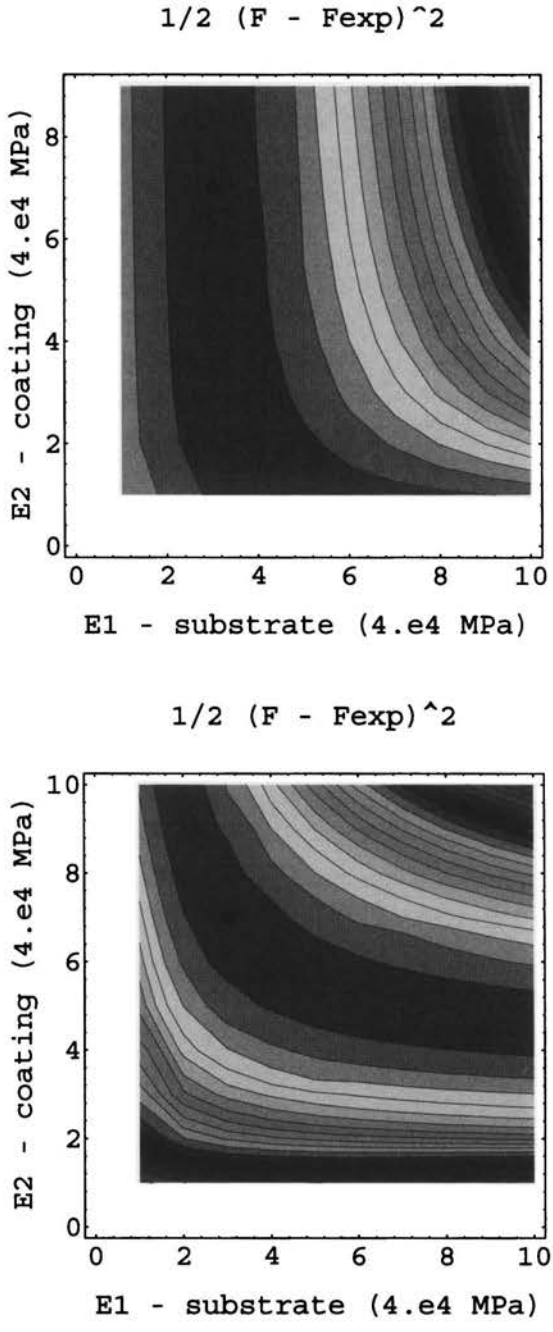


FIGURE 4.5. Contourplots of $\mathcal{J}_1$ for a deep ($U^{\text{exp}} = 0.2\,\text{mm}$) and $\mathcal{J}_2$ for a small indentation ($U^{\text{exp}} = 2.0\,\text{mm}$).

## 4.3. Notes

A list of further references concerning both linear and nonlinear material behaviour is given at the end of the next Chapter.

## 4.4. References


1. M. BONNET, H.D. BUI, and A. CONSTANTINESCU, Principes variationnels et exploitation de mesures de champs en élasticité, *Séminaire Mésures de Champs, Clermont Ferrand, 29 avril 2002*, 2002.

2. M. BONNET, H.D. BUI, and A. CONSTANTINESCU, Principes variationnels et exploitation de mesures de champs en élasticité, *Mécaniques et Industries*, 2002.

3. D.B. FOGEL, *Evolutionary Computations: Towards a New Philosophy of Machine Intelligence*, IEEE Press, 1995.

4. D.E. GOLDBERG, *Genetic Algorithms in Search, Optimization and Machine Learning*, Addison Weslay, 1989.

5. R. FLETCHER, *Practical Methods of Optimization*, John Wiley & Sons, New York, 1987.

6. G.H. GOLUB and C.H. VAN LOAN, *Practical Methods of Optimization*, John Wiley & Sons, New York, 1987.

7. D. BERTSEKAS, *Linear Network Optimization*, MIT Press, Cambridge Massachusetts, 1991.

8. A. CONN, N.I.M. GOULD, and PH.L. TOINT, *Lancelot: a Fortran package for large scale optimization*, Springer Verlag, Heidelberg, Berlin, New York, 1992.

9. B. DELATTRE, D. IVALDI, and C. STOLZ, Identification du chargement thermique par contrôle optimal, *Rev. Eur. Elèments Finis*, 2002.

10. P. MICHALERIS and D.A. TORTORELLI, Design sensitivity analysis: an overview and review, *Inverse Problems in Engineering*, 1, 1995.

11. N. TARDIEU and A. CONSTANTINESCU On the determination of elastic coefficients from indentation experiments, *Inverse Problems*, 16(3):577–588, 2000.

12. N. TARDIEU *Identification de Lois de Comportement Élastoviscoplastique par Indentation*, Ph.D. thesis, Ecole Polytechnique, France, 2000.

13. N. KIKUCHI and J.T. ODEN, *Contact Problems in Elasticity: A Study of Variational Inequalities and Finite Element Methods*, SIAM, Philadelphia, 1984.

14. L. BOURGEOIS, *Contrôle Optimal et Problèmes Inverses en Plasticité*, Ph.D. thesis, Ecole Polytechnique, France, 1997.

15. H.D. BUI, *Introduction aux Problèmes Inverses en Mécanique des Matériaux*, Eyrolles, Paris / CRC Roca Baton, 1993.

# Chapter 5

# Sensitivity computations: nonlinear case

In this chapter we shall not get into all details of the sensitivity computations for a nonlinear material behaviour. We shall only briefly present the class of standard generalized materials [1, 2] of the Perzyna type [3] and then discuss the two main types of sensitivity computations:

- *Direct Differentiation Method*
  The direct differentiation method will be illustrated in the case of parameters identification of a rock mass from measurements around a tunnel [4].
- *Adjoint State Method*
  The adjoint state method will be illustrated in the case of identification of constitutive parameters aluminum from anisothermal traction compression experiments [5] and for parameters of various materials from indentation experiments [6, 7, 8].

We would also like to emphasize that a series of other research teams have been working on these subjects and that the techniques and developments are similar even if the application are different. A short list is briefly discussed in Sec. 5.2 at the end of the Chapter.

## 5.1. Standard generalized material behaviour

We pass now to generalized materials without work hardening [1, 2]. This constitutive behaviour is completely determined by the elastic compliance tensor $\boldsymbol{S}(\boldsymbol{c})$ and by the pseudo-potential of dissipation $\Phi = \Phi(\boldsymbol{\sigma}, \boldsymbol{c})$. The latter is assumed to be twice differentiable with respect to $\boldsymbol{\sigma}$. $\boldsymbol{c}$ is the vector of the material parameters characterizing the material behaviour (Young's modulus, elasticity limit, etc.).

*Time continuous expression*

In the time continuous description, the constitutive law is expressed by the classical set of equations:

$$\boldsymbol{\varepsilon}(\dot{\boldsymbol{u}}) = \boldsymbol{S}(\boldsymbol{c}) : \dot{\boldsymbol{\sigma}} + \dot{\boldsymbol{\varepsilon}}^{\mathrm{p}}, \tag{5.1}$$

$$\dot{\boldsymbol{\varepsilon}}^{\mathrm{p}} = \frac{\partial \Phi(\boldsymbol{\sigma}, \boldsymbol{c})}{\partial \boldsymbol{\sigma}}, \tag{5.2}$$

where the dot $\dot{}$ denotes the time derivative and $\boldsymbol{\varepsilon}^{\mathrm{p}}$ is the viscoplastic strain.

*Time discretized expression*

In a time discretization, the previous equations are expressed as:

$$\boldsymbol{\varepsilon}(\Delta \boldsymbol{u}_i) = \boldsymbol{S} : \Delta \boldsymbol{\sigma}_i + \Delta \boldsymbol{\varepsilon}_i^{\mathrm{p}}, \tag{5.3}$$

$$\Delta \boldsymbol{\varepsilon}_i^{\mathrm{p}} = \frac{\partial \Phi(\boldsymbol{\sigma}_i, \boldsymbol{c})}{\partial \boldsymbol{\sigma}} \Delta t. \tag{5.4}$$

*Examples*

The following classical constitutive laws can be expressed under this formalism:

- The Maxwell viscoelastic material: the pseudo potential $\Phi$ is given by

$$\Phi(\boldsymbol{\sigma}_i, \boldsymbol{c}) = \frac{1}{2} \boldsymbol{\sigma}_i : \boldsymbol{M} : \boldsymbol{\sigma}_i,$$

  where $\boldsymbol{M}$ is a fourth-order tensor. The plastic strain increment is determined by

$$\Delta \boldsymbol{\varepsilon}_i^{\mathrm{p}} = \boldsymbol{M} : \boldsymbol{\sigma}_i \, \Delta t.$$

- The Norton–Hoff viscoplastic material: the pseudo potential $\Phi$ is given by

$$\Phi(\boldsymbol{\sigma}_i, \boldsymbol{c}) = \frac{K}{m+1} \langle \frac{(\boldsymbol{\sigma}_i)_{\mathrm{eq}} - \sigma^Y}{K} \rangle_+^{m+1},$$

where $\sigma^Y$ is the elasticity limit, $\langle \cdot \rangle_+$ denotes the positive part of function and $(\cdot)_{\text{eq}}$ is the equivalent Mises stress. The plastic strain increment is determined by:

$$\Delta\varepsilon_i^{\text{p}} = \frac{3}{2}\langle\frac{(\sigma_i)_{\text{eq}} - \sigma^Y}{K}\rangle_+^m \frac{\tilde{\boldsymbol{\sigma}}_i}{(\sigma_i)_{\text{eq}}}\Delta t,$$

where $\tilde{\boldsymbol{\sigma}}_i$ is the deviator of $\boldsymbol{\sigma}_i$.

**Equations of the direct problem ($\mathcal{P}$).** The governing equations of the direct problem consist of the equilibrium and constitutive equations, the boundary conditions and a set of initial values for the different fields. In the time-discretized formulation the *equilibrium and constitutive equation in* $\Omega$ have the following form:

$$\text{div}(\Delta\boldsymbol{\sigma}_i) = 0, \tag{5.5}$$

$$\boldsymbol{\varepsilon}(\Delta\boldsymbol{u}_i) = \boldsymbol{S} : \Delta\boldsymbol{\sigma}_i + \frac{\partial\Phi(\boldsymbol{\sigma}_i, \boldsymbol{c})}{\partial\boldsymbol{\sigma}}\Delta t. \tag{5.6}$$

### 5.1.1. Example: rock mass identification around a tunnel

In this Section we will briefly revisit the mathematical formulas developed in [4] for the direct differentiation approach applied to the identification of constitutive parameters of a rock mass around a tunnel. The input measurements pertain to displacement and pressure around the tunnel. The model involves all the construction steps of the tunnel: excavation, installation of the lining and functioning.

**The direct problem ($\mathcal{P}$).** Before excavation, at time $t = 0$, we assume that the rock mass is in its natural state given by the initial statically admissible stress state:

$$\boldsymbol{\sigma} = \boldsymbol{\sigma}_0 \tag{5.7}$$

and that all the other mechanical fields are equal to zero. The evolution of the rock mass is described by the following system of equations, written in rate form as:

- Balance equation on $\Omega \times T$ and imposed tractions on the boundary on $\Gamma_t \times T$:

$$\begin{cases} \text{div}\dot{\boldsymbol{\sigma}} + \dot{\boldsymbol{f}} = 0, \\ \dot{\boldsymbol{\sigma}}\boldsymbol{n} = \dot{\boldsymbol{t}}^d. \end{cases} \tag{5.8}$$

- Small strain equations on $\Omega \times T$ and displacement boundary conditions on $\Gamma_u \times T$:

$$\begin{cases} \boldsymbol{\varepsilon}(\dot{\boldsymbol{u}}) = \dfrac{1}{2}\left(\boldsymbol{\nabla}\dot{\boldsymbol{u}} + \boldsymbol{\nabla}^T\dot{\boldsymbol{u}}\right), \\ \dot{\boldsymbol{u}} = \dot{\boldsymbol{u}}^d. \end{cases} \tag{5.9}$$

- Elasto-viscoplastic constitutive law of Perzyna type [3] for the rock mass on $\Omega_X \times T$:

$$\begin{cases} \dot{\boldsymbol{\sigma}} = \boldsymbol{C} : (\dot{\boldsymbol{\varepsilon}} - \dot{\boldsymbol{\varepsilon}}^{\mathrm{vp}}), \\ \dot{\boldsymbol{\varepsilon}}^{\mathrm{vp}} = \dfrac{\partial \phi(\boldsymbol{\sigma})}{\partial \boldsymbol{\sigma}}. \end{cases} \tag{5.10}$$

where $\phi$ is a pseudo-potential functional of the stress tensor [3].
The expression of $\phi$ for the Norton–Hoff law is given by:

$$\phi(\boldsymbol{\sigma}) = \frac{K}{N+1}\left\langle \frac{\sigma_{\mathrm{eq}} - \sigma_Y}{K} \right\rangle^{N+1}, \tag{5.11}$$

where :

$\sigma_{\mathrm{eq}}$ is the Von Mises equivalent stress,

$\sigma_Y$ is the yield limit in MPa,

$N$ is the viscoplastic exponent,

$K$ is the viscosity coefficient in $\mathrm{MPa} \cdot \mathrm{s}^{1/N}$.

- Elastic behaviour for the lining on $\Omega_\ell \times [t_l, t_f]$:

$$\dot{\boldsymbol{\sigma}} = \boldsymbol{C_l} : \dot{\boldsymbol{\varepsilon}}. \tag{5.12}$$

The numerical integration of the initial boundary value problem is classically done by finite elements in space and finite difference in time. An extensive presentation of these techniques is given in [9, 10].

At this point let us recall the weak formulation of the preceding problem which will be used in the sequel for the description of the direct differentiation method. On the discretized time interval $[t_n, t_{n+1}]$, the weak formulation at time $t = t_{n+1}$ can be written using a forward Euler (implicit) scheme for the time integration and a radial return mapping for the local plastic integration [9]:

*Find* $\boldsymbol{u}_{n+1} \in \mathcal{U}$, $\boldsymbol{\epsilon}^{\text{vp}}_{n+1}$ *and* $\boldsymbol{\sigma}_{n+1}$ *satisfying:*

$$\begin{cases} \int_{\Omega} \boldsymbol{\varepsilon}(\boldsymbol{v}) : \boldsymbol{\sigma}_{n+1} d\Omega - \int_{\Omega} \boldsymbol{v} \boldsymbol{f}_{n+1} d\Omega - \int_{\Gamma_t} \boldsymbol{v} \boldsymbol{t}^d_{n+1} d\Gamma = 0 \qquad \forall \boldsymbol{v} \in \mathcal{V}, \\ \boldsymbol{\sigma}_{n+1} = \boldsymbol{C} : \left(\boldsymbol{\varepsilon}\left(\boldsymbol{u}_{n+1}\right) - \boldsymbol{\varepsilon}^{\text{vp}}_{n+1}\right) - \boldsymbol{\sigma}_0, \\ \boldsymbol{\varepsilon}^{\text{vp}}_{n+1} = \boldsymbol{\varepsilon}^{\text{vp}}_{n} + \Delta t_{n+1} \dfrac{\partial \phi\left(\boldsymbol{\sigma}_{n+1}\right)}{\partial \boldsymbol{\sigma}}, \end{cases} \tag{5.13}$$

*where all fields* $X(t_{n+1})$ *at time* $t = t_{n+1}$ *are denoted by* $X_{n+1}$ *and* $\Delta t_{n+1} = t_{n+1} - t_n$.

$\mathcal{U}$ *and* $\mathcal{V}$ *are the classical functional spaces:*

$$\begin{cases} \mathcal{U} = \left\{ \boldsymbol{u} \in H^1(\Omega) \mid \boldsymbol{u}_{n+1} = \boldsymbol{u}^d(t_{n+1}) \text{ on } \Gamma_u \right\}, \\ \mathcal{V} = \left\{ \boldsymbol{v} \in H^1(\Omega) \mid \boldsymbol{v} = 0 \text{ on } \Gamma_u \right\}. \end{cases} \tag{5.14}$$

Let us now discuss the computational details imposed by the excavation of tunnel and the installation of lining. The FEM computations will be performed on the domain $\Omega_X \cup \Omega_\ell$ for all time steps. Before the effective installation of the lining, the mechanical influence of $\Omega_\ell$ has to be neglected and therefore the Young moduli of the lining has been such that $E_l \ll E_m$. The different steps can now be described in the following way:

- For $t \in [-\infty, 0]$, the non-excavated domain is at equilibrium with an initial stress state. The FEM boundary condition should be: $\boldsymbol{\sigma}.\boldsymbol{n}|_{\Gamma_\ell} = \boldsymbol{\sigma}_0.\boldsymbol{n}$ Due to the negligible stiffness in $\Omega_\ell$ this is practically equivalent with the real condition: $\boldsymbol{\sigma}.\boldsymbol{n}|_{\Gamma_{X\ell}} = \boldsymbol{\sigma}_0.\boldsymbol{n}$.
- For $t \in [0, t_\ell]$, the tunnel is already excavated but the lining is not active. The boundary $\Gamma_{Xl}$ of the rock mass is free of traction. Using the same argument as before, we impose: $\boldsymbol{\sigma}.\boldsymbol{n}|_{\Gamma_\ell} = \boldsymbol{0}$ Due to the negligible stiffness in $\Omega_\ell$ this is practically equivalent to the real condition: $\boldsymbol{\sigma}.\boldsymbol{n}|_{\Gamma_{X\ell}} = \boldsymbol{0}$.
- For $t \in [t_\ell, t_f]$, the elastic lining is set. The boundary condition is now given by: $\boldsymbol{\sigma}.\boldsymbol{n}|_{\Gamma_\ell} = \boldsymbol{0}$ However, at this point the stiffness of the lining is no longer negligible and therefore the traction between lining and rock mass expressed by $\boldsymbol{\sigma}.\boldsymbol{n}|_{\Gamma_{X\ell}}$ is no more zero.

**The inverse problem ($\mathcal{P}^{-1}$).** In the inverse problem the constitutive parameters are unknown. This drawback will be supplemented with a series of measurements, for example:

- convergence of the tunnel wall;
- displacement measurements, by extensometers, within the rock mass;
- pressure cells on the lining or at the interface between the lining and the rock mass.

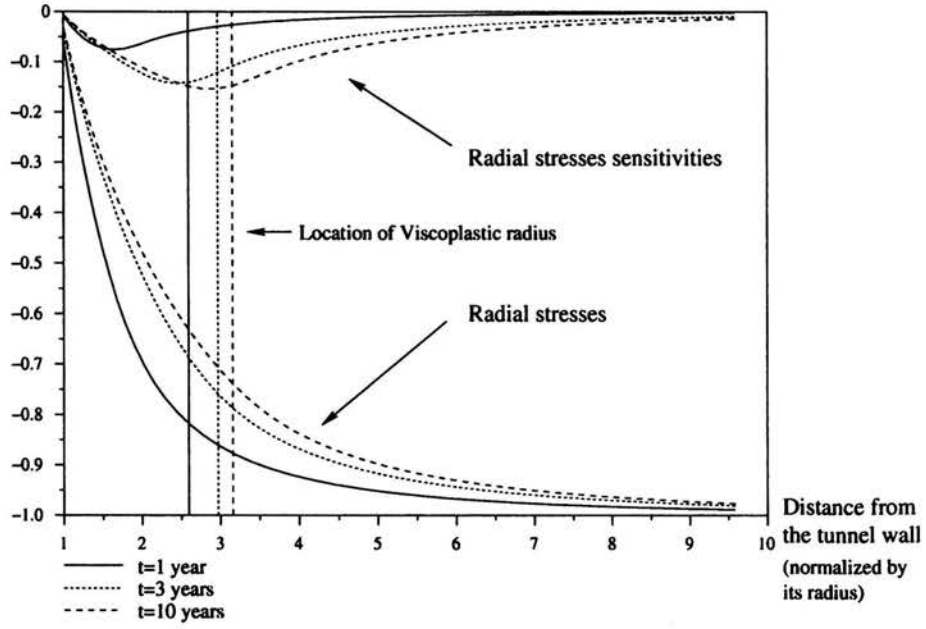


FIGURE 5.1. Evolution of $\sigma_{rr}/\sigma_0$ and $\delta_N\sigma_{rr}/\sigma_0$ function of $r$ unlined tunnel.

A general formulation of this identification problem is:

*Find* $\boldsymbol{c} = \{E, N, \sigma_Y, K\}$ *from displacement and force measurements performed during the time interval* $T$.

This problem is now reformulated as the minimization of cost functional measuring the distance between measurements and the calculated estimations:

$$J(\boldsymbol{c}) = \frac{1}{2}\sum_{i=1,k}\sum_{j=1,p}\left(\frac{\boldsymbol{u}(\boldsymbol{c}, t_i, \boldsymbol{x}_j) - \boldsymbol{u}_{\text{mes}}(t_i, \boldsymbol{x}_j)}{w_{u_{ij}}}\right)^2 + \frac{1}{2}\sum_{i=1,k}\sum_{j=1,p}\left(\frac{\boldsymbol{t}(\boldsymbol{c}, t_i, \boldsymbol{x}_j) - \boldsymbol{t}_{\text{mes}}(t_i, \boldsymbol{x}_j)}{w_{t_{ij}}}\right)^2,$$

where $\boldsymbol{u}$ and $\boldsymbol{t}$ are displacements and tractions calculated by direct computations, $\boldsymbol{u}_{\text{mes}}$ and $\boldsymbol{t}_{\text{mes}}$ are measured quantities, $t_i, \boldsymbol{x}_j$ are respectively the time instants and the location of the measurements, $w_t$ and $w_u$ are weights.

The gradient of the preceding cost functional can be written as follows:

$$\frac{\partial J}{\partial c_l} = \sum_{i=1,k} \sum_{j=1,p} \frac{\boldsymbol{u}(\boldsymbol{c}, t_i, \boldsymbol{x}_j) - \boldsymbol{u}_{\text{mes}}(t_i, \boldsymbol{x}_j)}{w_{u_{ij}}^2} \frac{\partial \boldsymbol{u}}{\partial c_l}(\boldsymbol{c}, t_i, \boldsymbol{x}_j) + \sum_{i=1,k} \sum_{j=1,p} \frac{\boldsymbol{t}(\boldsymbol{c}, t_i, \boldsymbol{x}_j) - \boldsymbol{t}_{\text{mes}}(t_i, \boldsymbol{x}_j)}{w_{t_{ij}}^2} \frac{\partial \boldsymbol{t}}{\partial c_l}(\boldsymbol{c}, t_i, \boldsymbol{x}_j).$$

In the sequel we shall use the *direct differentiation method* to calculate the gradient. More precisely, this method allows to calculate exactly not only $\dfrac{\partial J}{\partial \boldsymbol{c}}$ as in the *adjoint state method* but also the values of the sensitivities of all mechanical fields $\dfrac{\partial \boldsymbol{u}}{\partial c_l}, \dfrac{\partial \boldsymbol{\sigma}}{\partial c_l}, \ldots$ in each point and at each instant. We recall that this method requires the solution of $n$ additional viscoelastic problems, where $n$ is the number of parameters. This method will be described in the next paragraph.

**Direct Differentiation Method.** Let $c_i$ denote a constitutive parameter, $\delta_{c_i}\boldsymbol{u}$ and $\delta_{c_i}\boldsymbol{\sigma}$ the related sensitivities of the displacement and stress field, respectively.

The direct differentiation of the classical initial boundary problem in elasto-viscoplasticity will lead to a somehow similar system of partial differential equations, where the constitutive equation is always similar to a viscoelastic law.

The differentiation of the equilibrium and compatibility equations is straightforward since the divergence and gradient are linear operators. The boundary and initial conditions are also easily derived. In particular, if the boundary conditions do not depend on the constitutive parameters $c_i$, the sensitivity problem has homogeneous boundary conditions.

**Differentiation of the discretized constitutive law.** The pseudo-potential is a function of the parameters $c_i$ and the stress field also depends on $c_i$. Therefore we have: $\phi(\boldsymbol{\sigma}(c_i), c_i)$.

The differentiation of equation (5.11) and (5.10) thus gives:

$$\delta_{c_i}\boldsymbol{\sigma}_{n+1} = \frac{\partial \boldsymbol{C}}{\partial c_i} : \left(\boldsymbol{\varepsilon}\left(\boldsymbol{u}_{n+1}\right) - \boldsymbol{\varepsilon}^{\mathrm{vp}}_{n+1}\right) + \boldsymbol{C} : \left(\boldsymbol{\varepsilon}\left(\delta_{c_i}\boldsymbol{u}_{n+1}\right) - \delta_{c_i}\boldsymbol{\varepsilon}^{\mathrm{vp}}_{n+1}\right) + \frac{\partial \boldsymbol{\sigma}_0}{\partial c_i}, \quad (5.15)$$

$$\delta_{c_i}\boldsymbol{\varepsilon}^{\mathrm{vp}}_{n+1} = \delta_{c_i}\boldsymbol{\varepsilon}^{\mathrm{vp}}_{n} + \Delta t_{n+1}\frac{\partial^2 \phi\left(\boldsymbol{\sigma}\left(c_i\right), c_i\right)}{\partial \boldsymbol{\sigma}\partial c_i} + \Delta t_{n+1}\frac{\partial^2 \phi\left(\boldsymbol{\sigma}_{n+1}\right)}{\partial \boldsymbol{\sigma}^2}\delta_{c_i}\boldsymbol{\sigma}_{n+1}. \quad (5.16)$$

Combining the last equations we derive the following constitutive law for the sensitivity fields:

$$\begin{aligned}\delta_{c_i}\boldsymbol{\sigma}_{n+1} = {} & \boldsymbol{\Xi}_{n+1} : \boldsymbol{\varepsilon}\left(\delta_{c_i}u_{n+1}\right) \\ & + \boldsymbol{\Xi}_{n+1} : \left[\boldsymbol{C}^{-1} : \frac{\partial \boldsymbol{C}}{\partial c_i} : \left(\boldsymbol{\varepsilon}\left(u_{n+1}\right) - \boldsymbol{\varepsilon}^{\mathrm{vp}}_{n+1}\right)\right] \\ & + \boldsymbol{\Xi}_{n+1} : \left[\boldsymbol{C}^{-1} : \frac{\partial \boldsymbol{\sigma}_0}{\partial c_i} - \delta_{c_i}\boldsymbol{\varepsilon}^{\mathrm{vp}}_{n} - \frac{\partial^2 \phi\left(\boldsymbol{\sigma}_{n+1}\left(c_i\right), c_i\right)}{\partial \boldsymbol{\sigma}\partial c_i}\Delta t_{n+1}\right],\end{aligned} \quad (5.17)$$

where $\boldsymbol{\Xi}_{n+1}$ is the consistent tangent operator [9, 11, 12] defined by:

$$\boldsymbol{\Xi}_{n+1} = \left(\boldsymbol{C}^{-1} + \Delta_{n+1}t\frac{\partial^2 \phi\left(\boldsymbol{\sigma}_{n+1}\right)}{\partial \boldsymbol{\sigma}^2}\right)^{-1}. \quad (5.18)$$

This constitutive relation is of the viscoelastic type, the response of the stress sensitivity at time $t_{n+1}$ depends linearly on the displacement sensitivity at time $t_{n+1}$ and known sensitivities at $t_n$.

**Weak form of the sensitivity problem ($\mathcal{P}^s$).** Following a similar method as in the direct problem (5.13), the initial boundary value problem for the sensitivity can be written in the following weak form:

*Find $\delta_{c_i}\boldsymbol{u}_{n+1} \in \mathcal{W}$ and $\delta_{c_i}\boldsymbol{\sigma}_{n+1}$ satisfying:*

$$\int_{\Omega} \boldsymbol{\varepsilon}\left(\boldsymbol{v}\right) : \delta_{c_i}\boldsymbol{\sigma}_{n+1}d\Omega - \int_{\Omega} \boldsymbol{v}\frac{\partial \boldsymbol{f}_{n+1}}{\partial c_i}d\Omega - \int_{\Gamma_t} \boldsymbol{v}\frac{\partial t^d_{n+1}}{\partial c_i}d\Gamma = 0 \quad \forall \boldsymbol{v} \in \mathcal{W}. \quad (5.19)$$

The constitutive law for the sensitivity is described by Eq. (5.17) mentioned above. At time $t = 0$ the initial conditions have the following form:

$$\delta_{c_i}\boldsymbol{\sigma} = \frac{\partial \boldsymbol{\sigma}_0}{\partial c_i}, \qquad \delta_{c_i}\boldsymbol{u} = 0. \quad (5.20)$$

$\mathcal{W}$ is the space of admissible displacements defined by

$$\mathcal{W} = \left\{ \delta_{c_i}\boldsymbol{u} \in H^1(\Omega) \mid \delta_{c_i}\boldsymbol{u}_{n+1} = \frac{\partial \boldsymbol{u}^d_{n+1}}{\partial c_i} \text{ on } \Gamma_u \right\}. \tag{5.21}$$

**Incremental form of $(\mathcal{P}^s)$.** To get insight into the structure of the computation which is performed step by step, let us denote:

$$\delta_{c_i}\boldsymbol{u}_{n+1} = \delta_{c_i}\Delta\boldsymbol{u} + \delta_{c_i}\boldsymbol{u}_n. \tag{5.22}$$

Then, the weak incremental formulation reads:

*Find $\delta_{c_i}\Delta\boldsymbol{u} \in \mathcal{W}$ and $\delta_{c_i}\boldsymbol{\sigma}_{n+1}$ satisfying:*

$$\begin{aligned}
&\int_\Omega \boldsymbol{\varepsilon}(\boldsymbol{v}) : \boldsymbol{\Xi}_{n+1} : \boldsymbol{\varepsilon}(\delta_{c_i}\Delta\boldsymbol{u})\, d\Omega = \int_\Omega \boldsymbol{v}\frac{\partial \boldsymbol{f}_{n+1}}{\partial c_i} d\Omega + \int_{\Gamma_T} \boldsymbol{v}\frac{\partial \boldsymbol{t}^d_{n+1}}{\partial c_i} d\Gamma \\
&\quad + \int_\Omega \boldsymbol{\varepsilon}(\boldsymbol{v}) : \boldsymbol{\Xi}_{n+1} : \frac{\partial^2 \phi(\boldsymbol{\sigma}_{n+1}(c_i), c_i)}{\partial \boldsymbol{\sigma}\partial c_i} \Delta t_{n+1} d\Omega \\
&\quad - \int_\Omega \boldsymbol{\varepsilon}(\boldsymbol{v}) : \boldsymbol{\Xi}_{n+1} : \boldsymbol{C}^{-1} : \frac{\partial \boldsymbol{C}}{\partial c_i} : \left( \boldsymbol{\varepsilon}(\Delta\boldsymbol{u}) - \Delta t_{n+1}\frac{\partial \phi(\boldsymbol{\sigma}_{n+1})}{\partial \boldsymbol{\sigma}} \right) d\Omega \\
&\quad - \int_\Omega \boldsymbol{\varepsilon}(\boldsymbol{v}) : \boldsymbol{\Xi}_{n+1} : \boldsymbol{C}^{-1} : \delta_{c_i}\boldsymbol{\sigma}_n d\Omega \qquad \forall \boldsymbol{v} \in \mathcal{V},
\end{aligned} \tag{5.23}$$

with the following constitutive law:

$$\begin{aligned}
\delta_{c_i}\boldsymbol{\sigma}_{n+1} &= \boldsymbol{\Xi}_{n+1} : \boldsymbol{\varepsilon}(\delta_{c_i}\Delta\boldsymbol{u}) \\
&\quad + \boldsymbol{\Xi}_{n+1} : \left[ \boldsymbol{C}^{-1} : \delta_{c_i}\boldsymbol{\sigma}_n + \boldsymbol{C}^{-1} : \frac{\partial \boldsymbol{C}}{\partial c_i} : \left( \boldsymbol{\varepsilon}(\Delta\boldsymbol{u}) - \Delta t_{n+1}\frac{\partial \phi(\boldsymbol{\sigma}_{n+1})}{\partial \boldsymbol{\sigma}} \right) \right] \\
&\quad - \boldsymbol{\Xi}_{n+1} : \frac{\partial^2 \phi(\boldsymbol{\sigma}_{n+1}(c_i), c_i)}{\partial \boldsymbol{\sigma}\partial c_i} \Delta t_{n+1},
\end{aligned} \tag{5.24}$$

and the initial conditions specified by Eq. (5.20).

**Identification results.** The complete mechanical interpretation of the identification results is presented in [4]. Let us just notice that this type of analysis permits to obtain not only the gradient of the cost functional, but also the time and space distribution of the sensibility of different fields, see for example Figs. 5.1 and 5.3.

$$
\begin{array}{ccc}
\boldsymbol{u}_n & & \boldsymbol{u}_{n+1} \\
\boldsymbol{\sigma}_n & \longrightarrow & \boldsymbol{\sigma}_{n+1} \\
\boldsymbol{\epsilon}_n^{\mathrm{vp}} & & \boldsymbol{\epsilon}_{n+1}^{\mathrm{vp}} \\
 & & \downarrow \\
 & & \boldsymbol{\Xi}_{n+1} \\
 & & \text{force terms (see Eq. (5.23))} \\
 & & \downarrow \\
\delta_{c_i}\boldsymbol{u}_n & & \delta_{c_i}\boldsymbol{u}_{n+1} \\
\delta_{c_i}\boldsymbol{\sigma}_n & \longrightarrow & \delta_{c_i}\boldsymbol{\sigma}_{n+1}
\end{array}
$$

FIGURE 5.2. Scheme of a time step for the direct and sensitivity problem.

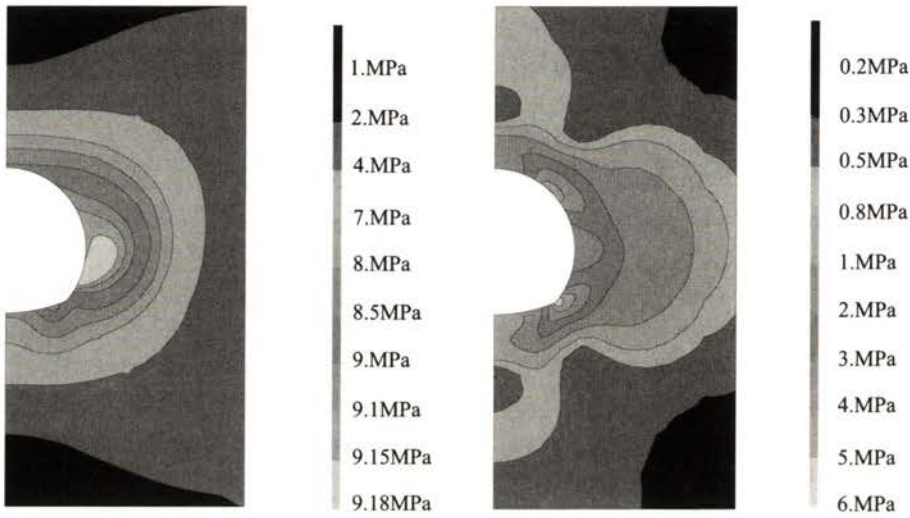


FIGURE 5.3. Von Mises of $\boldsymbol{\sigma}$ (Yield Limit 3 MPa) and $\delta_N\boldsymbol{\sigma}$.

### 5.1.2. Example: anisothermal identification of parameters

In this Section we shall give the development of the adjoint state method used for the identification of temperature dependent material parameters from anisothermal traction–compression experiments of specimens [5]. To simplify the equations of the problem we assume that the strain and stress states are uniaxial.

**The direct Problem ($\mathcal{P}$).** If the strain $\varepsilon(t)$ and temperature $\theta(t)$ are considered as functions of time $t \in [0, T]$ then the stress $\sigma$ and the viscoplastic

strain $\varepsilon_{\text{vp}}$ can be calculated as function of time from the equations of the following model:

$$\begin{cases} \dot{\sigma} = \dfrac{d}{dt}\big(E(\theta)\cdot(\varepsilon - \varepsilon_{\text{vp}})\big), \\ \dot{\varepsilon}_{\text{vp}} = \left\langle \dfrac{J_2(\sigma,\varepsilon_{\text{vp}}) - \sigma_y(\theta)}{\eta(\theta)} \right\rangle^{\mathtt{m}(\theta)} \operatorname{sgn}\left(\dfrac{2}{3}\sigma - H(\theta)\varepsilon_{\text{vp}}\right), \end{cases} \tag{5.25}$$

with the the initial conditions:

$$\sigma(0) = 0, \qquad \varepsilon_{\text{vp}}(0) = 0. \tag{5.26}$$

We have denoted by:

$$J_2(\sigma,\varepsilon_{\text{vp}}) = \left|\sigma - \frac{3}{2}H(\theta)\varepsilon_{\text{vp}}\right|, \tag{5.27}$$

and by $\langle . \rangle$ the positive part of its argument.

Therefore the model is determined by 5 temperature-dependent parameters:

$$\mathcal{P}(\theta) = \big(E(\theta), \sigma_y(\theta), H(\theta), \eta(\theta), \mathtt{m}(\theta)\big),$$

namely, the Young modulus $E$, the yield limit $\sigma_Y$, the hardening parameter $H$, the viscosity $\eta$, and the power coefficient $m$. These parameters have to be recovered from experiments performed under cyclic loading conditions. As all parameters are temperature dependent, this leads to the identification of some dozens of scalar values.

**The inverse problem ($\mathcal{P}^{-1}$).** In experiments and consequently in the numerical simulations the temperature and strain histories $(\theta(t), \epsilon(t))$ were imposed and the stress history was measured and respectively calculated. Let us denote by $\sigma_{\text{exp}}(\mathcal{P})$ the experimentally measured stress and by $\sigma_{\text{comp}}(\mathcal{P})$ the calculated stress history, depending on the given loading and also on the material parameters $\mathcal{P}$.

Consequently we can now define the identification problem for the parameters $\mathcal{P}$ as a minimization problem for the following cost functional:

$$\mathcal{J}(\mathcal{P}) = \frac{1}{2T}\int_0^T |\sigma_{\text{exp}}(t) - \sigma_{\text{comp}}(\mathcal{P},t)|^2 dt, \tag{5.28}$$

defined over a complete experiment.

In the case were the identification involves a series of independent experiments, a cost functional defined as a linear combination of functionals of the preceding type can be used. These formulations are the continuous equivalent of the classical nonlinear least square problem.

**The adjoint state method.** As stated in the previous discussions, the adjoint state method redefines the minimization problem of $\mathcal{J}$ as constrained minimization problem and replaces the search of the minimum of $\mathcal{J}$ by the search of the saddle point of well chosen Lagrangian $\mathcal{L}$.

In order to construct the Lagrangian $\mathcal{L}$, let us introduce two adjoint fields $\varepsilon^*$ and $\sigma^*$ which will play the role of Lagrange multipliers for our system.

The Lagrangian $\mathcal{L}(\mathcal{P}, \varepsilon_{\text{vp}}, \sigma, \varepsilon^*, \sigma^*)$ is defined by the sum of the cost functional $\mathcal{J}$ and of variational formulation of the equations of the *direct problem* described by (5.25) and (5.26):

$$\mathcal{L}(S, \mathcal{P}(\theta), \varepsilon_{\text{vp}}, \sigma, \varepsilon^*, \sigma^*) = \mathcal{J}(S, \sigma) - \int_S \left[\dot{\varepsilon}_{\text{vp}} - g(\mathcal{P}(\theta), \sigma, \varepsilon_{\text{vp}})\right] \cdot \sigma^* dt$$
$$- \int_S \left[\dot{\sigma} - \frac{dE}{d\theta}\dot{\theta} \cdot (\varepsilon - \varepsilon_{\text{vp}}) - E(\theta) \cdot (\dot{\varepsilon} - \dot{\varepsilon}_{\text{vp}})\right] \cdot \varepsilon^* dt, \quad (5.29)$$

where $g(\mathcal{P}(\theta), \sigma, \varepsilon_{\text{vp}})$ is the viscoplastic flow function represented by the right hand side of equation (5.25). $S$ defines the time interval on which the parameters will be identified. Its is obvious that the identification process also depends on this parameter, however for the sake of simplicity we shall assume that this interval is specified at the beginning of the process and considered as fixed. The saddle point of the Lagrangian is given by the optimality conditions:

$$\frac{\partial \mathcal{L}}{\partial \varepsilon^*_{\text{vp}}} \cdot \delta\varepsilon^*_{\text{vp}} = 0, \qquad \frac{\partial \mathcal{L}}{\partial \sigma^*} \cdot \delta\sigma^* = 0, \quad (5.30)$$

$$\frac{\partial \mathcal{L}}{\partial \varepsilon_{\text{vp}}} \cdot \delta\varepsilon_{\text{vp}} = 0, \qquad \frac{\partial \mathcal{L}}{\partial \sigma} \cdot \delta\sigma = 0. \quad (5.31)$$

The derivation of the first two conditions, with respect to the adjoint variables, defines the solution of the *direct problem* (5.25) and (5.26).

The derivatives of the last two conditions, with respect to the direct variables are:

$$\frac{\partial \mathcal{L}}{\partial \varepsilon_{\mathrm{vp}}} \cdot \delta\varepsilon_{\mathrm{vp}} = -\int_S \varepsilon^* \cdot \left(\frac{dE}{d\theta}\dot{\theta} \cdot \delta\varepsilon_{\mathrm{vp}} + E(\theta)\delta\dot{\varepsilon}_{\mathrm{vp}}\right)dt - \int_S \sigma^* \cdot \left(\delta\dot{\varepsilon}_{\mathrm{vp}} - \frac{\partial g}{\partial \varepsilon_{\mathrm{vp}}} \cdot \delta\varepsilon_{\mathrm{vp}}\right)dt$$

$$= -\left[\delta\varepsilon_{\mathrm{vp}} \cdot (E(\theta)\varepsilon^* + \sigma^*)\right]_0^{t_{\mathrm{f}}} + \int_S (E(\theta)\dot{\varepsilon}^* + \dot{\sigma}^*) \cdot \delta\varepsilon_{\mathrm{vp}}dt$$

$$- \frac{3}{2}\int_S \sigma^* H(\theta) \cdot \frac{\mathtt{m}(\theta)}{\eta(\theta)} \left\langle \frac{J_2 - \sigma_y(\theta)}{\eta(\theta)} \right\rangle^{\mathtt{m}(\theta)-1} \cdot \delta\varepsilon_{\mathrm{vp}}dt, \quad (5.32)$$

$$\frac{\partial \mathcal{L}}{\partial \sigma} \cdot \delta\sigma = \frac{\partial \mathcal{J}}{\partial \sigma} \cdot \delta\sigma - \int_S \delta\dot{\sigma} \cdot \varepsilon^* dt + \int_S \frac{\partial g}{\partial \sigma} \cdot \sigma^* dt = \int_S (\sigma_{\mathrm{exp}} - \sigma)\delta\sigma dt - \left[\delta\sigma \cdot \varepsilon^*\right]_0^{t_{\mathrm{f}}}$$

$$+ \int_S \dot{\varepsilon}^* \delta\sigma dt + \frac{3}{2}\int_S \sigma^* \frac{\mathtt{m}(\theta)}{\eta(\theta)} \left\langle \frac{J_2 - \sigma_y(\theta)}{\eta(\theta)} \right\rangle^{\mathtt{m}(\theta)-1} \delta\sigma dt, \quad (5.33)$$

and define the *adjoint problem.*

Therefore the *adjoint problem* is given by the following system of ordinary differential equations:

$$\begin{cases} \dot{\sigma}^* - \dfrac{3}{2}H(\theta) \cdot \dfrac{\mathtt{m}(\theta)}{\eta(\theta)} \left\langle \dfrac{J_2 - \sigma_y(\theta)}{\eta(\theta)} \right\rangle^{\mathtt{m}(\theta)-1} \cdot \sigma^* + E(\theta) \cdot \dot{\varepsilon}^* = 0, \\ \dfrac{3}{2}\dfrac{\mathtt{m}(\theta)}{\eta(\theta)} \left\langle \dfrac{J_2 - \sigma_y(\theta)}{\eta(\theta)} \right\rangle^{\mathtt{m}(\theta)-1} \cdot \sigma^* + (\sigma_{\mathrm{exp}} - \sigma) + \dot{\varepsilon}^* = 0, \end{cases} \quad (5.34)$$

with the *final* conditions:

$$\sigma^*(t_{\mathrm{f}}) = 0, \qquad \varepsilon^*(t_{\mathrm{f}}) = 0. \quad (5.35)$$

The adjoint problem is therefore a linear system of ordinary differential equations in $\sigma^*$, $\varepsilon^*$ to be integrated backward in time. This may seem awkward, but it expresses actually just the integration by parts made during the process.

For a given set of material parameters $\mathcal{P}$ let us choose a solution pair of the direct problem $(\varepsilon, \sigma)$ and the corresponding solution $(\varepsilon^*, \sigma^*)$ of the adjoint problem. For these functions, we obtain by definition of the La-

grangian $\mathcal{L} \equiv \mathcal{J}$. Moreover, writing the first order variation of the Lagrangian at this point we obtain:

$$\frac{\mathcal{J}}{\partial \mathcal{P}} = \frac{\partial \mathcal{L}}{\partial \mathcal{P}}. \tag{5.36}$$

The derivatives of the cost functional with respect to the material parameters are expressed by the following series of equations:

$$\frac{\partial \mathcal{J}}{\partial E} = -\int_{t_0}^{t_{\max}} (\dot{\varepsilon}^c - \dot{\varepsilon}^{\mathrm{vp}}) \cdot \varepsilon^* dt, \tag{5.37}$$

$$\frac{\partial \mathcal{J}}{\partial H} = \frac{3}{2} \int_{t_0}^{t_{\max}} \varepsilon^{\mathrm{vp}} \frac{\mathtt{m}}{\eta} \left\langle \frac{J_2 - \sigma_y}{\eta} \right\rangle^{\mathtt{m}-1} \cdot \sigma^* dt, \tag{5.38}$$

$$\frac{\partial \mathcal{J}}{\partial \sigma_y} = \int_{t_0}^{t_{\max}} \left\langle \frac{J_2 - \sigma_y}{\eta} \right\rangle^{\mathtt{m}-1} \operatorname{sgn}\left(\frac{2}{3}\sigma - H\varepsilon^{\mathrm{vp}}\right) \cdot \sigma^* dt, \tag{5.39}$$

$$\frac{\partial \mathcal{J}}{\partial \mathtt{m}} = -\int_{t_0}^{t_{\max}} \log\left(\left\langle \frac{J_2 - \sigma_y}{\eta} \right\rangle\right) \left\langle \frac{J_2 - \sigma_y}{\eta} \right\rangle^{\mathtt{m}} \operatorname{sgn}\left(\frac{2}{3}\sigma - H\varepsilon^{\mathrm{vp}}\right) \cdot \sigma^* dt, \tag{5.40}$$

$$\frac{\partial \mathcal{J}}{\partial \eta} = \int_{t_0}^{t_{\max}} \frac{J_2 - \sigma_y}{\eta^2} \left\langle \frac{J_2 - \sigma_y}{\eta} \right\rangle^{\mathtt{m}-1} \mathtt{m} \cdot \operatorname{sgn}\left(\frac{2}{3}\sigma - H\varepsilon^{\mathrm{vp}}\right) \cdot \sigma^* dt. \tag{5.41}$$

In order to simplify the preceding equations, we have not denoted explicitly the evolution of the parameters as a function of temperature.

This evolution was considered in the sequel as multi-linear and expressed under the following form:

$$\mathcal{P}(\theta) = \sum_{i=1}^{N-1} \left( \frac{\mathcal{P}_{i+1} - \mathcal{P}_i}{\theta_{i+1} - \theta_i} \cdot \theta + \frac{\mathcal{P}_i \theta_{i+1} - \mathcal{P}_{i+1} \theta_i}{\theta_{i+1} - \theta_i} \right) \cdot \mathcal{H}(\theta, \theta_i, \theta_{i+1}), \tag{5.42}$$

where $\mathcal{H}(\theta, \theta_i, \theta_{i+1}) = 1$ if and only if $\theta \in [\theta_i, \theta_{i+1}]$. During the identification process the values $\theta_i$ were predefined and only the values of the parameters $\{\mathcal{P}_i\}_{i=1,\ldots,N}$ were determined.

### 5.1.3. Example: indentation problem

We proceed to the presentation of the equations corresponding to the application of the adjoint state method for identification of material parameters from indentation experiments. For more details the reader is referred to a series of papers [6, 7, 8, 13].

**The inverse problem ($\mathcal{P}^{-1}$).** In the present inverse problem, one wants to identify the parameters of the material behaviour $\boldsymbol{c}$ from the knowledge of the indentation curve $(U^{\text{exp}}, F^{\text{exp}})$. $\boldsymbol{c}$ is assumed to belong to in a closed convex set $\mathcal{Q}$ of $\mathbb{R}^n$ $(n \geq 2)$.

This inverse problem can be expressed as a minimization problem of a well-defined cost functional and is the nonlinear equivalent of the one presented in the preceding chapter for an elastic material behaviour.

Since the direct problem is driven by the imposed displacement of the punch $U$, it is natural to express the cost functional as a function of the resultant force $F$. A possible formulation of the inverse problem $(\mathcal{P}^{-1})$ is:

*Find $\boldsymbol{c} \in \mathcal{Q}$ minimizing:*

$$\mathcal{J}(\boldsymbol{c}) = \frac{1}{2}\sum_{i=0}^{I}\left(F_i^{\text{comp}}(\boldsymbol{c}) - F_i^{\text{exp}}\right)^2 = \frac{1}{2}\sum_{i=0}^{I}\left(\int_{\Gamma_C} p_i(\boldsymbol{c})d\Gamma - F_i^{\text{exp}}\right)^2,$$

*where $F^{\text{comp}}$ is the calculated resultant force from the direct problem driven by $U^{\text{exp}}$.*

**Equations of the direct problem ($\mathcal{P}$).** The governing equations of the direct problem consist of the equilibrium and constitutive equations, the boundary and contact conditions and a set of initial values. The contact conditions on $\Gamma_C$ are expressed using the Lagrange multipliers $p_i \in N$, where $N = \{q \in (H^{1/2}(\Gamma_C))' \mid q \leq 0\}$ is a closed convex set and $(H^{1/2}(\Gamma_C))'$ denotes the dual of $H^{1/2}(\Gamma_C)$ (see [14]).

The punch is driven by its vertical displacement $U_i$ at time $t_i$. At the same moment, the gap $g_i$ between the surface $\Gamma_C$ and the punch is expressed by $g_i = g + U_i - u_i^n$.

*Equilibrium and constitutive equation in* $\Omega$:

$$\operatorname{div}(\Delta\boldsymbol{\sigma}_i) = 0, \tag{5.43}$$

$$\boldsymbol{\varepsilon}(\Delta\boldsymbol{u}_i) = \boldsymbol{S} : \Delta\boldsymbol{\sigma}_i + \frac{\partial\Phi(\boldsymbol{\sigma}_i, \boldsymbol{c})}{\partial\boldsymbol{\sigma}}\Delta t. \tag{5.44}$$

*Boundary conditions*:

$$\Delta\boldsymbol{\sigma}_i \cdot \boldsymbol{n} = 0 \quad \text{on} \quad \Gamma_F, \tag{5.45}$$

$$\Delta\boldsymbol{u}_i = 0 \quad \text{on} \quad \Gamma_D. \tag{5.46}$$

*Contact conditions*:

$$(\Delta u_i^n - g_i - \Delta U_i)(q - p^{i+1}) \geq 0 \quad \forall q \in N, \tag{5.47}$$

$$\Delta\sigma_i^{nn} = \Delta\boldsymbol{\sigma}_i \cdot \boldsymbol{n} \cdot \boldsymbol{n} = \Delta p_i, \tag{5.48}$$

$$\Delta\sigma_i^{nt} = (\Delta\boldsymbol{\sigma}_i \cdot \boldsymbol{n} - \Delta\sigma_i^{nn} \cdot \boldsymbol{n}) \cdot \boldsymbol{t} = 0. \tag{5.49}$$

*Initial conditions*:

$$\boldsymbol{\sigma}_0 = 0 \quad \text{in} \quad \Omega, \tag{5.50}$$

$$\boldsymbol{u}_0 = 0 \quad \text{on} \quad \Omega, \tag{5.51}$$

$$\boldsymbol{\varepsilon}_0^{\mathrm{p}} \cdot \boldsymbol{n} = 0 \quad \text{on} \quad \Omega. \tag{5.52}$$

**The adjoint state method.** Let us recall again that the resolution of a constrained minimization problem is equivalent, under some regularity conditions, to finding the saddle point of a Lagrangian functional $\mathcal{L}$. In the case of the inverse problem ($\mathcal{P}^{-1}$), the Lagrangian $\mathcal{L}$ is introduced as a sum of the cost functional and a variational formulation of the direct problem ($\mathcal{P}$). In this case we will adjoin the Lagrangian technique used in the elastic contact problem in the preceding chapter to a Lagrangian technique developed in the case of nonlinear behaviour as the one presented in the preceding section.

For each variable of the direct problem, an adjoint variable, denoted by the star (*) as the superscript, is introduced. These adjoint variables are the Lagrange multipliers of the constraints, the equations of the direct problem.

According to the optimal control theory, all direct and adjoint variables will be considered as mutually independent. The relationships between them will be recovered from the stationarity conditions of the Lagrangian $\mathcal{L}$, characterizing the saddle point.

The Lagrangian functional has the following form:

$$\mathcal{L}(\boldsymbol{u},\boldsymbol{\sigma},p,\boldsymbol{u}^\star,\boldsymbol{\sigma}^\star,p^\star,\boldsymbol{c}) = \sum_{i=0}^{I}\mathcal{L}_i(\boldsymbol{u}_i,\boldsymbol{\sigma}_i,p_i,\boldsymbol{u}_i^\star,\boldsymbol{\sigma}_i^\star,p_i^\star,\boldsymbol{c}), \tag{5.53}$$

where

$$\begin{aligned}\mathcal{L}_i(\boldsymbol{u}_i,\boldsymbol{\sigma}_i,p_i,\boldsymbol{u}_i^\star,\boldsymbol{\sigma}_i^\star,p_i^\star) = \frac{1}{2}\Big(\int_{\Gamma_C} p_i d\Gamma - F_i^{\exp}\Big)^2 + \int_\Omega \operatorname{div}(\Delta\boldsymbol{\sigma}_i)\cdot\boldsymbol{u}_i^\star d\Omega \\ - \int_{\Gamma_F}\Delta\boldsymbol{\sigma}_i\cdot\boldsymbol{n}\cdot\boldsymbol{u}_i^\star d\Gamma + \int_{\Gamma_D}\Delta\boldsymbol{u}_i\cdot\boldsymbol{\sigma}_i^\star\cdot\boldsymbol{n}d\Gamma + \int_{\Gamma_C}(\Delta u_i^n - \Delta U_i - g_i)\cdot p_i^\star d\Gamma \\ - \int_\Omega\Big(\boldsymbol{\varepsilon}(\Delta\boldsymbol{u}_i) - \boldsymbol{S}:\Delta\boldsymbol{\sigma}_i - \frac{\partial\Phi(\boldsymbol{\sigma}_i,\boldsymbol{c})}{\partial\boldsymbol{\sigma}}\Delta t\Big):\boldsymbol{\sigma}_i^\star d\Omega \\ - \int_{\Gamma_C}(\Delta p_i - \Delta\boldsymbol{\sigma}_i^{nn})\cdot u_i^{n\star}d\Gamma - \int_{\Gamma_C}\Delta\sigma_i^{nt}\cdot u_i^{t\star}d\Gamma,\end{aligned}$$

and

- $\boldsymbol{u}_i, \boldsymbol{u}_i^\star \in (H^1(\Omega))^2$,
- $\boldsymbol{\sigma}_i, \boldsymbol{\sigma}_i^\star \in (L^2(\Omega))^4$,
- $p_i, p_i^\star \in N_i = \{q \in (H^{1/2})'(\Gamma_C) \mid q = 0 \text{ on } \Gamma_C/\Gamma_{C_i}\}$. Here $\Gamma_{C_i}$ is the effective contact surface at time $t_i$.

The complex form of this Lagrangian does not permit to draw any conclusions with regard to the existence and uniqueness of its saddle point. Nevertheless, necessary conditions of stationarity can be formally written in order to characterize this eventual saddle point.

The stationarity conditions of $\mathcal{L}$ are given by the following expressions:

$$\sum_{i=0}^{I}\Big\langle\frac{\partial\mathcal{L}_i}{\partial\boldsymbol{u}}, d\boldsymbol{w}_i\Big\rangle = 0 \qquad \forall d\boldsymbol{w}_i \in (H^1(\Omega))^2, \tag{5.54}$$

$$\sum_{i=0}^{I}\Big\langle\frac{\partial\mathcal{L}_i}{\partial\boldsymbol{\sigma}}, d\boldsymbol{\tau}_i\Big\rangle = 0 \qquad \forall d\boldsymbol{\tau}_i \in (L^2(\Omega))^4, \tag{5.55}$$

$$\sum_{i=0}^{I}\Big\langle\frac{\partial\mathcal{L}_i}{\partial p}, dq_i\Big\rangle = 0 \qquad \forall dq_i \in N_i, \tag{5.56}$$

$$\sum_{i=0}^{I}\Big\langle\frac{\partial\mathcal{L}_i}{\partial\boldsymbol{u}^\star}, d\boldsymbol{w}_i\Big\rangle = 0 \qquad \forall d\boldsymbol{w}_i \in (H^1(\Omega))^2, \tag{5.57}$$

$$\sum_{i=0}^{I} \left\langle \frac{\partial \mathcal{L}_i}{\partial \boldsymbol{\sigma}^\star}, d\boldsymbol{\tau}_i \right\rangle = 0 \qquad \forall d\boldsymbol{\tau}_i \in (L^2(\Omega))^4, \tag{5.58}$$

$$\sum_{i=0}^{I} \left\langle \frac{\partial \mathcal{L}_i}{\partial p^\star}, dq_i \right\rangle = 0 \qquad \forall dq_i \in N_i, \tag{5.59}$$

$$\sum_{i=0}^{I} \left\langle \frac{\partial \mathcal{L}_i}{\partial \boldsymbol{c}}, \boldsymbol{d} - \boldsymbol{c} \right\rangle \geq 0 \qquad \forall \boldsymbol{d} \in \mathcal{Q}, \tag{5.60}$$

where $\langle \cdot, \cdot \rangle$ represents in each equation the duality pairing for the corresponding functional spaces.

Calculating the derivatives with respect to the adjoint variables (Eqs. (5.57), (5.58) and (5.59)) leads to the set of equations:

$$\operatorname{div}(\Delta \boldsymbol{\sigma}_i) = 0 \quad \text{in} \quad \Omega, \tag{5.61}$$

$$\boldsymbol{\varepsilon}(\Delta \boldsymbol{u}_i) - \boldsymbol{S} : \Delta \boldsymbol{\sigma}_i - \frac{\partial \Phi(\boldsymbol{\sigma}_i, \boldsymbol{c})}{\partial \boldsymbol{\sigma}} \Delta t = 0 \quad \text{in} \quad \Omega, \tag{5.62}$$

$$\Delta \boldsymbol{\sigma}_i \cdot \boldsymbol{n} = 0 \quad \text{on} \quad \Gamma_F, \tag{5.63}$$

$$\Delta \boldsymbol{u}_i = 0 \quad \text{on} \quad \Gamma_D, \tag{5.64}$$

$$\left.\begin{aligned} \Delta u_i^n - g_i - \Delta U_i &= 0, \\ \Delta \sigma_i^{nn} &= \Delta p_i, \\ \Delta \sigma_i^{nt} &= 0, \end{aligned}\right\} \quad \text{on} \quad \Gamma_{C_i}. \tag{5.65}$$

The preceding calculation leads in the classical Lagrangian theory to the equations of the direct problem. In the present case, in contrast to the classical frame, the equations do not represent exactly the direct problem. However, if $(\boldsymbol{u}, \boldsymbol{\sigma}, p)$ are the solutions to $(\boldsymbol{\mathcal{P}})$, they obviously verify the above relations.

The derivation of $\mathcal{L}$ with respect to the direct variables (Eqs. (5.54), (5.55) and (5.56)) and a series of calculations: spatial integration by parts and use of the first order approximation $f_i \cdot \Delta g_i \approx f^{i+1} \cdot g^{i+1} - f^i \cdot g^i - \Delta f_i \cdot g^i$, gives the following set of equations:

$$\operatorname{div}(\Delta \boldsymbol{\sigma}_i) = 0 \quad \text{in} \quad \Omega, \tag{5.66}$$

$$\boldsymbol{\varepsilon}(\Delta \boldsymbol{u}_i^\star) = \boldsymbol{S} : \Delta \boldsymbol{\sigma}_i^\star - \frac{\partial^2 \Phi(\boldsymbol{\sigma}_i, \boldsymbol{c})}{\partial \boldsymbol{\sigma}^2} \Delta t : \boldsymbol{\sigma}_i^\star \quad \text{in} \quad \Omega, \tag{5.67}$$

$$\Delta \boldsymbol{\sigma}_i^\star \cdot \boldsymbol{n} = 0 \quad \text{on} \quad \Gamma_F, \tag{5.68}$$

$$\Delta \boldsymbol{u}_i^\star = 0 \quad \text{on} \quad \Gamma_D, \tag{5.69}$$

$$\left.\begin{aligned} \Delta u_i^{n\star} &= (F_i^{\text{calc}}(\boldsymbol{c}) - F_i^{\text{exp}}), \\ \Delta\sigma_i^{nn\star} &= \Delta p_i^{\star}, \\ \Delta\sigma_i^{nt\star} &= 0, \end{aligned}\right\} \quad \text{on} \quad \Gamma_{C_i}. \tag{5.70}$$

and the following final conditions at time $T$

$$\operatorname{div}(\boldsymbol{\sigma}_I^{\star}) = 0 \quad \text{in} \quad \Omega \tag{5.71}$$

$$\boldsymbol{\varepsilon}(\Delta\boldsymbol{u}_I^{\star}) = \boldsymbol{S} : \Delta\boldsymbol{\sigma}_I^{\star} \quad \text{in} \quad \Omega \tag{5.72}$$

$$\boldsymbol{u}_I^{\star} = 0 \quad \text{on} \quad \Gamma_D \tag{5.73}$$

$$\boldsymbol{\sigma}_I^{\star} \cdot \boldsymbol{n} = 0 \quad \text{on} \quad \Gamma_F \tag{5.74}$$

$$\left.\begin{aligned} u_i^{n\star} &= 0, \\ p_I^{\star} &= \sigma_I^{nn\star}, \end{aligned}\right\} \quad \text{on} \quad \Gamma_C. \tag{5.75}$$

This set of equations and the final conditions define a well-posed incremental problem with Dirichlet conditions on a part of the boundary and will be called the adjoint problem ($\boldsymbol{\mathcal{P}}^{\star}$).

The preceding calculations can be summarized as:

**Stationarity result:** *If $(\boldsymbol{u}, \boldsymbol{\sigma}, p)$ and $(\boldsymbol{u}^{\star}, \boldsymbol{\sigma}^{\star}, p^{\star})$ are, respectively, the solutions to the incremental direct and adjoint problem ($\boldsymbol{\mathcal{P}}$) and ($\boldsymbol{\mathcal{P}}^{\star}$), then the conditions (5.54), (5.55), (5.56), (5.57), (5.58) and (5.59) of stationarity of the Lagrangian $\mathcal{L}$ are verified.*

Moreover, if $(\boldsymbol{u}, \boldsymbol{\sigma}, p)$ is the solution to ($\boldsymbol{\mathcal{P}}$), then the Lagrangian $\mathcal{L}$ is reduced to the cost functional $\mathcal{J}$. Together with the expression of stationarity conditions (5.60) this implies that:

**Gradient computation:** *If $(\boldsymbol{u}, \boldsymbol{\sigma}, p)$ and $(\boldsymbol{u}^{\star}, \boldsymbol{\sigma}^{\star}, p^{\star})$ are, respectively, the solutions to the incremental direct problem ($\boldsymbol{\mathcal{P}}$) and to the incremental adjoint problem ($\boldsymbol{\mathcal{P}}^{\star}$), then the gradient of the cost functional $\mathcal{J}$ is given by:*

$$\nabla_{\boldsymbol{c}}\mathcal{J} = \sum_{i=0}^{I} \left( \int_{\Omega} \Delta\boldsymbol{\sigma}_i : \frac{\partial \boldsymbol{S}}{\partial \boldsymbol{c}} : \boldsymbol{\sigma}_i^{\star} + \frac{\partial^2 \Phi}{\partial \boldsymbol{\sigma} \partial \boldsymbol{c}} \Delta t : \boldsymbol{\sigma}_i^{\star} d\Omega \right). \tag{5.76}$$

Some remarks can be done about the preceding results:

- The adjoint problem is *not* a contact problem. Its loading is a Dirichlet condition (imposed displacement) on $\Gamma_{C_i}$, the effective contact surface of the direct problem.

- The adjoint problem is a time dependent system of partial differential equations on $[0, T]$ and a final condition given by a well-posed elasticity problem. Therefore the adjoint problem will be integrated from $T$ to 0 in the reversed time.
- The adjoint constitutive law is viscoelastic considered in the reversed time $i' \leftarrow I - i$:

$$\boldsymbol{\varepsilon}(\Delta \boldsymbol{u}^{\star}_{i'}) = \boldsymbol{S} : \Delta \boldsymbol{\sigma}^{\star}_{i'} + \boldsymbol{R} : \boldsymbol{\sigma}^{\star}_{i'} \, \Delta t,$$

where $\boldsymbol{R}$ is the fourth-order tensor:

$$\boldsymbol{R} = \frac{\partial^2 \Phi(\boldsymbol{\sigma}_{i'}, \boldsymbol{c})}{\partial \boldsymbol{\sigma}^2_{i'}}.$$

The pseudo-potential $\Phi$ has to be twice differentiable to ensure the existence of the adjoint state (for example, in the Norton–Hoff constitutive law, $m > 1$ is needed). From a numerical point of view, this leads to a linear problem at each time step and therefore a rapid integration.

- The parameters of the adjoint constitutive law depend on the parameters of the direct constitutive law, but also on the solution of the direct problem. Hence the solution to the adjoint problem is implicitly dependent on the solution of the direct problem.
- The equations of the adjoint problem in the reversed time describe a linear viscoelastic problem with Dirichlet boundary conditions and initial conditions, and is therefore well-posed.
- This method allows to compute of the gradient of the cost functional $\mathcal{J}$ using the solutions to the direct and adjoint problems, independently of the number of parameters involved. A rapid evaluation of the computational problem shows that gradient calculation takes $\approx 1.5$ the time for solving the direct problem due to the simplicity of the adjoint behaviour and the elimination of the contact condition. This is extremely interesting for problems with a large number of parameters. However, the intervention of the solution to the direct problem in the resolution of the adjoint problem, demands large memory space for keeping track of all the fields.

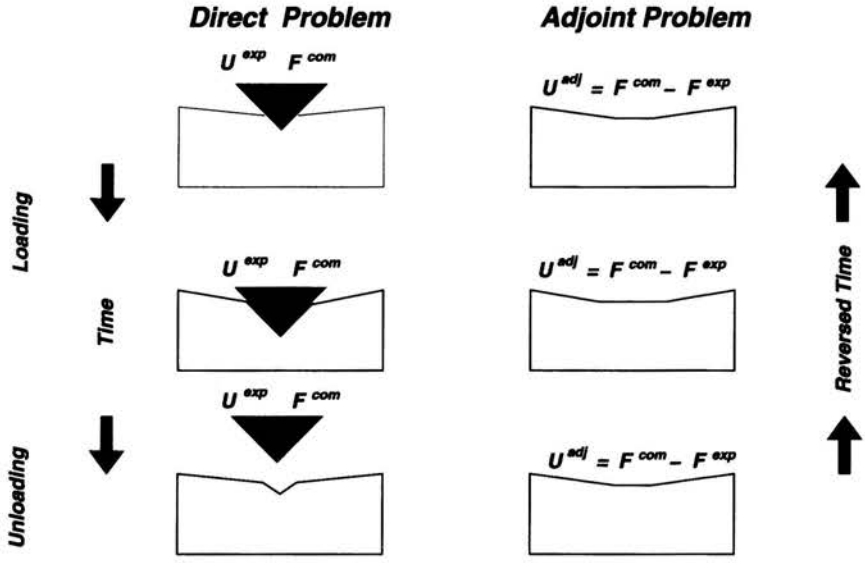


FIGURE 5.4. Evolution of the contact are in the direct indentation problem and definition of corresponding adjoint problem at each time step.

**Norton–Hoff material behaviour.** We recall that the viscoplastic Norton–Hoff constitutive law is expressed by:

$$\boldsymbol{\varepsilon}(\Delta \boldsymbol{u}_i) = \boldsymbol{S} : \Delta \boldsymbol{\sigma}_i + \Delta \boldsymbol{\varepsilon}_i^{\mathrm{p}}, \quad \text{where} \quad \Delta \boldsymbol{\varepsilon}_i^{\mathrm{p}} = \boldsymbol{M} : \boldsymbol{\sigma}_i \Delta t, \tag{5.77}$$

$$S_{ijkl} = \frac{1}{E}((1+\nu)\delta_{ik}\delta_{jl} - \nu\delta_{kl}\delta_{ij}), \tag{5.78}$$

$$\Delta \varepsilon_i^{\mathrm{p}} = \frac{3}{2}\langle \frac{(\sigma_i)_{\mathrm{eq}} - \sigma^Y}{K} \rangle_+^m \frac{\tilde{\boldsymbol{\sigma}}_i}{(\sigma_i)_{\mathrm{eq}}} \Delta t, \tag{5.79}$$

$$\boldsymbol{\varepsilon}(\Delta \boldsymbol{u}_i^*) = \boldsymbol{S} : \Delta \boldsymbol{\sigma}_i^* + \boldsymbol{M} : \boldsymbol{\sigma}_i^*, \tag{5.80}$$

where:

$$\boldsymbol{M} = -\frac{3}{2}\langle \frac{(\sigma_i)_{\mathrm{eq}} - \sigma^Y}{K} \rangle_+^m \frac{1}{(\boldsymbol{\sigma}_i)_{\mathrm{eq}}} \boldsymbol{J} + \frac{\tilde{\boldsymbol{\sigma}}_i \otimes \tilde{\boldsymbol{\sigma}}_i}{(\boldsymbol{\sigma}_i)_{\mathrm{eq}}^2} \frac{9}{4} \left[ \langle \frac{(\sigma_i)_{\mathrm{eq}} - \sigma^Y}{K} \rangle_+^m \frac{1}{(\boldsymbol{\sigma}_i)_{\mathrm{eq}}^2} - \frac{m}{K} \langle \frac{(\sigma_i)_{\mathrm{eq}} - \sigma^Y}{K} \rangle_+^{m-1} \right],$$

$$J_{ijkl} = (\delta_{ik}\delta_{jl} - \frac{1}{3}\delta_{kl}\delta_{ij}).$$

This formula already expresses a forward Euler integration scheme which has been programmed as such in the code.

One notes that the adjoint constitutive law is viscoelastic, nevertheless anisotropic and nonhomogenous.

**Numerical results.** Some numerical results will briefly be discussed next. The results correspond to simulated (see Table 5.1) and real indentation experiments (see Figs. 5.5, 5.7 and 5.6).

TABLE 5.1. Identification results with exact measurements for the Norton–Hoff material for the reference values $E^{\text{ref}} = 100000\,\text{MPa}$, $K^{\text{ref}} = 1500\,\text{MPa}\cdot\text{s}^{1/5}$, $m^{\text{ref}} = 5$ and $\sigma^{Y\text{ref}} = 500\,\text{MPa}$.

| Test | $E^{\text{ini}}$ [MPa] | $K^{\text{ini}}$ $\left[(\text{MPa}\cdot\text{s})^{\frac{1}{m}}\right]$ | $m^{\text{ini}}$ | $\sigma^{Y\text{ini}}$ [MPa] | $E^{\text{final}}$ [MPa] | $K^{\text{final}}$ $\left[(\text{MPa}\cdot\text{s})^{\frac{1}{m}}\right]$ | $m^{\text{final}}$ | $\sigma^{Y\text{final}}$ [MPa] |
|---|---|---|---|---|---|---|---|---|
| 1 | 130000 | 800 | 2 | 1000 | 99664.3 | 1533.36 | 5.38417 | 446.414 |
| 2 | 150000 | 1000 | 3 | 1000 | 100228.0 | 1524.64 | 5.00296 | 491.795 |
| 3 | 150000 | 2000 | 3 | 200 | 99429.3 | 1598.24 | 6.18529 | 343.533 |
| 4 | 150000 | 2000 | 8 | 1000 | 99288.9 | 1657.20 | 6.98908 | 246.959 |
| 5 | 70000 | 2000 | 8 | 200 | 99126.5 | 1682.47 | 6.94556 | 238.366 |
| 6 | 70000 | 3000 | 8 | 250 | 100598.0 | 1451.36 | 4.24316 | 602.651 |
| 7 | 70000 | 1000 | 3 | 250 | 99630.1 | 1521.18 | 4.94161 | 497.229 |
| 8 | 150000 | 1000 | 3 | 250 | 99778.0 | 1516.32 | 5.28676 | 464.255 |

We observe that the parameters have been identified within $\approx 5\%$ of the real values for tests 1, 2, 7 and 8. In other cases, only the Young modulus $E$ and the viscosity $K$ have been reasonably identified (1% error for $E$ and 1-10% for $K$). The power coefficient $m$ and the yield limit $\sigma^Y$ are in these cases still far away from the real values.

However, the final calculated indentation curves are always superposed with the experimental curve, meaning that the minimization of the geometrical distance between them has been achieved. This was also obtained for experimental indentation curves for different materials like nylon (see Fig. 5.5), aluminum (see Fig. 5.7) or polyethylene (see Fig. 5.6).

The previous results are a direct consequence of the poor sensitivity of the cost functional in this region of the parameter space. In order to illustrate this property we have plotted the values of the cost functional $\mathcal{J}$ on a plane of the parameter space determined by the following points:

- the reference point: $\boldsymbol{c} = (100000, 1500, 5, 500)$,
- the initial point in test 5: $\boldsymbol{c} = (70000, 2000, 8, 200)$,
- the final point in test 5: $\boldsymbol{c} = (99126, 1682, 6.95, 238)$.

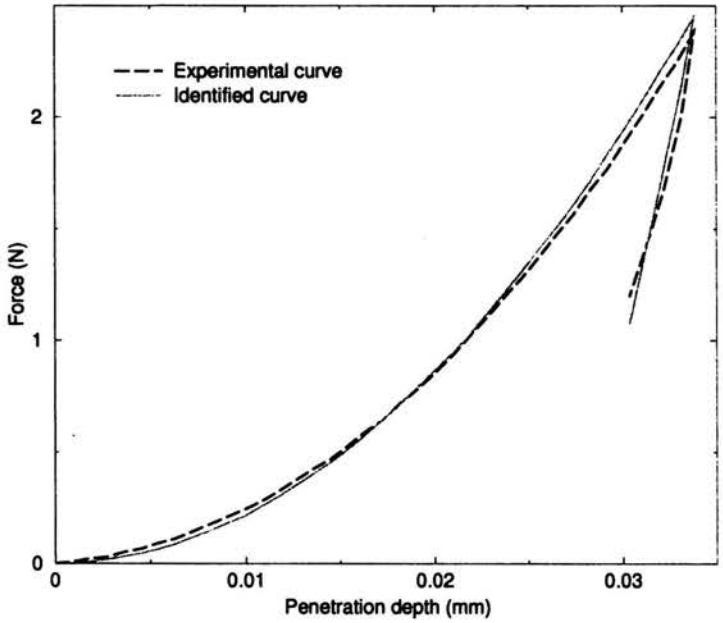


FIGURE 5.5. Experimental and identified indentation curve for nylon.

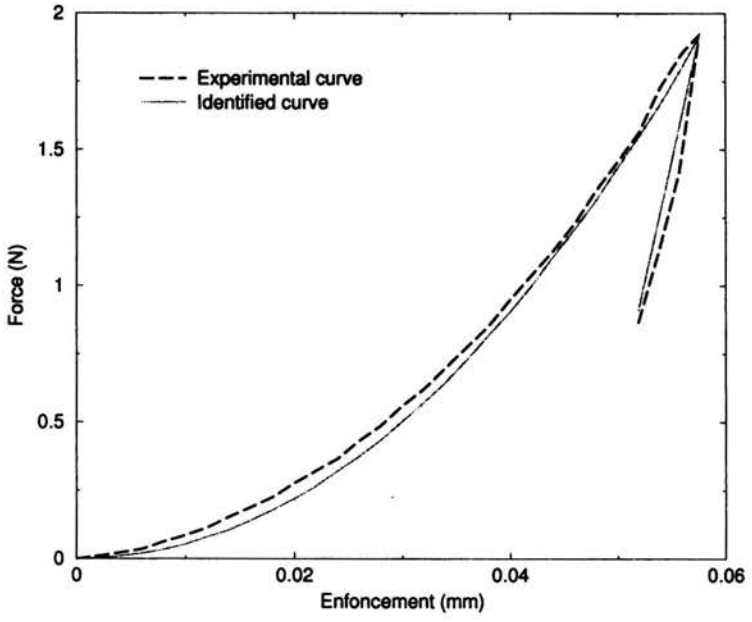


FIGURE 5.6. Experimental and identified indentation curve for polyethylene.

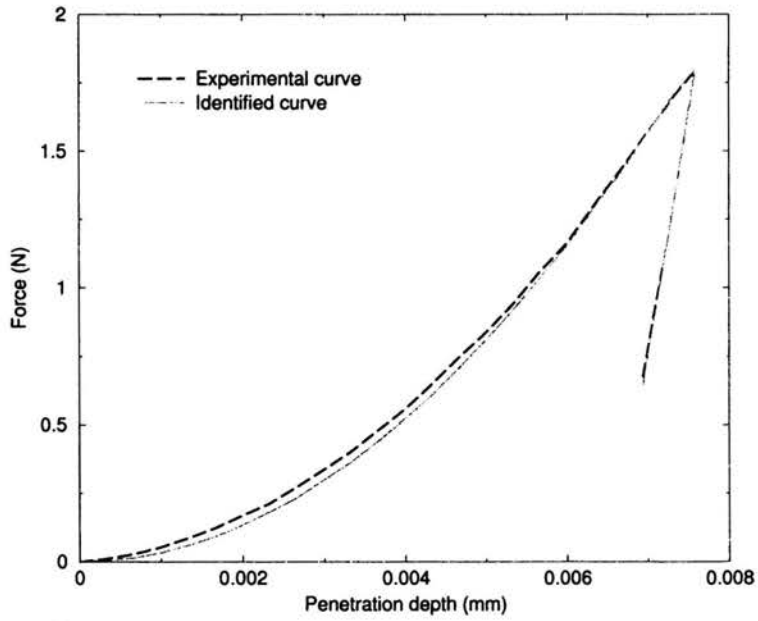


FIGURE 5.7. Experimental and identified indentation curve for a duraluminum.

Using a coordinate parametrization given by two orthogonal vectors, the parameter sets in this plane can be generated using the following formula:

$$\begin{aligned} E &= 100000 - 1315.4a - 80362.7b, \\ K &= 1500 + 273.917a + 714.075b, \\ m &= 5 + 2.93482a + 1.08013b, \\ \sigma^y &= 500 - 394.32a + 142.208b, \end{aligned} \tag{5.81}$$

where $a$ and $b$ are two real parameters.

In Fig. 5.8 we represented the values of the cost functional for the parameter sets generated with $(a, b) \in [-1, 1] \times [-0.5, 0.5]$. Two extreme values $(141200, 923, 2.11, 744)$, i.e $(a, b) = (-1, -0.5)$ and $(58500, 2131, 8.47, 176)$, i.e $(a, b) = (1, 0.5)$ show how spanned are the values covered in this region. The cost functional presents a deep and long valley where it is very difficult to converge to the minimum. A close inspection of the obtained values shows however, that there is a unique minimum in this region.

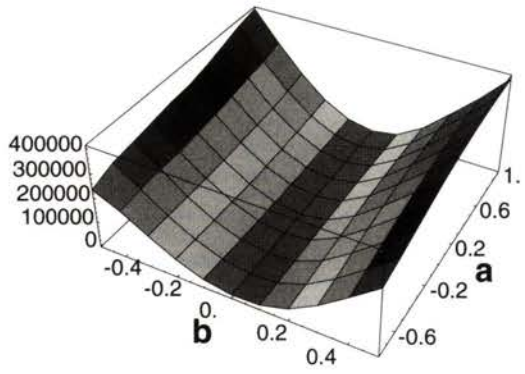


FIGURE 5.8. Shape of the cost functional $\mathcal{J}$ in the $(a, b)$ plane.

## 5.2. Notes

**Further reading on sensitivity analysis.** Some of the topics related to sensitivity analysis and nonlinear material behaviour can be found in the following list of papers and books:

- an excellent introduction to sensitivity analysis is the paper of Tortorelli and Michaleris [15],
- an introduction on the subject can be found in the articles and books [16, 17, 18, 19, 20],
- discussion of tangent operators in plasticity and their impact on sensitivity computations [21, 11, 12],
- applications are to be found for example in [22, 23, 24, 25, 26, 27, 28].

**Programming.** Programming sensitivity analysis for nonlinear material behaviour is a tricky subject. This is not necessarily due to complexity of the subject, but merely because of the difficulties of programming in given commercial finite element computer programmes.

As shown in the examples presented in the preceding Sections, choosing the direct differentiation method of the adjoint state method requires the integration of some general viscoelastic problems with data coming from the direct analysis. The manipulation of data and involved constitutive laws is not always straightforward in this context.

The examples presented before were programmed using the finite element language `gibiane` of the CAST3M computer code. The `gibiane` language has

all the programming possibilities of classical languages like `Fortran` and its operation act directly on the finite element fields. (Some general information about programming in CAST3M is given in [29]). Moreover, the integration of nonlinear material behaviour, i.e. the operator **pasapas** has a possibility of executing a series of commands given by the user, which made programming of the direct differentiation technique very elegant and permitted the usage of the already calculated decomposed tangent stiffness matrix.

## 5.3. References

1. B. HALPHEN and S. NGUYEN QUOC, Sur les matériaux standards généralisés, *Journ. de Mécanique*, 1975.

2. S. NGUYEN QUOC, On the elastic plastic initial-boundary value problem and its numerical integration, *International Journal for Numerical Methods in Engineering*, (11):817–832, 1977.

3. P. PERZYNA, Fundamental problems in viscoplasticity, *Advances in Appl. Mech.*, 9:243–377, 1966.

4. B LECAMPION, A. CONSTANTINESCU, and M.D. NGUYEN, Parameter identification for linned tunnels in viscoplastic media, *Int.J.Numerical and Analytical Methods in Geomechanics*, 26(12):1191–1211, 2002.

5. A. CONSTANTINESCU and L. VERGER, Indentification of a viscoplastic material behaviour under anisothermal conditions, in: D. Petit, D.B. Ingham, Y. Jarny, and F. Plourde (Eds.), *Eurotherm Seminar 68: Inverse problems and experimental design in thermal and mechanical engineering*, pp.221–228, Edizioni ETS, 2002.

6. A. CONSTANTINESCU and N. TARDIEU, On the identification of elastoviscoplastic constitutive laws from indentation tests, *Inverse Problems in Engineering*, 2000.

7. A. CONSTANTINESCU and N. TARDIEU, On the indentification of nonlinear constitutive laws from indentation tests, in: ASME (Ed.), *Inverse Problems in Engineering*, 1999.

8. A. CONSTANTINESCU and N. TARDIEU, Identification strategies for recovering material parameters from indentation experiments, in: M. Tanaka and G. Dulikravich (Eds.), *ISIP'2000 International Symposium on Inverse Problems in Engineering*, Elsevier, 2000.

9. J.C. SIMO and T.J.R. HUGHES, *Computational Inelasticity*, Springer, 1997.

10. J.C. SIMO and R.L. TAYLOR, Consistent tangent operators for rate-indenpendent elastoplasticity, *Computer Methods in Applied Mechanical Engineering*, (48):101–118, 1985.

11. C.A. VIDAL, H.S. LEE, and R.B. HABER, The consistent tangent operator for design sensitivity analysis of history-dependent response, *Computing Systems in Engineering*, 2(5/6):509–523, 1991.

12. C.A. VIDAL and R.B. HABER, Design sensitivity analysis for rate-independent elastoplasticity, *Computer Methods in Applied Mechanical Engineering*, pp.393–431, 1993.

13. N. TARDIEU, *Identification de lois de comportement élastoviscoplastique par indentation*, PhD thesis, Ecole Polytechnique, France, 2000.

14. N. KIKUCHI and J.T. ODEN, *Contact Problems in Elasticity: A Study of Variational Inequalities and Finite Element Methods*, SIAM, Philadelphia, 1984.

15. P. MICHALERIS and D.A. TORTORELLI, Design sensitivity analysis: An overview and review, *Inverse Problems in Engineering*, 1, 1995.

16. K. DEMS and Z. MRÓZ, Variational approach to sensitivity analysis in thermoelasticity, *J. Therm. Stress.*, 10:283–306, 1987.

17. J.J TSAY and J.S. ARORA, Nonlinear design sensitivity analysis for path dependent problems. Part 1: General theory. 81:183–208, 1989.

18. J.J TSAY and J.S. ARORA, Nonlinear design sensitivity analysis for path dependent problems. Part 2: Analytical examples. 81:209–228, 1989.

19. E.J. HAUG, K.Y. CHOI, and V. KOMKOV, *Design Sensitivity Analysis of Structural System*, Academic press, 1986.

20. M. KLEIBER, H. ANTUNEZ, T.D. TIEN, and P. KOWALCYK, *Parameter sensitivity in nonlinear mechanics*, Wiley, Chichester, 1997.

21. P. MICHALERIS, D.A. TORTORELLI, and C.A. VIDAL, Tangent operators and design sensitivity formulations for transient non-linear coupled problems with applications to elastoplasticity, *International Journal for Numerical Methods in Engineering*, 37, 1994.

22. A. GAVRUS, E. MASSONI, and J.L. CHENOT, The analysis of inelastic behaviour formulated as an inverse rheological approach, *Meas. Sci. Technol.*, 9:848–863, 1998.

23. R. MAHNKEN and E. STEIN, Parameter identification for viscoplastic models based on analytical derivatives of a least-square functionals and stability investigations, *Int. J. Plast.*, 12(4):451–479, 1996.

24. R. MAHNKEN and E. KUHL, Parameter identification of gradient enhanced damage models with the finite element method, *European Journal of Solid Mechanics*, 18:819–835, 1999.

25. G.Z. YANG and N. ZABARAS, An adjoint method for the inverse design of solidification processes with natural convection, *International Journal for Numerical Methods in Engineering*, 42:1121–1144, 1998.

26. J. CARRERA, G.A. GALARZA and A. MEDINA, Computational techniques for optimization of problems involving nonlinear transient simulations, *International Journal for Numerical Methods in Engineering*, 45(3):319–334, 1999.

27. N. ZABARAS, Y. BAO, A. SRIKANTH, and W.G. FRAZIER, A continum lagrangian sensitivity analysis for metal forming processes with applications to die design problems, *Int.J.Num.Meth.Engrg.*, 48:679–720, 2000.

28. S. STUPKIEWICZ, J. KORELC, M. DUTKO, and T. RODIC, Shape sensitivity analysis of large deformation frictional contact problems, *Comput.Meth.Appl.Mech.Engrg.*, 191:3555–3581, 2002.

29. A. CONSTANTINESCU, M. DRAGON, and J. KICHENIN, Programming engineering applications using the object oriented FEM code CASTEM 2000, in: M. Henderson (Ed.), *SIAM Workshop on Object Oriented Methods for Interoperable Scientific and Engineering Computing, October 21-24 1998, IBM Watson Research Center, NY USA*, SIAM, 1998.

PART II

# Unified Fatigue Modelling for Structural Applications Based on a Multiscale Approach and Shakedown Hypothesis

KY DANG VAN

# Preface

Fatigue failure is the final result of complex microscopic phenomena which occur under cyclic loading. Traditionally this phenomenon is studied different ways depending on the fatigue regime and on the field of interest: fatigue limit analysis, life prediction in high or in low cycle fatigue, thermal fatigue, etc. The diversity of the proposed approaches is so great that design engineers meet many difficulties to have a clear idea of the fatigue calculations which have to be done. The purpose of this paper is to present *a unified approach to both high and low cycle fatigue based on shakedown theories and dissipated energy.* The discussion starts with a recalling of fatigue phenomena at different scales (microscopic, mesoscopic, and macroscopic). Then some useful aspects of shakedown theory in relation with fatigue are presented. Applications to modelling of high cycle fatigue is then introduced: for instance, some multiaxial fatigue criteria (Dang Van, Papadopoulos) are essentially based on the hypothesis of elastic shakedown at the mesoscopic scale and therefore on a bounded cumulated dissipated energy. Discussion of some aspects of high cycle fatigue in presence of notches or stress concentration locus is done. In the low cycle fatigue regime, some recent results show that we can speak of a plastic shakedown at both mesoscopic and macroscopic scale and a cumulated energy bounded by the failure energy. These ideas are also justified by some infrared thermography test results permitting a direct determination of the fatigue limit.

# Chapter 1

# Introduction to fatigue analysis of structures

Current industrial design is highly concerned by fatigue because this phenomenon is the main failure mode of mechanical structures undergoing variable loads. This type of failure occurs after the repetition of several load cycles (from a few to millions) to the specimen or the mechanical component. Because of the very important implications of fatigue failures in the economy and on the security, many research efforts (in academic as well as industrial laboratories) are devoted to the development of design methods against fatigue.

During a long period, starting with the pioneering work of Wöhler (1860) and ending in the late fifties, high-cycle fatigue (HCF) was one the most significant topic for engineers and researchers. Mechanical engineers were mainly interested in establishing S-N curves and in determining fatigue limits for metallic materials because they are concerned with the effect on lifetime of external loadings. During this period only simple methods like beam theory were available for engineering computations. The stress evaluated in that way is most of the time uniaxial and simple so that S-N curves approach is in adequation with these computational tools. However, scientists are aware of the need of more general criteria and the first multiaxial criteria were proposed quite early in the beginning of the last century.

In the sixties two new approaches for studying fatigue were introduced.

First, a special interest occurred in studying low-cycle fatigue (LCF). Instead of developing stress approaches, Manson and Coffin proposed fatigue

models based on the strain amplitude or the plastic strain amplitude. Their models were derived from uniaxial tests in tension–compression where the longitudinal strain amplitude was imposed. Application of Manson–Coffin approach to structure necessitates inelastic analysis. This is at the origin of important development of inelastic constitutive equations which are necessary to perform this type of fatigue analysis on structures using this theory (Mróz, Chaboche, Lemaitre,...).

Nearly at the same time Paris proposed to use linear fracture mechanics approach for studying fatigue crack propagation. He had first to overcome the doubts of the reviewers of the fatigue journals who ignore at that time this new subject. This new way for studying this old science has rapidly a great audience. With the help of new experimental devices the development of research on fatigue crack propagation became "à la mode" and increases exponentially. Nowadays some authors (see for instance K. Miller [ ]) consider that, in fact, fatigue is only a crack propagation phenomenon and fatigue limit corresponds to a fatigue crack propagation threshold.

These two new trends for studying fatigue are favoured by new experimental devices and more and more precise observations. The two cited approaches showed their effectiveness in some cases for structures in the aeronautical and nuclear industry. However, these successes were obtained when the stress or the strain cycle were uniaxial and simple. As stresses and strain are often multiaxial and present a complex path during a loading cycle, application of these models is then difficult and the predicted results are often not in reasonable agreement with test results. Nevertheless these new fatigue approaches has so much success that the more classical domain of high cycle was more or less neglected: few new ideas concerning this field of application was proposed despite the great number of existing fatigue criteria. Surprisingly, the only theoretical tools mostly used by the mechanical industries are always those developed during the 19th or at the beginning of the $20^{th}$ century. Nowadays S-N curve, Goodman–Haigh diagram or Gerber diagram approach are still used as design tools to predict fatigue resistance of mechanical structures, even if they are only applicable in uniaxial situations. The computational methods like FEM or integral equations methods are much more efficient in comparison with beam theory so that the stress and the strain states on structures are defined not only by nominal stress or strain value but by fields of tensorial components. The S-N curve method is then clearly not sufficient and more sophisticated methods are needed. This is particularly true when

the fatigue resistance of mechanical structures which have to resist to complex cyclic loadings is evaluated, which necessitates the use of multiaxial fatigue criteria. In the high cycle regime, many proposals exist. They are mostly based on stress or stress amplitude parameters, corresponding for instance to adaptation of plasticity criteria to fatigue applications. For instance, many fatigue criteria are obtained by replacing Tresca or Mises equivalent stress by similar quantities formulated by using amplitude of stress. Predictions are often poor and not in reasonable agreement with experiments so that the design of structures which have to resist to fatigue (and particularly to high cycle fatigue) is still a problem: engineers have to perform difficult and time consuming experiments to find fatigue limit of mechanical structures. This is done generally on the structure itself, which necessitates iterative experiments on one to one scale test models.

The need of more efficient design methods, the generalization of finite elements calculations favor the development of researches. Therefore, a significant effort has been put into for deriving reliable fatigue computational methods applicable to the previous situations. Beside the fatigue crack propagation methods (which are not studied hereafter), the actual prediction techniques are generally based on multiaxial fatigue criteria using a stress approach in the HCF regime and on strain or inelastic strain approaches in the LCF domain. The materials fail in both domains in similar ways, however, nowadays the approaches for modelling these two types of fatigue are different.

In the present paper a unified approach is proposed in order to overcome this difficulty. It is derived from a HCF multiaxial fatigue theory based on a multiscale approach [1], from some recent results in LCF and shakedown theories [2, 3, 4].

# Chapter 2

# Short description of fatigue mechanisms: the necessity of a multiscale approach

Phenomena which cause fatigue failure differ from those which can be observed in static failures. It can be caused by a preexisting crack or defect which lead to stress concentration; in that case, it is traditional to consider that it is mainly a problem of propagation after a short period of incubation. However, in the absence of such defects, an initiation period is necessary for the formation of the first detectable cracks which will lead to the final breakage. This period can take a great part of the fatigue life, particularly in the high cycle fatigue regime. In this regime, even if no plastic strain is detected at the engineering scale, one can observe plastic slip bands localized in some grains. Since the first observations by Gough, many other scientists have studied the microstructural changes in fatigue, and particularly the mechanisms of the formation of persistent slip bands and the associated intrusion extrusion phenomena. As noted by J. Polak, the characteristic feature of the cyclic deformation is an inhomogeneous distribution of the cyclic strain in the material. This is particularly true when the applied load is low corresponding to the high cycle fatigue. It is then difficult to derive computational methods which can be employed by engineers for quantitative prediction of the fatigue resistance of mechanical structures. By studies based only on macroscopic approaches: before crack initiation, the observable behavior of the material does not show any deviation from elasticity. Though not detectable at the macroscopic scale, it is precisely the evolution of irreversible processes

(broadening of the persistent slip bands) which take place at the level of the metallic grains which leads to the initiation of first cracks. The introduction of the grain scale is thus suitable to model correctly and to capture the main features of mechanisms of plastic deformation which are not detectable at the macroscopic scale when the specimen is subjected to low or moderate cyclic loads.

In discussing fatigue phenomena we shall distinguish three scales:

- the microscopic scale of dislocations,
- the mesoscopic scale of grains,
- the macroscopic scale representing phenomena at the scale of engineers.

In a simplified analysis one can say that fatigue phenomena start generally with appearance of slip bands in grains which broaden progressively during first cycles. The proportion of grains in which slip bands develop increases with the applied load.

In the *high-cycle fatigue regime* (HCF), as the material behaviour seems to be purely elastic; no inelastic behaviour (plastic or viscous) is detected in general and consequently the use of stress or strain at this engineering scale is equivalent. In practice stress is often preferred to strain. However, at a *mesoscopic* level, plasticity occurs in certain number of grains and generates a *heterogenous* plastic strain. Only misoriented crystals undergo plastic slip corresponding to a heterogeneous distribution of micro cracks. The initiation of first visible crack, at the macroscopic scale, represents a large part of the fatigue life.

The *low-cycle fatigue regime* (LCF) implies significant macroscopic deformations leading to irreversible deformations detectable at this level. At the mesoscopic level, the metal grains are subjected to plastic deformation in a more homogeneous manner than in the HCF regime. The first micro cracks in the persistent slip bands appear quite early in the life of the structure. The strain and the plastic strain are no more related to the stress through a simple relations but depend strongly on the loading path. For instance, it is well-known that two similar stress state may correspond to completely different plastic strain history. Thus the use of stress parameter or strain is not equivalent.

*In both LCF and HCF damage phenomena occur in the grains*, and therefore the use of mesoscopic fields seem to be relevant for studying fatigue phenomena. Let us recall, that the macroscopic fields (stress $\Sigma$, strain $E$,

plastic strain $P$, etc.) are in a certain sense approximately the mean value of the mesoscopic fields (stress $\sigma$, strain $\epsilon$, plastic strain $p$, etc.). The macroscopic fields are therefore supposed constant in a small volume, surrounding the point under consideration. In the theories of polycrystalline aggregates, this volume is called "representative volume element" or RVE. For instance, the mesoscopic stress $\sigma$ and the macroscopic stress $\Sigma$ are related by the following formula:

$$\sigma = A.\Sigma + \rho, \tag{2.1}$$

where $\rho$ is the local residual stress and $A$ is the elastic stress localization tensor. $A$ is the identity tensor if local and macroscopic elastic moduli are similar. This relation *shows that it is incorrect to use* $\Sigma$ for characterizing phenomena which occur at the grain scale since the *local stress* $\sigma$ *is not proportional to* $\Sigma$ and does not include information about $\rho$. More precisely, fatigue criteria using maximum stress (or some combination of maximum stress) are only valid for loading paths for which they are derived by correlating experimental results; therefore they cannot be extended to take account of multiaxial loadings, and as consequently they cannot be used practically for mechanical design. However, this way to proceed is very often used even if it is not valid.

As fatigue is caused by irreversible phenomena let us compare the dissipated energy at both mesoscopic and macroscopic scales. It is well-known (see for instance [1]) that the total macroscopic work rate is the mean value in the RVE of the local total work rate. However, the equality between the mesoscopic and macroscopic energy does not hold for plastic dissipation as proven by H. D. Bui and recalled also in [1]. The difference between macroscopic plastic dissipation and mean value of mesoscopic plastic dissipation decreases with increasing plastic strain, as the plastic heterogeneity from grain to grain decreases. This also justifies why macroscopic plastic deformation is a reasonable approximation in LCF.

The evaluation of the local mesoscopic fields from the macroscopic ones is in general a difficult task since *the material is locally heterogeneous and has to be considered as a structure when submitted to complex loading histories.* Depending on the loading characteristics one can accept different simplifying assumptions which will permit to find a solution to the problem. The multiscale approaches in fatigue that we promote are precisely based on the use of mesoscopic parameters instead of engineering macroscopic quantities. *In order to derive a unified theory of fatigue, we shall assume that the elastic*

*shakedown occurs at the level of the microstructure as well as at the macroscopic one.*

Before studying the application of the shakedown theory to the microstructure, let us examine some physical models which were at the origin of the proposed approach.

# Chapter 3

# On some physical modellings of fatigue

The first multiscale fatigue model was proposed by Orowan [5]. In fact, this model is only qualitative. Orowan wants to give a plausible explanation of fatigue fracture near the fatigue limit. In this regime, the stress could be well below the macroscopic yield limit. To derive his model, this author observes that fatigue is generally due to stress concentrations, heterogeneity, etc., and that the first fatigue phenomena are microscopic and local i.e. they appear in some grains which have undergone plastic deformations. These deformations are localized in intra-crystalline shear bands, the rest of the matrix behaves elastically because the macroscopic plastic strain is negligible. The first cracks initiate precisely in these shear bands.

Using such an approach, Orowan proposed the following model depicted in Fig. 3.1.

A weak plastic element is embedded between two elastic springs, which impose their deformation to the whole system. The weak element undergoes plastic strains $\Gamma$ and hardens. If the plastic behaviour of this element is governed by pure isotropic hardening, as shown in Fig. 3.1, then its response tends towards an elastic shakedown state precluding fatigue. The limit state in that case oscillates between A (the corresponding shear is $\tau$) and B (the corresponding shear is $-\tau$). The local shear loading is symmetric even if the prescribed external loading is not symmetric. Then, if the limit range is smaller than some definite value, there is no fatigue. On the contrary, fatigue occurs if this condition is not satisfied.

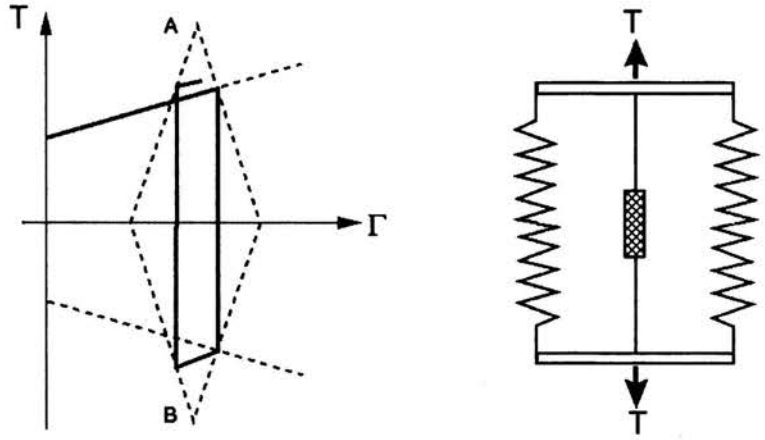


FIGURE 3.1. Schematic representation of fatigue crack initiation after Orowan [5].

Orowan's model is interesting, however it contains an error, because it does not take into account the generation of residual stress arising from incompatibility between the weak plastic element and the elastic matrix.

A very simple generalization of Orowan's model can be proposed based on the use of Lin–Taylor model [1].

Let us consider an inclusion submitted to a uniform plastic strain $p$ and embedded in an elastic matrix. Let $L$ and $l$ be respectively the elastic compliance of the matrix and the inclusion. Suppose that under external loading, the total strain of the matrix and of the inclusion are the same (Lin–Taylor model):

$$E = \varepsilon^{\mathrm{e}} + p. \tag{3.1}$$

Multiplying both sides of the previous relation by $l$ and taking into account the elastic stress-strain relations:

$$\sigma = l : \varepsilon^{\mathrm{e}}, \tag{3.2}$$

$$E = L^{-1} : \Sigma, \tag{3.3}$$

one obtains:

$$\sigma = l : L^{-1} : \Sigma - l : p. \tag{3.4}$$

This relation is similar to Eq. (2.1), where $l : L^{-1}$ is a localization tensor that concentrates the stress (tensor $A$ of Eq. (2.1)) and $l : p$ corresponds to the local residual stress induced by the mesoplasticity (plasticity in the

grain). Then similarly to Orowan's model, the fatigue crack initiation criterion in high cycle regime can be formulated using local stress tensor $\sigma$ in the stabilized state. The proposed criterion will be detailed later in Sec. 5.1.

If one assumes that elastic shakedown occurs before fatigue, then local plastic deformation $p$ and residual stress field $\rho$ become independent of time after a certain number of loading cycles, whereas the local stress as well as the macroscopic stress varies cyclically. If the possibility of shakedown coincide with fatigue limit, then it is possible to characterize limit state by the associated hardening parameter, as it was proposed by Y. V. Papadopoulos [6].

Let us notice that if macroscopic plastic deformation occurs, then Eq. (3.4) must be modified:

$$\sigma = l : L^{-1} : \Sigma - l : \left(p - E^{\mathrm{p}}\right), \tag{3.5}$$

which is similar to the famous Kröner–Eshelby equation which is very popular among specialists of polycristalline theories.

The local residual stress is now related to the difference between plastic deformation of the matrix and of the grain. In the high cycle regime, it is natural to suppose that near the fatigue limit, both plastic deformations are stabilized (elastic shakedown at both scale of material description).

However, if the loading is such that stabilization is not possible, the number of cycle for fatigue failure is low. This regime corresponds to low cycle (plastic) fatigue.

Formulae (3.4)-(3.5) show that the residual stress is a function of the plastic deformation and of the elastic modulus of the material. More generally, the residual stress is a functional of the plastic deformation and is proportional to the elastic moduli.

# Chapter 4

# Elastic shakedown of an elastoplastic structure

Under cyclic loadings, an elastoplastic mechanical structure may have three possible asymptotic responses after a certain numbers of cycles (which could be infinite):

- elastic shakedown which corresponds to stabilization on a pure elastic response,
- elastoplastic shakedown when this response is stabilized on an elastoplastic cycle,
- ratcheting when their is no possible stabilization.

The static theorem of Melan gives a sufficient condition for elastic shakedown for a structure made of elastic perfectly plastic material. It can be stated as follows:

> *If there exist a time $\theta$ and a fixed (i.e. independent of time t) self-equilibrated stress field $R(x)$ and a safety coefficient $m$ such that $\forall$ point $x$ of the structure and $t > \theta$*
>
> $$g\big(m(\Sigma_{\text{el}}(x,t) + R(x))\big) < k^2,$$
>
> *the structure will shakedown elastically.*

$\Sigma_{\text{el}}$ is the stress response of the structure under the same external loading, but under the assumption that the constitutive material has a pure elastic behaviour.

(This formulation, due to W. Koiter, differs slightly from the original formulation of Melan).

Demonstration and discussions of this theorem was given in a famous paper of Professor W. Koiter [2]. In his paper, Koiter draws attention to the fact that this theorem and its proof do not say anything about the magnitude of plastic deformation which may occur before the structure reaches its shakedown state. It is clear that too large plastic deformation gives a solution, which has no physical meaning. But, Professor Koiter added that if *"the total amount of plastic work performed in the loading is accepted as suitable criterion for assessing the overall deformation, boundedness of the overall deformation may be proved if the structure has a safety factor* $m > 1$ *with respect to shakedown."*

We do not reproduce more detail of this discussion; *we shall retain the condition that total plastic work must be bounded to ensure acceptable bounds on plastic deformation.*

Melan's theorem was extended by different authors to account for more realistic material behaviour. In particular, generalization to elastoplastic material combining linear kinematic and isotropic hardening by Mandel et al. [3] (and Q. S. Nguyen but with an other formalism which will be recall hereafter) is particularly interesting. However, these theorems are difficult to apply, because the fixed stress field $R(x)$ must be self-equilibrated, a condition which is not easy to fulfil.

That's why Mandel et al. give another proposal, which is a *necessary condition* of elastic shakedown. This last condition can be summarized as followed (J. Mandel, B. Halphen, J. Zarka [3]):

> *Shakedown occurs if it exists a fixed stress tensor* $\Sigma^*$ *(not necessarily self-equilibrated) such that*
>
> $$\forall t > \theta, g\left(\Sigma_{\text{el}}(x,t) - \Sigma^*\right) - K^{*2}(P_{\text{eq}}) \leqslant 0.$$
>
> *The isotropic hardening parameter* $K$ *is supposed to be an increasing function of equivalent plastic strain* $P_{\text{eq}}$ *beyond some limit* $K^*$. $K^{*2}(P_{\text{eq}})$ *is the maximum acceptable value of the yield radius.*

Thus, at the shakedown limit, $\Sigma^*$ is the centre of the of the smallest hypersphere surrounding the local loading path $\Sigma_{\text{el}}(x,t)$, the radius of which is $K^*(P_{\text{eq}})$.

This theorem is very useful in fatigue.

At that point of the presentation, it is interesting to recall a proposal of J. Zarka [6] for studying asymptotic responses of structures made of elastoplastic linear kinematic hardening material submitted to cyclic loadings. For such material, the yield function can be written as follows:

$$\forall t > \theta \quad g\big(\Sigma(x,t) - cP(x,t)\big) - K^{*2} \leqslant 0, \tag{4.1}$$

where $c$ is the linear kinematic hardening parameter, which is of the order of magnitude smaller than the elastic modulus. Since $\Sigma = \Sigma_{el} + R$, the previous inequality can be rewritten as follows:

$$\forall t > \theta \quad g\big(\Sigma_{el}(x,t) + R(x,t) - cP(x,t)\big) - K^2 \leqslant 0. \tag{4.2}$$

$R$ must be self-equilibrated, but no such condition is required for $\Sigma^* = -(R - cP)$. At the shakedown state $R$ and $P$ and consequently $\Sigma^*$ are independent of time.

Let us return to the Melan–Koiter sufficient shakedown condition. Koiter's reasoning can be also extended to strain hardening material in the framework of the generalized standard material theory as introduced by Q. S. Nguyen et al. and recalled in [7]. (Most of the classical metallic material belong to this class). The boundedness of the dissipation (which corresponds to plastic work plus work induced by generalized strain hardening parameters) assures that the plastic deformation as well as strain hardening parameters are bounded (see [4]). Since these results are not familiar to fatigue specialists, it is necessary to recall some important points of these theories:

Let us begin first with the classical case of a perfectly elastic plastic material. The elastic domain is defined by

$$g(\Sigma) - k^2 \leqslant 0, \tag{4.3}$$

and the associated plastic flow rule can be written as follows as follows:

$$\dot{P} = \mu \frac{\partial g}{\partial \Sigma} = N_c(\Sigma), \qquad g \leqslant 0, \qquad \mu \geqslant 0, \qquad \mu g = 0. \tag{4.4}$$

Here $\mu$ is the plastic multiplier which is non-negative. One can see easily that the plastic flow direction is normal to the plasticity convex at the point $\Sigma$, which can be denoted by

$$\dot{P} = N_c(\Sigma). \tag{4.5}$$

The dissipation rate is:

$$D(\dot{p}) = \Sigma \dot{P}. \tag{4.6}$$

The proof of the classical Melan–Koiter theorem for elastic perfectly plastic material can be performed in two steps:

1. in the first step, it is proved that under the previous assumptions, the dissipated energy is bounded,
2. in the second step, one demonstrates that the distance between $\Sigma(x,t)$ and $\Sigma_{el}(x,t)$ tends toward a constant value.

Only demonstration of the first step is recalled in the following.

Taking account of the property (4.5), one has for all plastically admissible stress field $\Sigma^*$:

$$\int_V (\Sigma - \Sigma^*) : \dot{P} dV \geqslant 0. \tag{4.7}$$

Choosing $\Sigma^* = m(R + \Sigma_{el}(t))$, which is plastically admissible by assumption, the following inequality is derived:

$$\int_V (\Sigma - R - \Sigma_{el}) : \dot{P} dV \geqslant \frac{m-1}{m} \int_V \Sigma \dot{P} dV. \tag{4.8}$$

Since $(\Sigma - R - \Sigma_{el})$ is self-equilibrated and the rate of displacement field $\dot{u} - \dot{u}_{el} = 0$, the application of virtual work principle gives:

$$\begin{aligned} 0 &= \int_V (\Sigma - R - \Sigma_{el}) : (\dot{E} - \dot{E}_{el})\, dV \\ &= \int_V \left[ (\Sigma - R - \Sigma_{el}) : P + (\Sigma - R - \Sigma_{el}) : M : (\dot{\Sigma} - \dot{R} - \dot{\Sigma}_{el}) \right] dV, \end{aligned} \tag{4.9}$$

where $M$ is the elasticity matrix. One concludes that:

$$-\int_V (\Sigma - R - \Sigma_{el}) : M : (\dot{\Sigma} - \dot{R} - \dot{\Sigma}_{el})\, dV \geqslant \frac{m-1}{m} \int_V \Sigma : \dot{P}\, dV. \tag{4.10}$$

After time integration, one obtains the following inequality

$$I(t_0) - I(t) \geqslant \frac{m-1}{m} W^p, \tag{4.11}$$

where $W^p$ is the plastic work and $I(t)$ is defined by:

$$I(t) = \int_V \tfrac{1}{2} (\Sigma - R - \Sigma_{el}) : M : (\Sigma - R - \Sigma_{el})\, dv. \tag{4.12}$$

The dissipated energy is thus bounded.

This result can be extended to more general elastoplastic behaviour, due to the *general standard material concept* introduced first by Q. S. Nguyen et al. [7]. Beside the usual strain parameters $E$ and $P$, these authors introduced a set of strain hardening parameters denoted symbolically by $\beta$. It is then possible to define a potential energy $W(E, P, \beta)$, from which one derives the family of "associated generalised forces" $A(\Sigma, A_p, A_\beta)$. More precisely:

$$\Sigma = \frac{\partial W}{\partial E}, \qquad A_p = -\frac{\partial W}{\partial P}, \qquad A_\beta = -\frac{\partial W}{\partial \beta}. \tag{4.13}$$

The elastic domain is a convex of the "generalised forces" space defined by:

$$g(A_p, A_\beta) \leqslant 0. \tag{4.14}$$

The constitutive equations can be written in a symbolical way like in perfect plasticity:

$$\dot{\alpha} = N_C(A), \tag{4.15}$$

where $\alpha = (P, \beta)$. The previous equation corresponds to (generalised) normality rule, like in perfect plasticity (Eq. 4.5). More precisely:

$$\dot{P} = \mu \frac{\partial g}{\partial A_p}, \qquad \dot{\beta} = \mu \frac{\partial g}{\partial A_\beta}, \qquad g \leqslant 0, \qquad \mu \geqslant 0, \qquad \mu g = 0. \tag{4.16}$$

The maximum dissipation principle which can be written for all $A^* \in C(\alpha)$ ($A^*$ is said to be plastically admissible):

$$A.\dot{\alpha} \geqslant A^*.\dot{\alpha} \tag{4.17}$$

results from the normality rule and the convexity of $C$. This expression is an extension of Hill's maximum principle (or Drucker's postulate) to generalised elastoplastic behaviour.

The corresponding Melan–Koiter theorem for generalised standard material then reads:

> *Elastic shakedown occurs, whatever the initial state of the structure, if there exists a field of internal parameters $\alpha^*$ and a safety coefficient $m > 1$ such that the associated generalised force field $A^*(t)$ is plastically admissible $\forall t > T$.*

Under these assumptions, Q. S. Nguyen [5] demonstrates the following inequality:

$$I(t_0) - I(t) \geqslant \frac{m-1}{m} \int_{t_0}^{t} \int_{V} A.\dot{\alpha}\, dV, \tag{4.18}$$

where $I(t) = \int_V W(E - E^*, \alpha - \alpha^*)\, dV$.

This expression is similar to inequality (4.11) corresponding to classical Melan–Koiter theorem for elastic perfectly plastic material.

The dissipated energy being bounded, the set of parameters $\alpha$ representing the plastic strain and the internal hardening parameters are also bounded.

Let us notice that the only assumption on the inelastic strain $P$ is that $\alpha = (P, \beta)$ must fulfil the normality law. Except this requirement $P$ could be purely deviatoric or can include a hydrostatic part.

# Chapter 5

# Application of the shakedown theory to fatigue

We propose to apply the shakedown theory to the microstructure in order to derive a unified fatigue model valid for structural applications. The main assumptions of this model are the following:

- Near the fatigue limit but below it, elastic shakedown takes place at all scales of material description, at the macroscopic scale as well as at the mesoscopic scale. In particular the local plastic dissipation must be bounded.
- If the loading history is such that elastic shakedown is not possible, then the local admissible dissipation is bounded. *This bound corresponds to fatigue initiation energy.* The number of cycle necessary to dissipated this energy corresponds to the initiation period.

## 5.1. Application to fatigue limit criterion

In the high cycle regime, only few misoriented grains (with respect to the loading) undergo plastic deformation in localized slip bands. Under the fatigue limit, i.e., the threshold between the infinite and finite lifetime, the dissipation at the macroscopic scale is bounded and therefore the dissipated energy per cycle decreases to become after a while negligible (see Fig. 5.1).

In engineering applications, it is therefore not easy to characterize it by evaluating directly the accumulated plastic strain, and consequently it is dif-

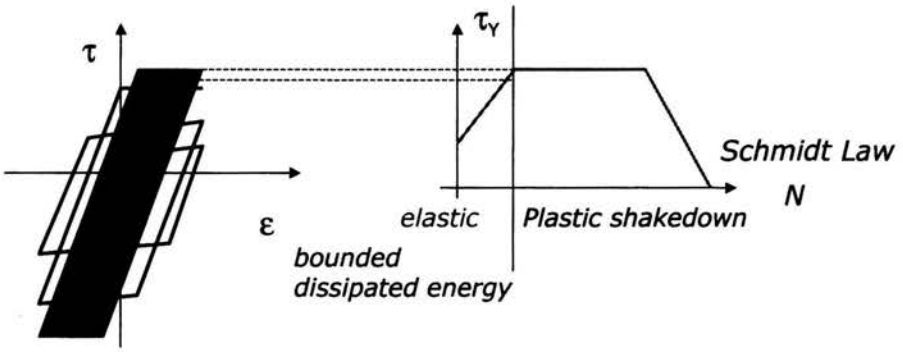


FIGURE 5.1. Elastic and plastic shakedown at the mesoscopic scale. Two types of limit cycles (elastic and plastic shakedown) are shown on the left. Initiation period corresponds to the number of cycles separating the elastic and plastic shakedown on the right.

ficult to calculate dissipated energy cycle by cycle as it was done by I. V. Papadopoulos [8]. This calculation is in fact only a way to construct a theoretical model of fatigue than to derive a proposal for practical applications.

It is the reason why two different ways were explored:

1. When the loading characteristics correspond to the fatigue limit, then the asymptotic stabilized stress state is contained in a limit yield surface defined by the limit radius $K^*$. Papadopoulos in an early work proposes a theory in which $K^*$ depends (linearly) on the maximum hydrostatic tension induced by the loading cycle [9].
2. In 1973, Dang Van, generalizing the idea of Orowan, proposed to consider the mesoscopic current stress state at the apparent stabilized (shakedown) state as the relevant parameters in order to formulate a polycyclic multiaxial fatigue resistance criterion. More precisely, the proposed criterion is a combination of mesoscopic shear $\tau(t)$ and the concomitant hydrostatic pressure $p_H(t)$.

The formulation of the proposed criterion is the following:

*if* $\tau(t) + ap_H(t) - b > 0$, *where* $a$ *and* $b$ *are material constants, then the fatigue will occur.*

The two coefficients $a$ and $b$ can be determined by two simple fatigue experiments; for instance, $b$ corresponds to the fatigue limit in simple shear.

General application of this criterion requires:

- first to evaluate the mesoscopic stress tensor knowing the macroscopic stress cycle; this can be done under the assumption of elastic shakedown near the fatigue limit by constructing the smallest hypersphere surrounding the macroscopic loading path as it is suggested the theorem of Mandel et al. Details of this construction is given in [1];
- second one must consider the plane on which the set $(\tau(t), p_H(t))$ is a "maximum" relative to the criterion. This computation can be done as follows:

The maximum local shear at any time $t$ is given by

$$\tau(t) = \text{Tresca}\left(\sigma(t)\right) = \max_{I,J} |\sigma_I(t) - \sigma_J(t)|. \tag{5.1}$$

The stresses $\sigma_I(t)$, $\sigma_J(t)$ are the principal stresses at time $t$.

The quantity that quantifies the danger of fatigue occurrence is defined by

$$d = \max_t \frac{\tau(t)}{b - a\, p_H(t)}. \tag{5.2}$$

$d$ is calculated over a period, and the maximum is to be taken over the cycle.

It is frequent in the applications in high cycle fatigue (elastic regime) to use *the concept of local equivalent stress* for a life duration $N_i$ defined by

$$\tau_{0,i} = \tau + a_i\, p_H. \tag{5.3}$$

For the fatigue limit $\tau_{0,i}$ corresponds to material constant $b$, but is different from b in general because $\tau_{0,i}$ and $a_i$ depend of $N_i$. If $a_i$ (slope of the fatigue line in $\tau - p_H$ diagram) depends weakly on $N_i$, taking $a_i \approx a$, it is possible to define the local equivalent stress by

$$\tau_0 = \tau + a\, p_H. \tag{5.4}$$

Very often $\tau$ and $p_H$ are maximum at the same time, so that is sufficient in some applications to plot $\tau_{\max}$ versus $p_{H\max}$ (cf. [10]).

## 5.2. Comments on notch effect in high cycle fatigue

The presence of defects like notches, cracks, and inclusions on mechanical structures induce an increase of the local stress and strain which is very harmful for the fatigue resistance. In order to take account of the notch effect,

it is traditional to distinguish the theoretical stress concentration factor $K_t$ and the fatigue concentration factor $K_f$.

$K_t$ is defined for notched test specimen as the ratio between maximum local stress (tension or shear) in the vicinity of the notch and the nominal stress (tension or torsion).

$K_f$ is the ratio between the fatigue resistance (in tension or in torsion) of the notched specimen and the fatigue resistance of a smooth specimen submitted to the same type of load. It is observed that $K_f$ differs from $K_t$ in a complex way. The explanation of this dependence is very simple if we accept the validity of the proposed model. Indeed, it is assumed that near the fatigue limit, elastic shakedown should occur at both the macro and the mesoscale.

Shakedown at macro scale means that at a point $x$ in the vicinity of the notch there exists a macroscopic residual stress field $R$ such that

$$\Sigma(x,t) = K_t.\Sigma_{el}(x,t) + R(x). \tag{5.5}$$

Relation (2.1) can be rewritten:

$$\sigma = A\big[K_t.\Sigma_{el}(x,t) + R(x)\big] + \rho(x). \tag{5.6}$$

Since mesoscopic stress tensor $\sigma$ intervenes in the fatigue criterion, there is no simple relation between $K_t$ and $K_f$ .

## 5.3. Application to low cycle fatigue

Plastic fatigue or low cycle fatigue is very much studied since the pioneering work of Manson and Coffin. In order to fit experimental results, these authors proposed to use the amplitude of plastic strain as a relevant parameter. These tests were uniaxial and strain was controlled. In that case it is clear that the stress is related to the plastic strain amplitude in the stabilized state so that the plastic dissipation is a function of strain amplitude.

However, in the case of cycles involving more complex stress state there is no such relation, since it is well-known that *in plasticity the response depends closely on the loading path and on the constitutive equations.* Generalisation to 3D formulation of elastoplastic cyclic curve is a convenient way to do, but which is not backed up by any theoretical background. In view of plastic fatigue applications, many elastoplastic or elastoviscoplastic constitutive

equations were proposed in the eighties (cf.: J. L. Chaboche, J. Lemaitre, Z. Mróz, ...), and summarised for instance in [11]. By numerical computations, it is then possible to evaluate plastic strain amplitude or plastic dissipated energy; let us notice, however, that for general cyclic loading paths, there is (on the contrary to uniaxial loading mentioned previously) no evident relation between those two quantities. Criteria based on plastic strain amplitude are then not equivalent to those based on plastic dissipation. The following question arises: what is the "good" parameter in plastic fatigue from a practical as well as from a theoretical point of view? Basing on the previous discussion we prefer to use a criterion based on a limitation of the local dissipation, since this feature ensures that the corresponding deformation is also bounded, which is a natural necessary condition for no rupture. Moreover,

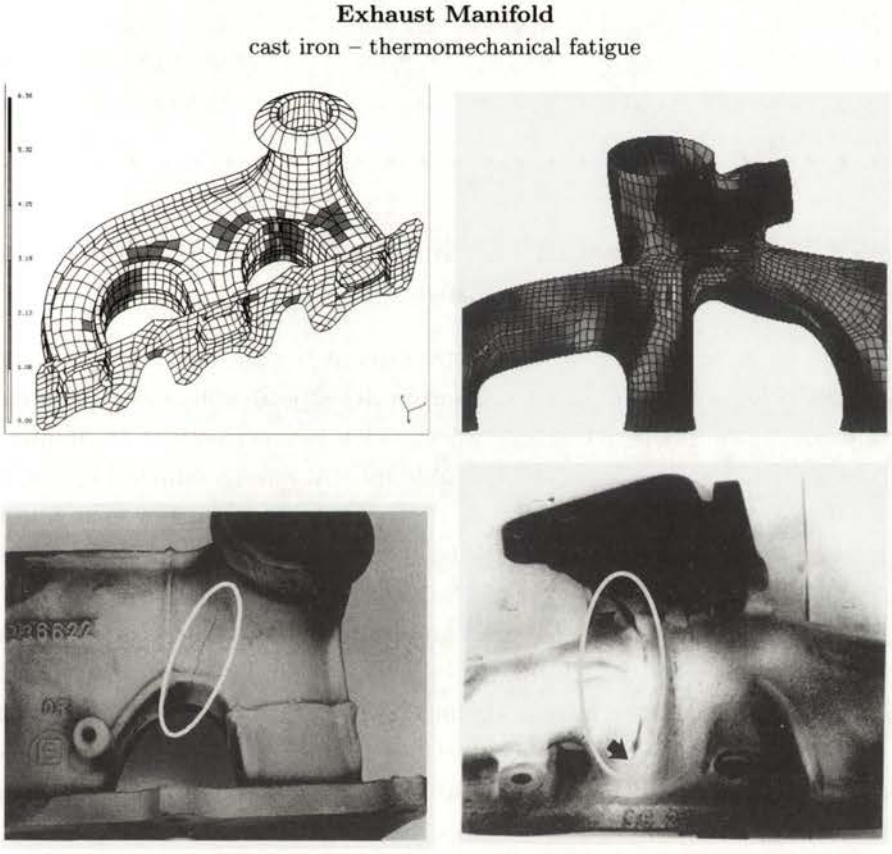


FIGURE 5.2. Prediction of crack initiation on exhaust manifolds subjected to thermomechanical cyclic loadings.

dissipation is easy to calculate, without any ambiguity, and presents many advantages particularly in problems involving thermomechnical loadings which are very frequent and important in mechanical industries (engines, power plants, etc.). Such a typical problem is studied by E. Charkaluk et al. [12]. The mechanical structure is an exhaust manifold which is submitted to gas pressure and temperature varying in a wide range. Since this structure is clamped on the engine body, thermomechanical stresses arise inducing inelastic deformations and low cycle fatigue and even creep fatigue. For such a problem, the approaches deriving from classical LCF are not efficient , since the stress varies with the temperature, for a given plastic strain. The use of a criterion based on a bound on dissipated energy, first identified in laboratory test specimens (isothermal strain controlled LCF tests and thermal fatigue tests on clamped specimens), then applied to the industrial structure for the prediction of the fatigue life (locus of crack and life duration) give very good results. This methodology was already successfully applied to the design of structures submitted to thermomechanical loadings (exhaust manifold shown in Fig. 5.2, cylinder head, etc.).

## 5.4. Interpretation of the infrared thermographic evaluation of the fatigue limit

Evaluation of fatigue limit by conventional testing methods (stair case, etc.) take a lot of time. In order to shorten the experiments, some researchers proposed to use infrared thermography which is a convenient technique for producing heat images from the invisible radiant energy emitted by the test specimen submitted to cyclic loading at an adequate frequency. The temperature rise can be thus captured by the thermographic camera as it is shown in Fig. 5.3.

When the load is increased, one can observe at the same time an increase of the temperature of the specimen. As it was shown by Luong et al. [13, 14], the manifestation of the fatigue damage is revealed by a break of the curve temperature (or also intrinsic dissipation) versus the intensity of the cyclic load as it is shown in Fig. 5.4. Figure 5.4(a) corresponds to determination of the fatigue limit of XC 55 steel by rotating bending test. Figure 5.4(b) corresponds to test done in order to evaluate the fatigue limit of an automotive connecting rod. In both cases, the results obtained very quickly by the method using infrared thermography are similar to those obtained by classical

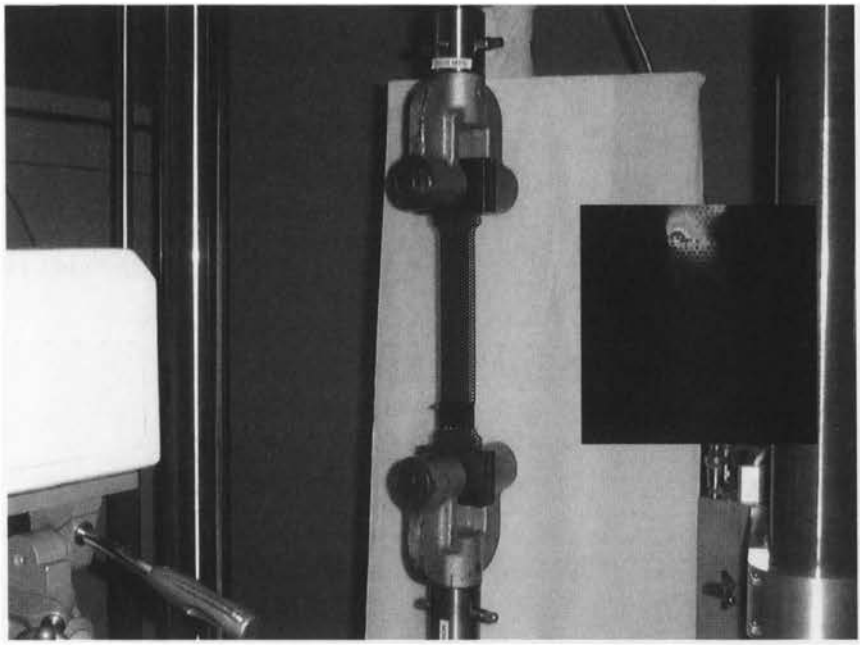

FIGURE 5.3. Determination of fatigue limit using thermographic camera.

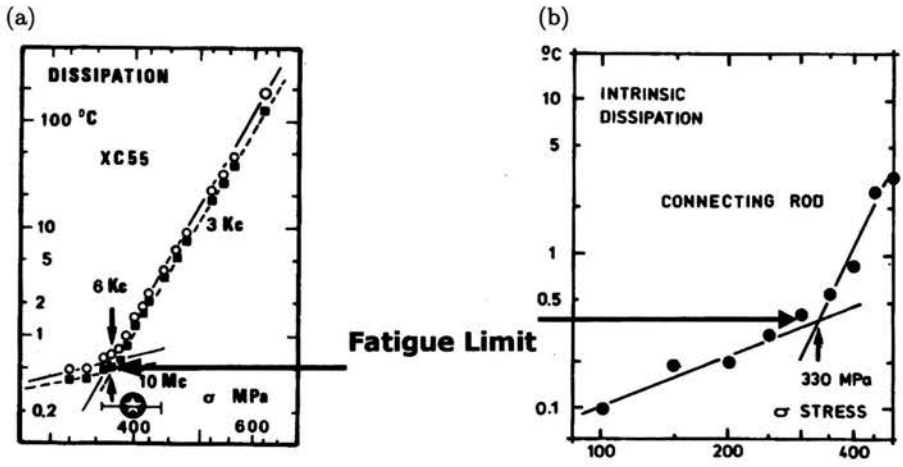


FIGURE 5.4. (a) Fatigue limit in rotating bending. (b) Fatigue limit of a connecting rod.

fatigue tests. Until now there is no convincing explanation of this coincidence. In the proposed theory of fatigue, the reason of this coincidence is very clear: the fatigue limit corresponds to a threshold on dissipative energy; below this threshold, dissipation is bounded, and as a consequence plastic strain (and internal strain hardening parameters) are finite as it was shown by W. Koiter for perfectly plastic material and extended by Q. S. Nguyen to generalized standard material (most of the metallic strain hardening material belongs to this class). The break on the curves of Fig. 5.4(a) and (b) corresponds to two different dissipative rate regimes.

# Chapter 6

# Conclusion

During more than one and a half century metal fatigue has been the subject of numerous research studies conducted by scientists of different fields: mechanical engineers, material scientists, physicists, chemists, etc. Although progress was done in an understanding of physical phenomena, many difficulties still exist to achieve an interdisciplinary consensus in the way to model fatigue crack initiation. Depending on the discipline, points of view are often very different. A mechanical approach has been presented which seems promising: it is based on shakedown hypothesis. Many applications to industrial structures submitted to complex multiaxial loadings are already successfully done; some of these applications, in the domain of high cycle fatigue as well as in plastic or viscoplastic creep fatigue regime have been shown this paper.

In final conclusion, lets us recall a sentence written in 1963 by Professor Daniel Drucker which summarizes very elegantly our proposal [14]: *"when applied to the microstructure there is a hope that the concepts of endurance limit and shakedown are related, and that fatigue failure can be related to energy dissipated in idealized material when shakedown does not occur"*. It seems that this sentence was not known by the fatigue scientist community.

# Bibliography


1. K. DANG VAN, Fatigue analysis by the multiscale approach, in: K. Dang Van and I.V. Papadopoulos (Eds.), *High Cycle Metal Fatigue, From Theory to Applications*, C.I.S.M. Courses and Lectures No. 392, Springer 1999.

2. W.T. KOITER, General theorems for elastic-plastic solids, in: J.N. Sneddon and R. Hill (Eds.), *Progress in Solid Mechanics*, Vol.1, North-Holland, Amsterdam, pp.165-221, 1960.

3. J. MANDEL, B. HALPHEN, J. ZARKA, Adaptation d'une structure elastoplastique à ecrouissage cinématique, *Mech. Res. Comm.*, Vol.4, 309-314, 1977.

4. Q.S. NGUYEN, *Stability and Nonlinear Solid Mechanics*, J. Wiley & Sons, 2000.

5. E. OROWAN, Theory of the fatigue of metals, *Proc. Roy. Soc. London, A*, Vol.171, pp.79-106, 1939.

6. J. ZARKA, Direct analysis of elastic-plastic structures with overlay materials during cyclic loading, *Int. J. Num. Meth. in Eng.*, Vol.15, p.225.

7. B. HALPHEN, Q.S. NGUYEN, Sur les matériaux standards généralisés, *J. Mécanique*, Vol.14, pp.1-37, 1975.

8. I.V. PAPADOPOULOS, Multiaxial fatigue limit criterion of metals, in: K. Dang Van and I.V. Papadopoulos (Eds.), *High Cycle Metal Fatigue, From Theory to Applications*, C.I.S.M. Courses and Lectures No. 392, Springer 1999.

9. I.V. PAPADOPOULOS, *Fatigue Polycyclique des Métaux: une nouvelle Approche, Thèse de Doctorat*, Ecole Nationale des Ponts et Chaussées, Paris 1987.

10. J.L. FAYARD, A. BIGNONNET, K. DANG VAN, Fatigue design criterion for welded structures, *Fatigue Fract. Engng. Mater. Struct.*, Vol.19, 723-729, 1996.

11. J. LEMAITRE, J.L. CHABOCHE, *Mechanics of Solid Materials*, Cambridge University Press, 1990.

12. E. CHARKALUK, A. BIGNONNET, A. CONSTANTINESCU, K. DANG VAN, Fatigue design of structures under thermomechanical loading, in: *Fat. Fracture of Eng. Mat. Struct.*, 2001.

13. M.P. LUONG, K. DANG VAN, Infrared thermographic evaluation of fatigue limit in metal, *Proc. 27$^{th}$ QUIRT Eurotherm Seminar*, Paris.

14. M.P. LUONG, Infrared thermographic scanning of fatigue in metals, *Nuclear Eng. and Design*, Vol.158, pp.363-376, 1995.

15. D.C. DRUCKER, On the macroscopic theory of inelastic stress-strain-time-temperature behaviour, *Advances in Materials Research in the NATO Nations (AGAR Dograph 62)*, Pergamon press, pp.641-651, 1963.

**INSTITUTE OF FUNDAMENTAL TECHNOLOGICAL RESEARCH**
publishes the following periodicals:

ARCHIVES OF MECHANICS — bimonthly (in English)
ARCHIVES OF ACOUSTICS — quarterly (in English)
ARCHIVES OF CIVIL ENGINEERING — quarterly (in English)
ENGINEERING TRANSACTIONS — quarterly (in English)
COMPUTER ASSISTED MECHANICS AND ENGINEERING SCIENCES — quarterly (in English)
JOURNAL OF TECHNICAL PHYSICS — quarterly (in English)

Subscription orders for all journals edited by IFTR may be sent directly to:
*Editorial Office*
*Institute of Fundamental Technological Research*
*Świętokrzyska 21, p. 508*
*00-049 Warszawa, POLAND*